Cooperative effects in multivalent crown ether/ammonium assemblies

Inaugural Dissertation

to obtain the academic degree

Doctor rerum naturalium (Dr. rer. nat.)

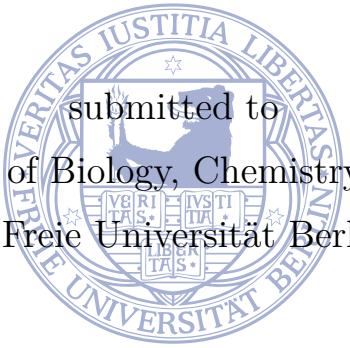

submitted to

the Department of Biology, Chemistry and Pharmacy

of Freie Universität Berlin

by

Larissa Katharina Sophie von Krbek, M.Sc.

from Berlin

2016

The research presented in this thesis was carried out under supervision of Prof. Dr. Christoph A. Schalley between November 2012 and October 2016 at the Department of Biology, Chemistry and Pharmacy of Freie Universität Berlin.

1st Reviewer:	Prof. Dr. Christoph A. Schalley
2nd Reviewer:	Prof. Dr. Beate Paulus
date of defence:	30 November 2016

Acknowledgements

Above all, I would like to express my deepest gratitude to Christoph A. Schalley for his excellent mentoring and supervision throughout my Ph.D. He gave me guidance, encouragement, and freedom to pursue my research interests. Our stimulating and inspiring discussions have broadened my scientific horizon and have promoted this thesis tremendously. Thank you for always welcoming other perspectives.

I am greatly indebted to Beate Paulus for co-examining this thesis.

I am deeply grateful to all my collaboration partners. I would like to mention in particular Stefan Hecht, Mirko Lohse, Karol Nowosinski, Beate Paulus, Marthe Solleder, and Marcus Weber. This thesis greatly profited from merging our various expertises. Our instructive and fruitful discussions were a deep pool of inspiration for me. I would like to single out Andreas J. Achazi here. Thank you for continuously digging deeper with me, thereby pushing our projects even further.

I have profited a lot from the excellent research environment in the Schalley group. Everyday lab work, discussions as well as lunch and coffee breaks would not have been so enjoyable without all current and former group members. Thanks are due to all of you; in particular Luca Cera, Thomas Heinrich, Henrik Hupatz, Karol Nowosinski, Stefan Schoder, Hendrik V. Schröder, Felix Schwarz, Ulrike Warzok, and—last but not least—Nora L. Traulsen for introducing me to the wonders of isothermal titration calorimetry. I gratefully acknowledge the contribution of the students I supervised: Tobias Biberger, Marius Gaedke, Tuğrul Kaynak, and Florian Korinth. Thanks are also due to the NMR and MS service teams together with Andreas Schäfer and Andreas Springer.

I am also greatly indebted to Jonathan R. Nitschke for giving me the opportunity to stay in his group at the University of Cambridge. Furthermore, I would like to thank all my friends and colleagues in Cambridge, who made my time there so enjoyable, especially Derrick A. Roberts and Ben S. Pilgrim.

The financial support by Ph.D. scholarships of the Studienstiftung des Deutschen Volkes and of the integrated RTG of the SFB 765 as well as the infrastructure provided by the Dahlem Research School are gratefully acknowledged.

Finally, I would like to express my gratitude to my friends and even more my family and David. Without their unconditional love and personal support, this thesis would not have come into being.

Abstract

Multivalency is a molecular organisation principle to generate strong and reversible intermolecular interactions. Generally speaking, there are two opposing design principles for constructing synthetic multivalent systems: the first exploits rigid and preorganised building blocks to reduce the entropic penalty of the binding event. Although widely used in supramolecular chemistry, such rigid complexes are sensitive to small geometric mismatches. The second concept—often found in nature—avoids this sensitivity by implementing adaptable, more flexible building blocks. At present, it remains unclear as to which approach leads to more stable multivalent interactions. Decoupling the multivalent association amplification into its component parts—allosteric and chelate cooperativity—can elucidate the operating principles behind the multivalent interaction, the impacts of structural flexibility, and promote a better understanding of the effect. In turn, a deeper understanding of these effects can inform a general "toolkit" for tuning multivalent interactions towards specific applications.

To address both questions regarding the general mechanisms governing the multivalency effect and the adaptability–preorganisation dichotomy, we investigated the cooperative effects in crown ether/ammonium assemblies with varying numbers of binding sites and different spacer lengths and flexibilities. The thermodynamic analysis by isothermal titration calorimetry was complemented by density functional theory calculations and molecular dynamics simulations. The combined approach revealed a number of effects operating in the systems. The ion-pairing between ammonium guests and their respective counterions strongly affects allosteric cooperativity in the guests. This is counterbalanced by the polarity of the chosen solvent. In the hosts, polarisable π-systems cause negative allosteric cooperativities. As expected, small geometric mismatches in rigid systems cause a significant drop in chelate cooperativity. The flexible guests are less affected by geometric mismatches and, surprisingly, generally exceed the more rigid structures in chelate cooperativity. The ability of flexible spacers to correct for small geometric mismatches between host and guest overcomes the entropic penalty incurred through conformational restriction during binding. Moreover, favourable secondary spacer–spacer interactions surpass any entropic penalty. A delicate balance between preorganisation and adaptability is at play when multiply bonded structures are concerned. From these findings, we derived our general toolkit: adaptable, complementary systems are

preferable over rigid preorganised systems with respect to strong, reliably working multivalent interactions.

Using our newly developed toolkit, we demonstrate the successful tuning of a photoswitch. Furthermore, we applied our design principle to program the self-assembly of di- and tetravalent porphyrin-based crown ether and ammonium building blocks into discrete assemblies. The rigidity of the porphyrin scaffold is necessary for complementarity and directionality of the interactions and rotational flexibility between porphyrin scaffold and binding sites for correction of possible mismatches. These and similar structures are promising building blocks for the construction of more complex assemblies inheriting function in the future.

Kurzzusammenfassung

Durch Multivalenz können auf molekularer Ebene starke und dennoch reversible Wechselwirkungen erzeugt werden. Dabei gibt es zwei gegensätzliche Ansätze, um dieses molekulare Organisationsprinzip zu optimieren: Im ersten Ansatz wird versucht, den Entropieverlust zu minimieren, der aus der Einschränkung der konformellen Freiheitsgrade im gebundenen Zustand herrührt. Dafür werden starre, vororganisierte Grundbausteine verwendet, welche bereits im ungebundenen Zustand wenig konformelle Freiheitsgrade besitzen. Sie haben jedoch den Nachteil, dass bereits kleine geometrische Unstimmigkeiten zwischen den Bindungspartnern ungünstige Spannungen im Komplex hervorrufen. Der zweite Ansatz versucht, diese Spannungen durch flexiblere, anpassungsfähige Grundbausteine zu umgehen. Viele Systeme in der Natur verwenden dieses zweite Konzept. In der supramolekularen Chemie ist jedoch das erste Konzept verbreitet. Die Untersuchung der kooperativen Effekte (allosterische und Chelatkooperativität) in einem multivalenten System kann Aufschluss darüber geben, welcher der beiden Ansätze zuverlässiger ist. Außerdem können Hinweise auf die Mechanismen, die der multivalenten Bindungsverstärkung zugrunde liegen, gewonnen werden.

Um beide Fragestellungen anzugehen, wurden die kooperativen Effekte in Kronenether/Ammonium-Komplexen abhängig von Flexibilität und Länge des Gastbausteins untersucht. Die thermodynamische Untersuchung mit isothermer Titrationskalorimetrie wurde durch Dichtefunktionaltheorie- und Moleküldynamikrechnungen ergänzt. Diese Untersuchungen deckten ein komplexes Zusammenspiel von Lösungsmittel- und kooperativen Effekten auf. Die allosterische Kooperativität in den Gastmolekülen wird hauptsächlich von der lösungsmittelabhängigen Ionenpaarbildung zu ihren Gegenionen hervorgerufen. In den Wirtmolekülen wird negative allosterische Kooperativität durch die Polarisierbarkeit ihrer π-Systeme verursacht. Die Chelatkooperativität in Komplexen mit flexiblen Gaststrukturen ist im Gegensatz zu den starren weitgehend unabhängig von strukturellen Unstimmigkeiten zwischen Wirt- und Gastmolekülen. Überraschenderweise haben Komplexe mit flexiblen Gaststrukturen generell höhere Chelatkooperativitäten als die mit starren. Die Anpassungsfähigkeit der flexiblen Strukturen scheint die Chelatkooperativität positiv zu beeinflussen. Dabei werden die durch die multivalente Bindung hervorgerufenen Entropieverluste kompensiert. Hinzu kommen enthalpisch günstige sekundäre Wechselwirkungen der Verknüpfungsstrukturen (*spacer*) zwischen den einzelnen Bindungsstellen. In multivalenten Systemen herrscht ein fragiles Gleich-

gewicht zwischen Anpassungsfähigkeit und Vororganisation. Für die Entwicklung eines verlässlich funktionierenden multivalenten Systems sollten komplementäre, anpassungsfähige Strukturen bevorzugt eingesetzt werden.

Mithilfe dieser Erkenntnisse konnten wir eine supramolekulare, multivalente Wechselwirkung nutzen, um die Funktion eines Photoschalters zu steuern. Die erworbenen Kenntnisse zum Anpassungsfähigkeits/Vororganisations-Gleichgewicht ermöglichten es uns, die Selbstanordnung (*self-assembly*) von di- und tetravalenten Kronenether- und Ammoniumbausteinen erfolgreich zu programmieren. Diese Strukturen sind vielversprechende Vorläufer für eine künftige Anwendung im Aufbau komplexerer Strukturen mit funktionalen Eigenschaften.

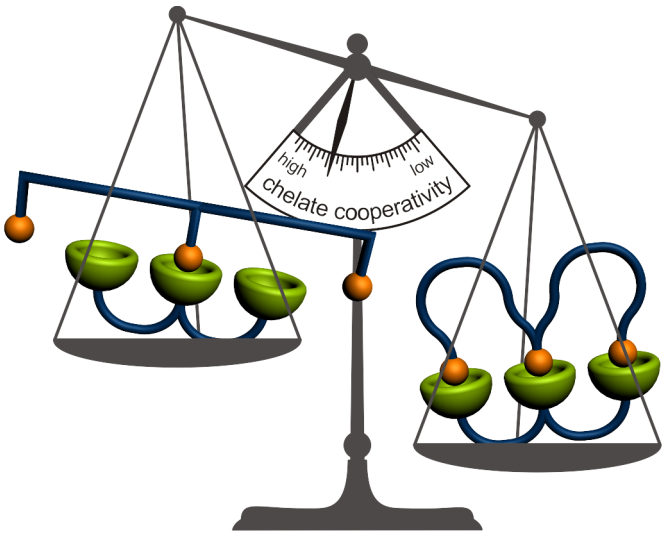

Contents

1 Introduction

Cooperative effects—the impact that one binding event has on subsequent events in a multiply bonded assembly—are the basis of the multivalent binding enhancement. The principle of multivalency—adopted from natural systems such as the DNA double helix—is a molecular organisation concept for the generation of strong but reversible bonds.[2–4] Strong interactions in multivalent systems are granted by the sheer number of weak binding sites. These render the multivalent interactions reversible which makes them preferable to equally strong monovalent interactions in many cases (Figure 1.1a).[2–4] While these statements may not be immediately intuitive, there are microscopic and macroscopic examples from daily life: the previously mentioned DNA double helix and the zipper (Figures 1.1b & c). In a zipper, one row of protruding teeth interdigitates with another row of teeth, thereby connecting both rows by a large number of weak, puzzle-piece type interactions. The connection between the rows is protected against pulling and shearing, but sequentially disconnecting the individual teeth, for example with a slider, separates the two rows easily. The slider renders the closure operation reversible just as

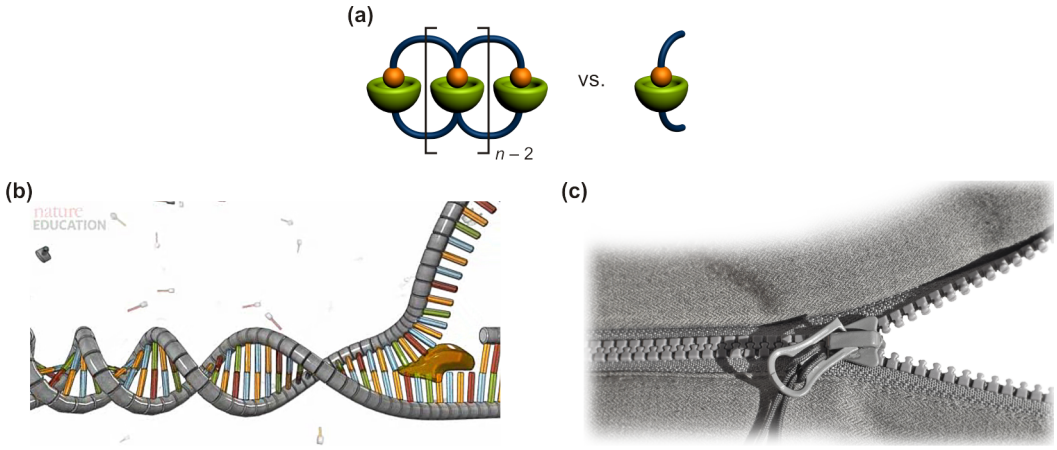

Figure 1.1. **(a)** Schematic representation of an *n*-valent assembly compared to a monovalent complex. **(b)** The DNA double helix[1] and **(c)** the zipper are microscopic and macroscopic examples for multivalent interactions, respectively.
Figure (b) adapted with permission from Nature Education[1] (© Nature Education). Special thanks to Hendrik V. Schröder who helped putting my winter coat on stage.

in the previously mentioned microscopic definition of multivalency. The DNA double strand can be regarded as a zipper on the microscopic scale with helicase corresponding to the slider.
How this multivalent binding amplification exactly operates is still an ongoing matter of current research.[2–4] One approach to elucidate this mechanism is to quantify the underlying cooperative effects in the multivalent systems: allosteric cooperativity, chelate cooperativity, and interannular cooperativity.[5,6] These cooperative effects can unravel the detailed association processes in multivalent systems and thereby inform a better understanding of the balancing effects in these complex systems.

Although the principal actions that underpin multivalent binding are still being uncovered, the exceptional properties of the multivalent bond have fuelled its increasing use in drug design,[2,7,8] biochemistry,[9] material sciences,[10] surface science,[11] and supramolecular chemistry.[12] In supramolecular chemistry, where individual small components assemble into larger, more complex structures, the principle of multivalent interactions is often used to render supramolecular synthesis[13–16] more efficient.
For an effective application of multivalent interactions, it is crucial not only to develop a deeper understanding of the details governing the multivalency effect, but also to develop a general "toolkit" to tune the association strengths according to the desired purpose. In most cases, that would probably be a strong, reliably operating interaction.

The classic approach to generate such high binding affinities relies on the rigid preorganisation of complementary building blocks. Cram[17,18] first introduced the concept of preorganisation in simple supramolecular complexes and Whitesides and co-workers[2,19] extended this principle to multivalent biological systems. Preorganised, rigid systems supposedly suffer from a lower entropic penalty upon binding compared to more flexible, less preorganised systems,[20,21] because bound and unbound species do not differ a lot with respect to conformational restriction. This principle has been used effectively to generate highly cooperative assemblies in the past.[4,10,12,19,22–24] However, these rigid structures are very sensitive towards geometric mismatches between the components, where even a slight discrepancy can lead to a drastic drop in binding affinity.[2,25]
These sensitivities might be a reason why many systems found in nature do not exhibit a very high degree of preorganisation. For instance, a single strand of DNA, as mentioned before (Figure 1.1b), has a highly flexible backbone, but is

very stable once entwined with a complementary partner. The main advantage of such a flexible backbone is its adaptability to small mismatches between the multiply bonded interaction partners. Hence, there might be an alternative way to generate strong multiple host–guest interactions that avoids the use of rigid, preorganised structures. The concept of adaptability is not completely unknown in supramolecular chemistry. It is, for example, used in foldamers—flexible oligomers which fold into conformationally ordered states.[26–29] Nevertheless, it has been scarcely used in multivalent systems so far.[30–33]
Two questions arise from these points. First, why did scientists adapt the principle of multivalency from nature, but did not also consider flexible, adaptable systems? Second, which approach is preferable for generating strong, reliably working interactions: the classical tactic of rigid preorganisation or nature's flexible adaptability?

To address both questions, the investigation of synthetic and, thus, designable multivalent supramolecular complexes is advantageous. Supramolecular complexes can be systematically varied with respect to parameters such as the number of binding sites or spacer flexibility, length and geometry. That means the complementarity and preorganisation of the two components can be modified. Such supramolecular model compounds need to meet several criteria to be suitable for this purpose: (i) easy synthetic accessibility, (ii) relatively strong binding interactions, and (iii) a well-understood monovalent binding motif. Crown ether/ammonium assemblies fulfil all of these conditions. The [18]crown-6/primary-ammonium-ion and [24]crown-8/secondary-ammonium-ion binding motifs are widely used building blocks for the generation of complex, programmed structures in supramolecular chemistry.[34–41] Thus, they were chosen as model systems in this research project.

Multivalent binding amplification, as the name suggests, is essentially a thermodynamic effect. For a thermodynamic analysis of the crown ether/ammonium assemblies, isothermal titration calorimetry (ITC) is a powerful tool. Unlike other analytical techniques used in supramolecular chemistry, it delivers the association constant K, the Gibbs free energy ΔG, the enthalpy ΔH and the entropy ΔS in a single experiment. Thus, using ITC does not only elucidate the cooperative effects of a multivalent system in a *double mutant cycle* (DMC) analysis, but also quantifies the impact of ΔH and entropy ΔS on the chelate cooperativity. The latter two have not been investigated in such detail before.
Supramolecular chemistry usually takes place in solution. Hence, even though the main interest focuses on the supramolecular complex, it is only a minor component of

the overall system. The solvent accounts for the major part of the molecules. Thus, the solvent can have crucial impact on the behaviour of the whole system including the supramolecular complex of interest. As a solution analytical technique, ITC can also be used to elucidate solvent effects. In crown ether/ammonium assemblies, where the dissociation of the ion pair precedes the assembly of the supramolecular architecture, the solvent can have a strong impact on binding behaviour.[42–46] Their solubility in a range of organic solvents of different polarities allows for addressing the questions of solvent and ion-pairing effects as well.

These aspects framed the research objective of this thesis as summarised in the following points:

- Synthesis and thorough thermodynamic analysis of the monovalent [18]crown-6/primary-ammonium-ion binding motif including solvent and counterion effects as a sturdy foundation to the following analyses of more complex assemblies (Figure 1.2a; Section 3.1).
- Quantification of all occurring cooperative effects in divalent [18]crown-6/primary-ammonium-ion complexes as well as in di- and trivalent [24]crown-8/secondary-ammonium-ion pseudorotaxanes to elucidate the detailed association mechanisms of multiply bonded structures. Analysis of solvent and ion-pairing effects in these crown ether/ammonium assemblies. (Figure 1.2b; Sections 3.2 & 3.3)
- Synthesis of divalent [18]crown-6/primary-ammonium-ion complexes with different guest spacer lengths and flexibilities. Use of the previously established approach to analyse the impact of the guest spacer length and flexibility on the cooperative effects to obtain a general "toolkit" for multivalent interactions with high binding amplifications (Figure 1.2c; Section 3.4).
- Use of the acquired knowledge to tune the function of a supramolecular photoswitch (Figure 1.2d; Section 3.5) and to design more complex supramolecular assemblies (Figure 1.2e; Section 3.6).

For the interpretation of experimental results and profound insight into the detailed association mechanisms of the investigated systems, the thermochemical analysis of divalent [18]crown-6/ammonium complexes is complemented by density functional theory (DFT) calculations and molecular dynamics (MD) simulations in close collaboration with Andreas J. Achazi, Beate Paulus, Marthe Solleder and Marcus Weber. Here, the simplicity of our chosen model systems comes into play again: they exhibit a limited molecular size suitable for these computational analyses.

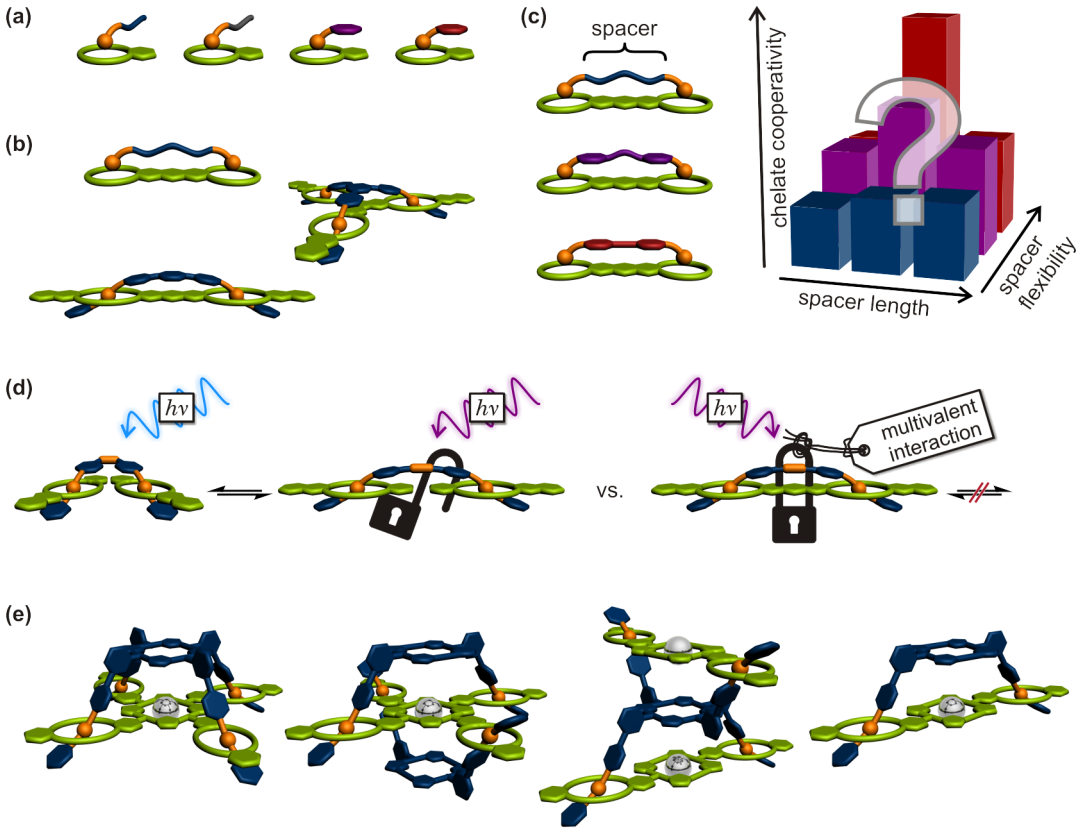

Figure 1.2. Graphical summary of the research objective: **(a)** Analysis of solvent and counterion effects in monovalent [18]crown-6/primary-ammonium-ion complexes. **(b)** Thermodynamic analysis of cooperative effects in di- and trivalent [18]crown-6/primary-ammonium-ion complexes and [24]crown-8/secondary-ammonium-ion pseudorotaxanes. **(c)** Systematic thermodynamic analysis of the impact of the guest spacer length and flexibility on the chelate cooperativity in the divalent assemblies. **(d)** Use of a multivalent interaction to tune the photochromic activity of a supramolecular assembly. **(e)** Construction of more complex supramolecular structures through multivalent interactions.

2 Theoretical background

2.1 Host–guest complexes

The relatively simple design of a host–guest complex (Figure 2.1) unites most of the core concepts of supramolecular chemistry. The host, a ring, bowl or cage-like molecule, binds to a guest through *reversible*, *non-covalent interactions*. The guest nicely fits into the host's cavity and, thus, the two components are *complementary* to each other respective to their interactions and their size. Host–guest complex formation is achieved simply by mixing the two components in solution where they spontaneously *self-assemble*; no external energy supply is required. Brownian motion of the molecules in solution lets the complementary binders eventually meet and "drop" into their *thermodynamic minimum*, the host–guest complex.

A few examples of typical complementary host and guest molecules and their complexes held together by various types of *non-covalent interactions* are depicted in Figure 2.2.[47–49] These non-covalent interactions range from strong ion–dipole interactions (50–200 kJ mol^{-1}) over hydrogen bonds (4–120 kJ mol^{-1}) to weak π–π (0–50 kJ mol^{-1}) and Van-der-Waals interactions (<5 kJ mol^{-1}).[47] The inclusion complexes with cucurbiturils and cyclodextrines are special cases. Held together only by the weak Van-der-Waals interactions, their host–guest-complex formation is mainly driven by solvophobic effects; the hydrophobic effect in particular. That is, they both exhibit a hydrophobic cavity which is poorly solvated in water. The respective guests are hydrophobic as well and solvated just as poorly. The main driving force to form the complex is to release the water in their solvation shells

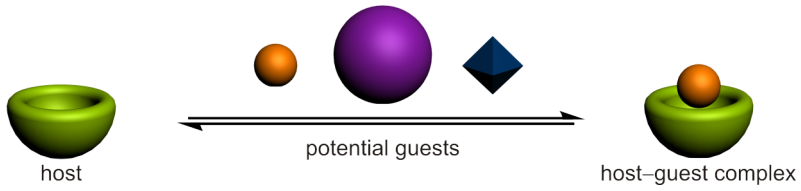

Figure 2.1. Schematic representation of size and shape-selective self-assembly of a host–guest complex.

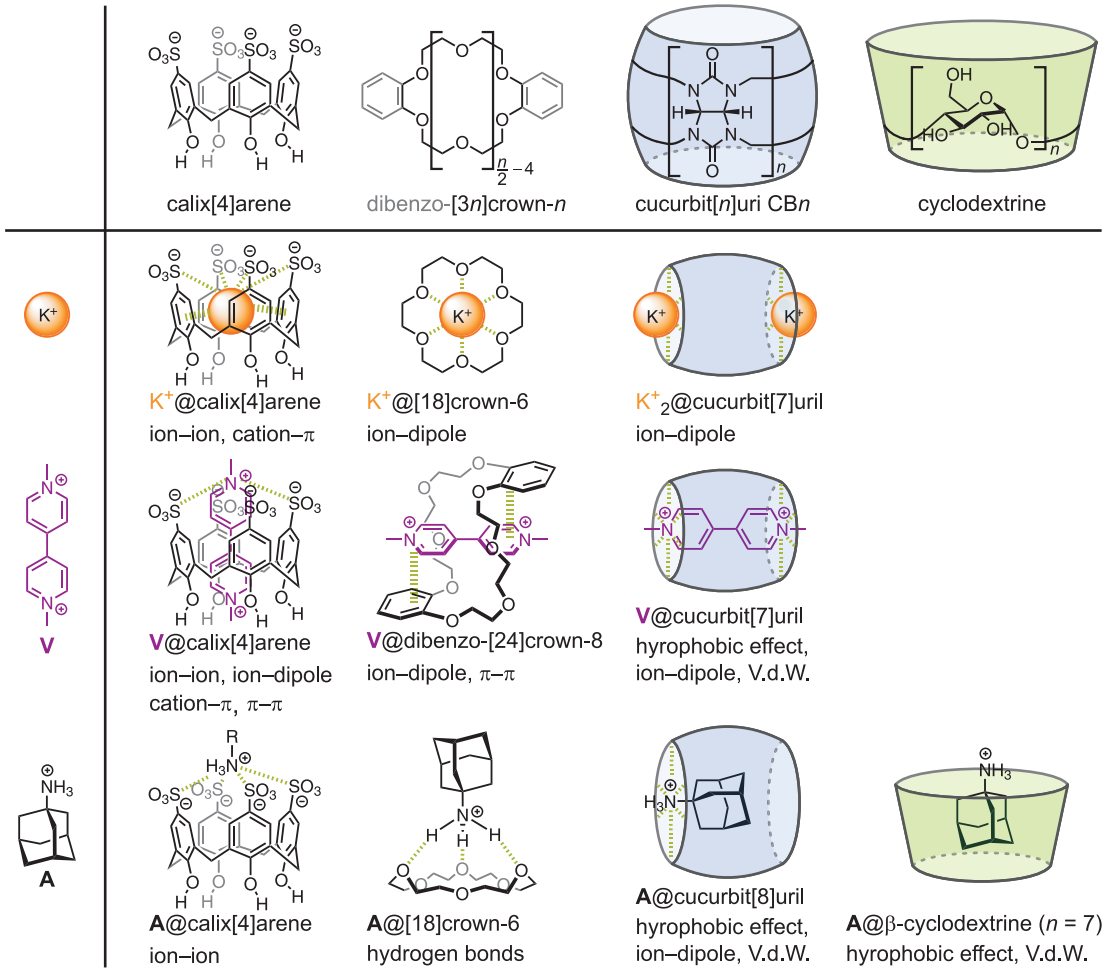

Figure 2.2. Examples of common supramolecular host molecules (top row) and typical guests (left column). Cells contain their host–guest complexes and the respective non-covalent interactions that hold the species together. A complex is formed, if host and guest are complementary with respect to both their size and their binding sites.

into the bulk thereby rising both the enhalpy and entropy of these water molecules. For the special case of the cucurbituril this phenomenon will be discussed in greater detail in Section 2.1.2.

Complementarity, both in size and interacting units, is crucial for strong host–guest interactions. The potassium cation, for example, is electron deficient and strongly interacts with dipoles such as polarised ether oxygens. Furthermore, the radius of the potassium cation (1.38 Å) and the inner cavity of [18]crown-6 (1.34–1.43 Å) perfectly fit together.[50] Hence, their host–guest interaction is exceptionally strong ($2.1 \cdot 10^6$ M^{-1} in methanol, $T = 25$ °C, counterion: ClO_4^-).[51]

Self-assembly describes the spontaneous and reversible association of monovalent building blocks to form organised aggregates.[47,48] *Reversibility* of the association

allows for error correction and the monovalent components eventually aggregate into the *thermodynamic-minimum* structure. The term "self-assembly" is usually attributed to the formation of larger structures, but the relatively simple generation of a host–guest complex from its individual components can be regarded as a basic form of self-assembly.

The expression "host–guest chemistry" was first introduced in 1974 by D. J. Cram [52] seven years after C. J. Pedersen [53,54] accidentally found the first host–guest complex: a crown ether/cation complex. Ever since, crown ethers and their host–guest complexes have been extensively studied [51,52,55–63] and used in the field of supramolecular chemistry, [35–40,64] but also for biologically inspired model systems. [65–67] In the field of supramolecular chemistry and in this thesis, the crown ether/ammonium binding motif is extensively used. Hence, this binding motif is described in greater detail in the following section.

2.1.1 The crown ether/ammonium binding motif

Depending on their ring size, crown ethers (nomenclature: [3n]crown-n, with n oxygen atoms in a 3n membered ring) can form host–guest complexes with different ammonium ions: primary, secondary and quaternary ammonium compounds (Figure 2.3). The simple ammonium cation (NH_4^+) was the first and simplest example of a crown ether/ammonium complex. It was the arbitrary choice, as its size is similar to the potassium cation which strongly binds to [18]crown-6 ($2.1 \cdot 10^6\ \mathrm{M}^{-1}$, methanol, $T = 25\,^\circ\mathrm{C}$, ClO_4^- [51]). Unlike the potassium ion, the ammonium ion does not sit in the ring plane but hovers above it in a side-on complex. Three hydrogen bonds to alternating crown ether oxygens support that structure (Figure 2.3, middle

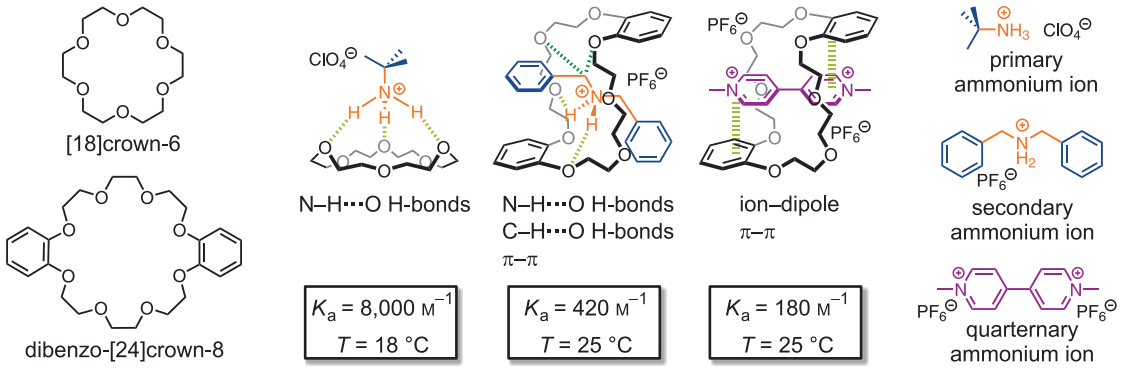

Figure 2.3. Three different examples of crown ether/ammonium complexes and the respective non-covalent interactions that hold the species together. Respective association constants [42,43,68] K_a were determined in acetone by NMR methods.

left).[37,59,69] These are only half as many non-covalent interactions as in the case of the potassium cation which might account for the one-order-of-magnitude lower association constant of NH_4^+ ($1.3 \cdot 10^5$ M^{-1}, methanol, $T = 25$ °C, ClO_4^- [51]). If one of the hydrogen atoms is substituted by an organic group (e.g. *t*Bu), the association constant of the primary ammonium ion exhibits a substantial drop ($3.7 \cdot 10^2$ M^{-1}, methanol, $T = 18$ °C, ClO_4^- [68]). In a less competing solvent, such as acetone (Section 2.1.2), the association constant rises considerably ($8.0 \cdot 10^3$ M^{-1}, acetone, $T = 18$ °C, ClO_4^- [68]). These [18]crown-6/primary ammonium ion complexes are usually formed and equilibrated within seconds and their exchange is on fast exchange on the NMR time scale.[68] This renders these complexes ideal for thermochemical investigation within an isothermal titration calorimeter and for investigation of rebinding effects in multiply bonded structures composed of this monovalent binding motif (for definition of rebinding effects, see Section 2.2).
The cavities of the two next larger crown ethers [21]crown-7 and [24]crown-8 are big enough for the ammonium ion to sit in the ring plane. Furthermore, their size allows for threading of the substituents of secondary ammonium ions (Figure 2.3, middle). In the case of a dibenzylammonium ion binding to dibenzo-[24]crown-8, the threaded structure—in contrast to a possible side-on complex—is supported by secondary C–H$\cdots$O hydrogen bonds of the bezylic hydrogens and π–π interactions between one benzo ring of the host and one benzyl ring of the guest.[37,47] The association constant of dibenzo-[24]crown-8/dibenzylammonium ion complex is one order of magnitude smaller that the [18]crown-6/primary ammonium ion system ($4.2 \cdot 10^2$ M^{-1}, acetone, $T = 25$ °C, PF_6^- [42]). The threaded complex assembles within minutes, but it is on slow exchange on the NMR time scale. Full error correction in more complex systems can last 15 hours and longer.[70] That can be a drawback in assembly of complex supramolecular structures. Good complementarity of host and guest and directionality of the binding sites might compensate for that (approach implemented in Section 3.6). The dibenzo-[24]crown-8/viologen dication complex exhibits considerably weaker interactions between host and guest($1.8 \cdot 10^2$ M^{-1}, acetone, $T = 25$ °C, PF_6^-) and is on fast exchange (NMR) again.[43]

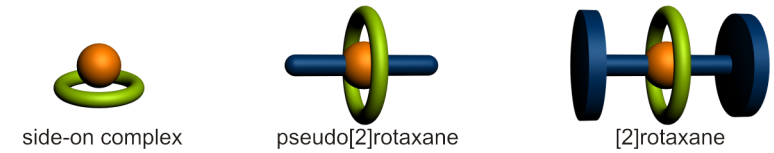

Figure 2.4. Schematic representations of a side-on complex, a pseudo[2]rotaxane and a [2]rotaxane. The number in brackets indicates of how many components the pseudorotaxane and rotaxane consist.

The threaded structures of the [24]crown-8/ammonium assemblies, per definition, are pseudorotaxanes. A pseudorotaxane is a special form of a host–guest complex in which the guest is axle-shaped and threaded through the ring- or wheel-shaped host (Figure 2.4). This thread can be extended with bulky stopper groups to form a mechanically interlocked molecule of wheel and axle: a rotaxane.

All host–guest complexes of crown ethers and primary or secondary ammonium ions have one particular characteristic in common: their acid/base responsiveness. Deprotonation of the ammonium ions weakens their hydrogen bonds to the crown ether considerably and the individual components dissociate. Protonation with acid can switch the interaction back "on". Thus, the crown ether/ammonium binding motif is not only a versatile binding site for pseudorotaxanes and rotaxanes, but also for rotaxane-based molecular shuttles or switches.

In a rotaxane-based molecular shuttle, the rotaxane thread contains two binding sites between which the wheel shuttles back and forth. In a rotaxane-based molecular switch, these two binding stations can be switched "on" or "off" by alternating stimuli (Figure 2.5). Thereby the potential energy landscape of the rotaxane switch is changed in favour of whichever binding site is switched on at the moment. The wheel performs a translational motion towards the respective binding site into its thermodynamic minimum. The height of the energetic barrier between two binding sites distinguishes the system between a shuttle and a switch. In a shuttle, the barrier is low and the wheel can freely shuttle back and forth between both stations, i.e. both thermodynamic minima. The difference in the thermodynamic minima dictates on which of the two stations the wheel sits with higher probability. In a switch, the barrier between both binding sites is high and the wheel is located on the stronger binding site. As usual with definitions, the transition between these two concepts is smooth and in most cases the truth is found somewhere in between. Many rotaxane-based molecular switches, for example, are more or less switchable molecular shuttles (Figure 2.5).

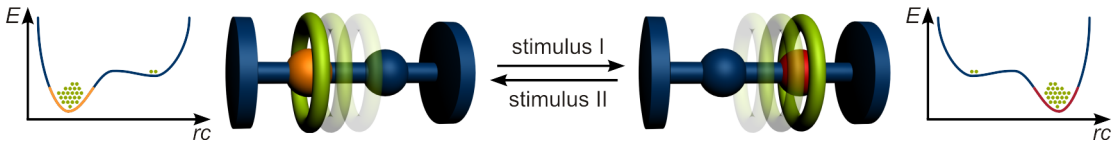

Figure 2.5. Schematic representation of a switchable [2]rotaxane-based molecular shuttle. Two alternating stimuli switch the binding sites "on"/"off" or "off"/"on" thereby generating different minima in the potential energy surfaces and causing a translational motion of the ring.

Stoddart and co-workers[71,72] reported the first crown-ether based molecular shuttles (Scheme 2.1, top). They implemented a dibenzylammonium unit and a viologen unit as binding stations into the thread. The ammonium binding station is considerably stronger than the viologen binding site due to hydrogen bonding (see above). Hence, the crown ether shuttles between both binding stations, but is mostly located at the ammonium site. Addition of base leads to deprotonation of the secondary ammonium ion and "switches off" hydrogen bonding. The crown ether performes a translational movement towards the now stronger viologen binding site where it is mostly located then. Addition of acid reverses the process.

The simplicity of this crown-ether based molecular shuttle found various applications in more complex systems such as molecular elevators[35,74] and muscles.[46] The first molecular elevator from Stoddart and co-workers[35,74] has three of these switchable shuttles implemented into a multiply threaded structure (Figure 2.6a). Within the base and acid strokes, the platform of the molecular elevator moves 7 Å downwards or upwards, respectively. The base stroke does not occur in the cartoon-like concerted fashion, but in a stepwise way of deprotonation and shuttling (Figure 2.6b). The 7 Å stroke might be used to generate forces of up to 200 pN which is more than one order of magnitude larger than those developed[75] by natural linear motors like myosin and kinesin. For this and other work on molecular motors, Stoddart, Sauvage, and Feringa were awarded the Nobel Price in Chemistry 2016.

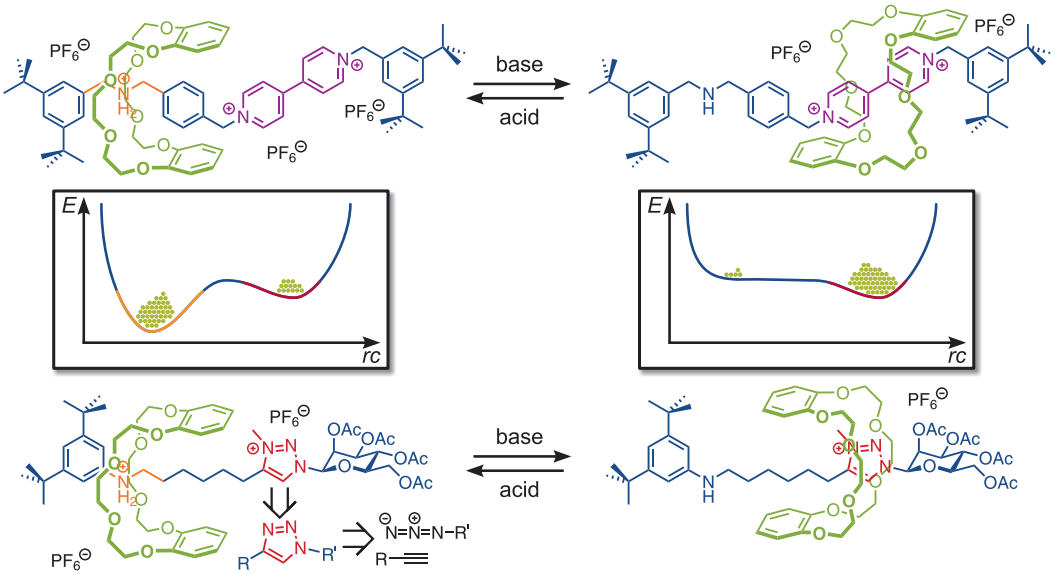

Scheme 2.1. Two similar approaches for acid/base-controlled crown ether/ammonium based [2]rotaxane shuttles by Stoddart and co-workers,[71] (top) and Coutrot and co-workers[73] (bottom). Schematic representation of the change in the energy landscape due to deprotonation/protonation is given in the middle.

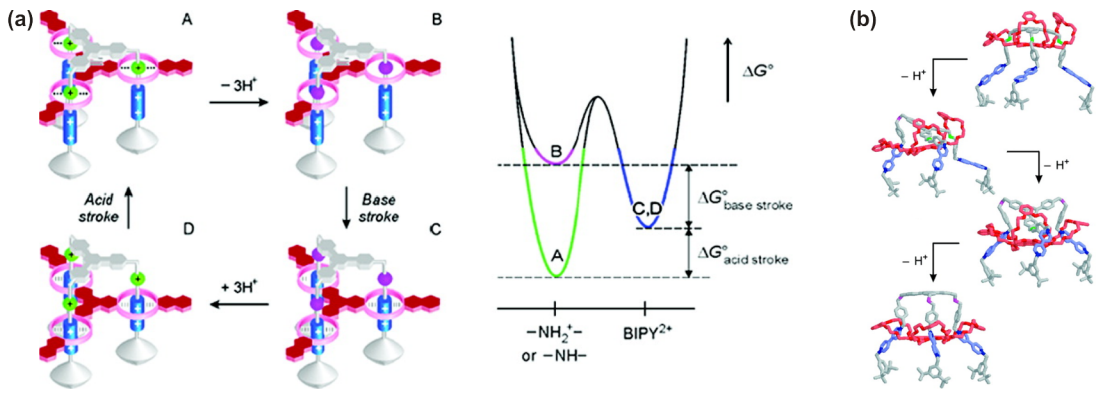

Figure 2.6. **(a)** Acid/base-controlled mechanical switching in a crown ether/ammonium based molecular elevator by Stoddart and co-workers (left).[35,74] The simplified potential energy landscape of the switching is depicted on the right. Reprinted with permission from Badjić et al.[35] (© 2006 American Chemical Society). **(b)** Stepwise motion of the crown-ether platform down the threads upon successive deprotonation of the three secondary ammonium groups (molecular mechanics calculations). Adapted with permission from Badjić et al.[74] (© 2004 American Association for the Advancement of Science).

Coutrot and co-workers[73,76] adapted Stoddart's[71,72] shuttle concept and considerably simplified it by exchanging the viologen by *N*-methyltriazolium (Scheme 2.1, bottom). They "clicked" a mannosyl stopper to the preformed crown ether/ammonium pseudorotaxane. Methylation of the triazole results in the secondary binding station. Their altered molecular shuttle works as nicely as the one previously reported from Stoddart and co-workers.[71,72] Due to the relative ease of synthesis, this approach is especially useful for more complex, multiply threaded shuttles.

The applicability of the secondary *N*-methyltriazolium binding station in more complex structures was later demonstrated in molecular pulleys,[77] elevators[38] and muscles.[78,79] Liu and co-workers,[38] successfully generated a doubly threaded—i.e. divalent—[2]rotaxane elevator (Figure 2.7). In this case, the "on"-state (left) is further stabilised by secondary spacer–spacer interactions between the guest's electron poor naphthalenediimide unit and the host's electron rich anthracene moiety.

These examples demonstrate that the crown ether/ammonium binding motif is a quite well understood binding site and a versatile building block for various purposes ranging from simple side-on complexes, pseudorotaxanes and rotaxanes over shuttles to molecular muscles. Therefore, it was chosen as monovalent binding motif for investigation of cooperative effects in multivalent systems in this work.

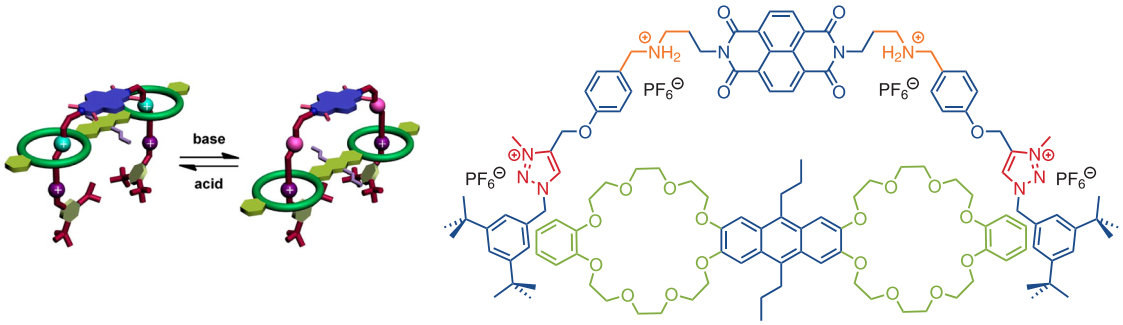

Figure 2.7. Schematic representation of the doubly threaded switchable [2]rotaxane shuttle by Liu and co-workers (left).[38] Chemical structures of individual wheel and axle components are depicted on the right.
Adapted with permission from Zhang et al.[38] (© 2013 American Chemical Society).

2.1.2 Solvent effects

Host–guest interactions are widely used to generate all kinds of complex structures including systems inheriting function and molecular machines. In many of these applications, the most prominent component of these systems is neglected: the solvent. The solvent surrounds the individual host and guest components as well as the host–guest complex in a solvation shell (Figure 2.8). Upon complex formation, the solvation shells around host and guest have to disrupt and the solvent molecules are released into the bulk. From that bulk, a solvation shell is reformed around the host–guest complex. overall, this process releases solvent molecules into the bulk and the entropy of the system increases. Hence, the solvent needs to be chosen carefully that it (i) solvates host, guest and host–guest complex and (ii) does not compete with the non-covalent interactions between host and guest. As the host–guest interactions are mostly ion–dipole interactions or hydrogen bonds, the common choice for non-competing solvents are unpolar, low-dielectricity constant solvents (e.g. chloroform, dichloromethane, etc.). Unpolar solvent molecules can neither serve as hydrogen-bond donor or acceptor and do not compete with ion–dipole interactions. The latter is, however, a disadvantage when it comes to the solvation of ionic species. They are rarely soluble in unpolar solvents and slightly

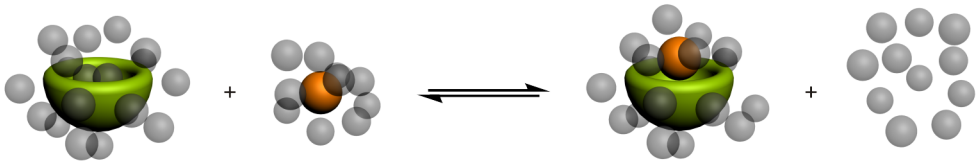

Figure 2.8. Host–guest association equilibrium showing the required desolvation of both components prior to complex formation. The solvent molecules (grey) thereby released into the bulk increase the entropy of the system.[47]

more competing polar, low-dielectricity constant solvents (e.g. acetonitrile, acetone, etc.) are used. If host–guest interactions are too strong to be measurable, they can be fine-tuned by changing to a more competing solvent. With these considerations in mind, the solvent is neglected as mostly passive component again.[47]

However, there are two cases which need to be considered with special care. The first regards mixtures of solvents with different polarity. Solubility issues or the wish for a slightly more competing solvent often require the use of mixtures of unpolar and (more) polar solvents. By gradually increasing the amount of the more polar component the dielectricity constant ε_r of the mixture increases as well. Although this is a linear relationship, the effect on the polar solutes is not always linear.[80] The more polar solvent tends to cluster around the polar sites of the solutes creating a higher local concentration of the polar solvent, i.e. a higher local dielectricity constant. Similarly, the less polar solvent is prone to cluster around the unpolar parts of the solutes.[81] Since the polar sites of the solutes are usually the binding sites in supramolecular complexes, the competition of these solvent mixtures is stronger than expected from the overall dielectricity constant of the solvent mixture. That often creates a non-linear behaviour of the host–guest association energies with respect to the gradual increase of the polar solvent fraction. It is likely, that the more polar the binding sites, e.g. ionic sites, the more pronounced is this non-linear behaviour of the solvent. This is also true if the two solvents differ strongly in polaritiy, e.g. the non-linearity is expected to be smaller for chloroform/acetonitrile mixtures than for chloroform/methanol mixtures.

The second special case is, if the release of solvent molecules into the bulk upon host–guest complex formation creates more energy than the actual host–guest interaction. This usually occurs, if the solvent–solvent interaction is a lot stronger than the solvent–solute interaction. In these so called solvophobic effects, release of the solvent into the bulk upon complex formation does not only increase the entropy of the overall system but also the enthalpy. In simple words: the individual components are barely soluble and badly solvated. Solvent molecules in these solvation shells are high in energy. The host–guest complex is usually better solvated; the solvent molecules in its solvation shell are a bit lower in energy. The released solvent molecules gain entropy but also interact more with the bulk, thereby gaining enthalpy as well.[82] Due to the strong hydrogen bonds between its individual molecules, water is most prominent for its solvophobic effects—the hydrophobic effect. That hydrophobic effect promotes complex formation in cyclodextrin complexes and contributes stongly to cucurbituril complex formation as well.

The contribution of the hydrophobic effect on cucurbituril complexes was recently elucidated by De Simone and co-workers.[83] In a combined approach of experimental thermodynamic (isothermal titration calorimetry, ITC) and computational molecular dynamics (MD) studies, they could show that the high binding affinities of unpolar guests to cucurbiturils CBn in water do not only originate from favourable interactions between host and guest, but also from a special form of the hydrophobic effect. Cucurbiturils CBn solvated in water contain a small number of water molecules in their hydrophobic cavity (Figure 2.9a). These water molecules are considerably higher in energy than molecules from the bulk water, because of (i) their hydrophobic environment the (ii) fact that they can only form half as many hydrogen bonds compared to bulk water (1.31 H bonds compared to 2.54). They mainly interact through weak dipole–dipole interactions. These high energy water molecules are released, if a host–guest complex is formed between the cucurbituril CBn and a hydrophobic guest (Figure 2.9b). The energy release of these water molecules upon interaction with the bulk is the main driving force for host–guest complex formation between cucurbiturils and hydrophobic guests.
These results do not only intriguingly demonstrate that the solvent is not always a passive component in host–guest association, but also show how a combined approach of experimental thermochemistry and computations can elucidate elaborate relations in greater detail than any of the methods could have done alone.

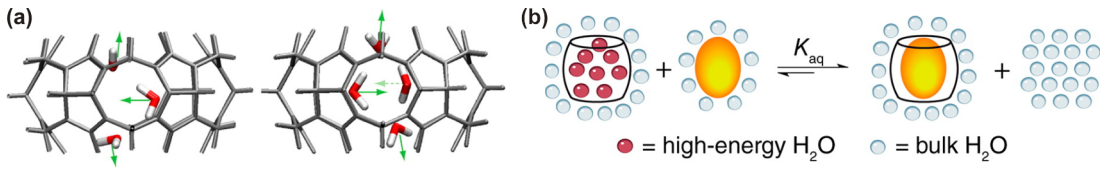

Figure 2.9. **(a)** Representative arragements of three (left) and four (right) water molecules inside the hydrophobic CB6 cavity.[83] **(b)** These high energy water molecules are released from the cavity upon binding of a hydrophobic guest.[83]
Adapted with permission from Biedermann et al.[83] (© 2012 American Chemical Society).

2.1.3 Counterion effects

Many of the discussed host–guest complexes involve cations which usually render the non-covalent interactions stronger. A paradigm for those is the crown ether/ammonium binding motif. The ammonium hydrogen bonds are strong, but deprotonation of the ammonium to the amine renders the interaction very weak and the complex dissociates as described above. These cationic species implicate a third important component into host–guest complex formation which is quite often neglected: the counter-anions. Usually, non-coordinating counterions such as PF_6^-, OTs^-, and $BArF_{24}^-$ are used and that approximation seems appropriate. However, the generally used low dielectric constant solvents do not only render the desired host–guest interaction but also ion–ion interaction between the opposing ions stronger. Unfortunately, that effect is most of the times not taken into account.

Gibson and co-workers[42,44] did comprehensive studies on the impact of ion pairing on host–guest complex formation of dibenzo-[24]crown-8 (**C8**) and dibenzylammonium salts (**A1** • X) in low dielectric constant solvents. They found that $\mathbf{A1}^+$ forms strong ion pairs with its counterion X^- ($X^- = PF_6^-$, BF_4^- or ($TFA^- = CF_3COO^-$)) whereas the host–guest complex $\mathbf{A1@C8}^+$ is not ion paired in these media (Scheme 2.2a). Therefore, the measured association constants for host–guest complex formation K_{exp} are strongly dependent on the nature of the anion and its concentration here (Table 2.1). The guest's ion pair **A1** • X needs to dissociate prior to complexation. Only the unpaired guest cation can then form a host–guest

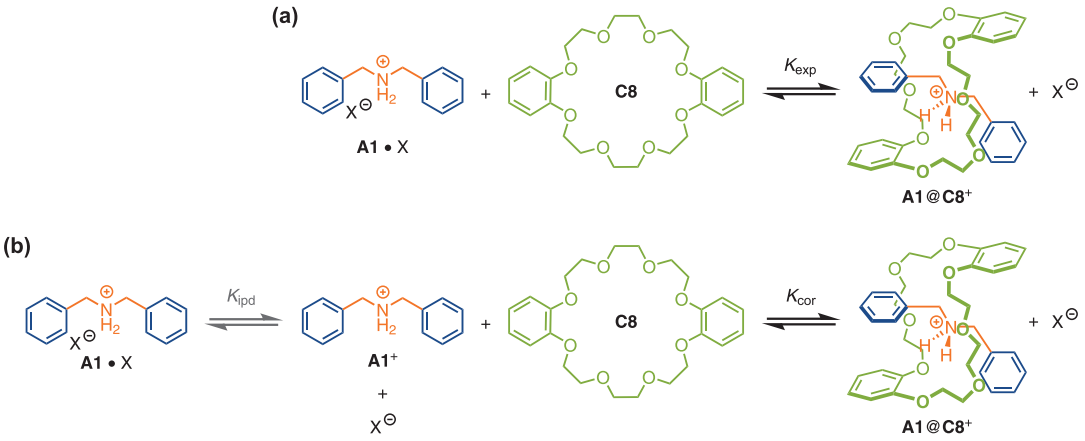

Scheme 2.2. **(a)** Association of a crown ether **C8** and an ammonium salt **A1** ▪ X in low dilelectric constant solvents. **A1** ▪ X forms strong ion pairs whereas in $\mathbf{A1@C8}^+$ the host prohibits ion pair formation. **(b)** Association of **C8** and $\mathbf{A1}^+$ corrected by the preliminary ion pair dissociation of **A1** ▪ X (K_{ipd}; $X^- = PF_6^-$, BF_4^- or ($TFA^- = CF_3COO^-$)).[42,44]

Table 2.1. Experimental association constants of **C8** and **A1** ▪ X (K_{exp}), corrected association constants of **C8** and $\mathbf{A1}^+$ (K_{cor}) and ion pair dissociation constants of **A1** ▪ X (K_{ipd}) in $CHCl_3/CH_3CN$ 3:2 (v/v).[42]

counterion	$\boldsymbol{K}_{\mathbf{exp}}$ $[\mathrm{M}^{-1}]$	$\boldsymbol{K}_{\mathbf{cor}}$ $[\mathrm{M}^{-1}]$	$\boldsymbol{K}_{\mathbf{ipd}}$ [M]
PF_6^-	450	509 ± 80	$6.94 \cdot 10^{-3}$
BF_4^-	1,300	500 ± 110	$3.92 \cdot 10^{-3}$
TFA^-	20	495 ± 30	$1.85 \cdot 10^{-4}$

complex with **C8** (Scheme 2.2b). If the experimental association constants K_{exp} are corrected by the ion pair dissociation constants K_{ipd} and the activity coefficients of the ammonium salts $\gamma_\pm$, all crown ether/ammonium complexes exhibited the same association constants K_{cor} (Eq. 2.1, Table 2.1).

$$\gamma_\pm^2 \, K_{exp} = K_{ipd} \, K_{cor} = \gamma_\pm^2 \, \frac{[\mathbf{A1@C8}^+] \, [X^-]}{[\mathbf{C8}] \, [\mathbf{A1} \bullet X]} \tag{2.1}$$

To conclude,[42,44] host–guest complexes involving ionic species have to be considered carefully in low dielectric constant solvents regarding (i) the nature of the counterion and (ii) the polarity of the solvent or the solvent mixture. (i) Weakly coordinating counterions such as PF_6^- are preferable. In the case of PF_6^-, the difference between the measured binding constant K_{exp} and the corrected K_{cor} was only marginal in the chosen solvent mixture ($CHCl_3/CH_3CN$ 3:2 (v/v); $450\ \mathrm{M}^{-1}$ and $510\ \mathrm{M}^{-1}$, respectively). (ii) There exists a trade-off between very unpolar solvents in which both the host–guest interaction is stronger and more polar solvents in which the ion pairs are completely dissociated, but the host–guest interaction is exceptionally weak as well. For example, in pure chloroform ion pairing of **A1** • PF_6 prevents any host–guest complexation with **C8**, whereas in acetone **A1** and PF_6^- seem to be fully dissociated. In the latter case, the association constant $K_{exp} = 420\ \mathrm{M}^{-1}$ is mostly independent on PF_6^- concentration, i.e. $K_{exp} = K_{cor}$, but slightly smaller than in the chloroform/acetonitrile mixture ($K_{cor} = 510\ \mathrm{M}^{-1}$). However, for analysis of the binding constants, this simple equilibrium is definitely preferable over a higher association constant.

Strongly competing counterions do not always have to be a negative side effect in supramolecular systems, as nicely demonstrated by Chiu and co-workers.[46] They deliberately used the strong interaction between secondary ammonium cations and fluoride anions in acetonitrile to switch “off” the crown ether/ammonium

interaction in a rotaxane switch. By successive addition and sequestering of fluoride anions, they effectively operated a crown ether/ammonium based molecular muscle (Scheme 2.3). Deprotonation of the ammonium ions, as in the shuttles described in Section 2.1.1 (Scheme 2.1 & Figure 2.7), did not lead to the expected contraction. The authors attribute this to the low acidity of the hydrogen bonded ammonium ions. The weak interaction of the crown ethers to the pyridinium moieties is not a good enough driving force to weaken the strong crown ether/ammonium hydrogen bonds enough to allow for their deprotonation.[46] Another factor is probably, that the energy difference between the amine and the pyridinium is not large enough to compensate for the strain generated by contracting the alkyl chain. The fluoride anions, however, interact strongly with the ammonium ions and force them out of the electron rich crown-ether cavity.[46] The contracted alkyl-ammonium chain probably forms a strongly ion-paired cluster with the fluoride anions (compare Figure 3.5, Section 3.3). This cluster effectively stabilises the contracted from and is only opened if the fluoride anions are sequestered by addition of $Ca(BF_4)_2$. Thereby, CaF_2 precipitates and the stretched form of the [2]rotaxane muscle is regained.

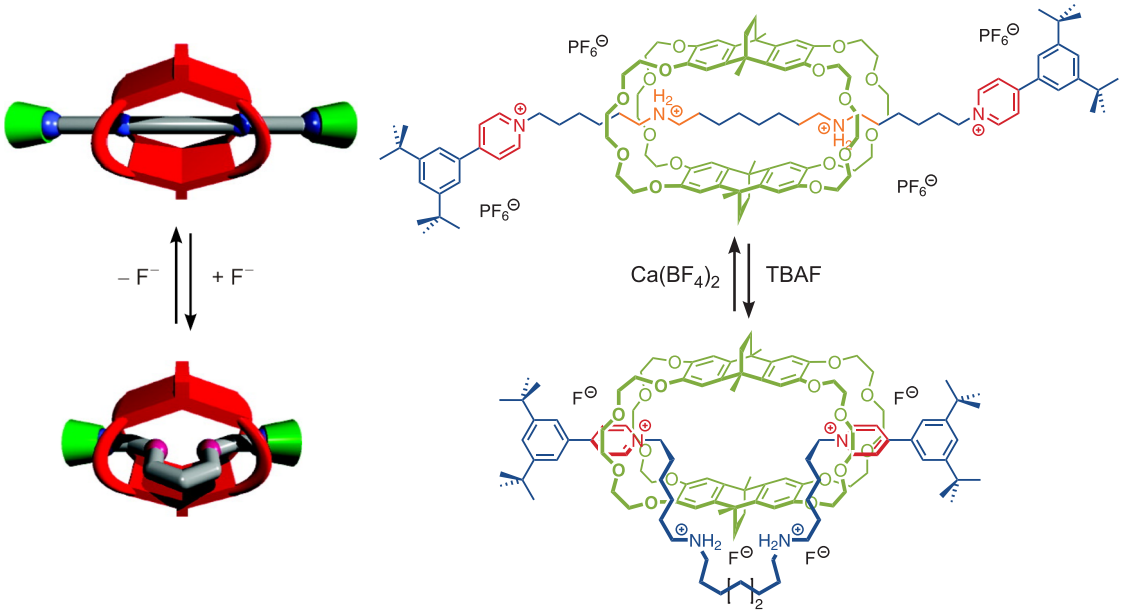

Scheme 2.3. Schematic representation of the [2]rotaxane-based molecular muscle by Chiu and co-workers (left).[46] Chemical structures of stretched and contracted forms are depicted on the right.
Cartoons adapted with permission from Chuang et al.[46] (© 2009 American Chemical Society).

2.2 Multivalency

In a multivalent assembly, an array of more than one weak reversible binding site generates a strong nonetheless reversible interaction. In these systems, a binding amplification is often observed: The multivalent interaction is stronger than its individual parts would indicate. This is sometimes referred to as the "multivalency effect".[4] As already mentioned in the Introduction, the principle of multivalency is found in nature and increasingly adapted in different fields of chemistry due its unique properties.[2–4,10–12]

Intriguing supramolecular examples of multivalent systems by Stoddart and co-workers[35,74] as well as Liu and co-workers[38] were already discussed in Section 2.1.1. Tanaka and co-workers[36,84,85] added another level of complexity to multiply threaded crown ether/ammonium rotaxanes. They reported the synthesis of a quadruply-threaded elevator (Figure 2.10a).[36] The scaffolds of host and guest contain copper(II) equipped phthalocyanines and porphyrines, respectively. The phosphoramidate stoppers can be deprotonated together with the ammonium binding sites by a base. The now negatively charged stopper units repel the crown

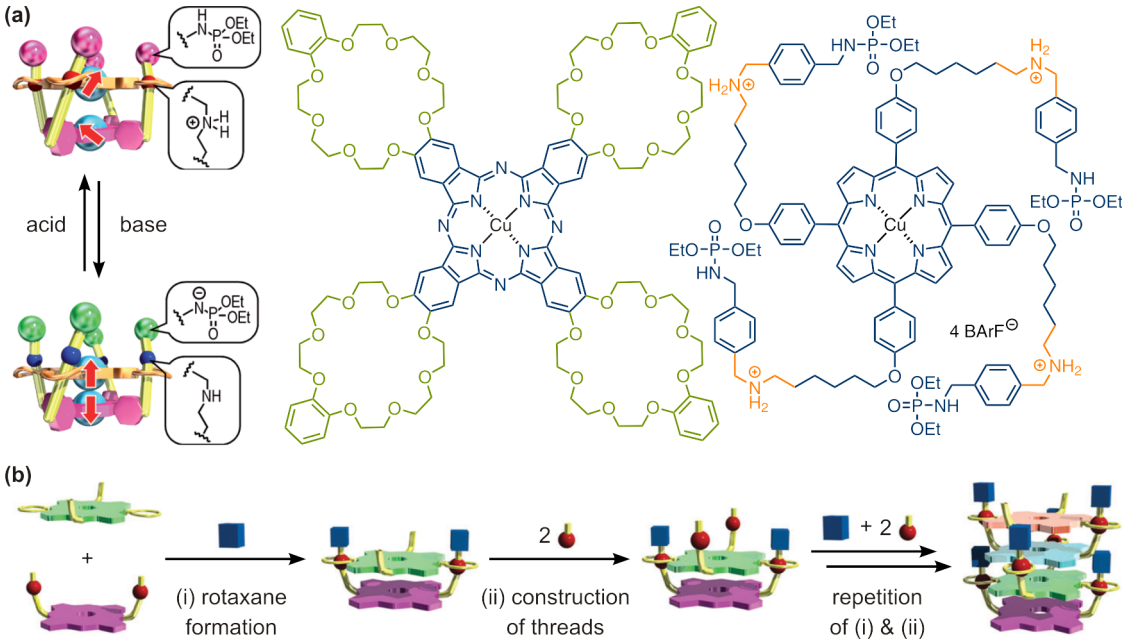

Figure 2.10. **(a)** Base/acid switching of the spin–spin coupling in a quadruply threaded molecular elevator.[36] Cartoons adapted with permission from Yamada et al.[36] (© 2012 Wiley-VCH Verlag GmbH & Co. KGaA, Weinheim). **(b)** Schematic representation of the stepwise synthesis of a porphyrin stack via repetitive formation of doubly threaded rotaxanes.[84] Cartoons adapted with permission from Yamada et al.[84] (© 2013 The Royal Society of Chemistry).

ethers and they perform a translational motion along the threads. This brings the two copper(II) equipped platforms in close proximity and a coupling of the spins of the two copper(II) ions is observed. The process is reversed by addition of acid. Later, Tanaka and co-workers[84] demonstrated that similar structures can be used to sequentially synthesise a porphyrin stack (Figure 2.10b).

The fact that these[36,84,85] and other systems[35,38,74] assemble into discrete structures rather than random oligomers is due to the "multivalency effect". It is a powerful tool, but the underlying principles that govern its properties, such as the binding amplification, are sparsely understood. One of the objectives of this thesis was to further elucidate these core concepts of multivalent systems. In the following, a brief summary of the current state of research apart from the results of this thesis is given.

The term multivalency describes an array of multiple, i.e. more than one ($n \geq 2$), host–guest complexes connected by spacers (Figure 2.11a). If a multivalent complex has only one type of binding site, it is termed homomultivalent. Heteromultivalency denotes an assembly containing more than one type of interaction site. Multivalent complexes between hosts and guests with different numbers of binding sites are possible as well (Figure 2.11b).[4,86] When considering the association mechanism of a trivalent complex and the possible partly bound states therein (Figure 2.12), it becomes obvious why a reversible monovalent interaction is mandatory in a effectively operating multivalent system: It allows for error correction. The lower the barrier between the bound and unbound states of an interaction site, the

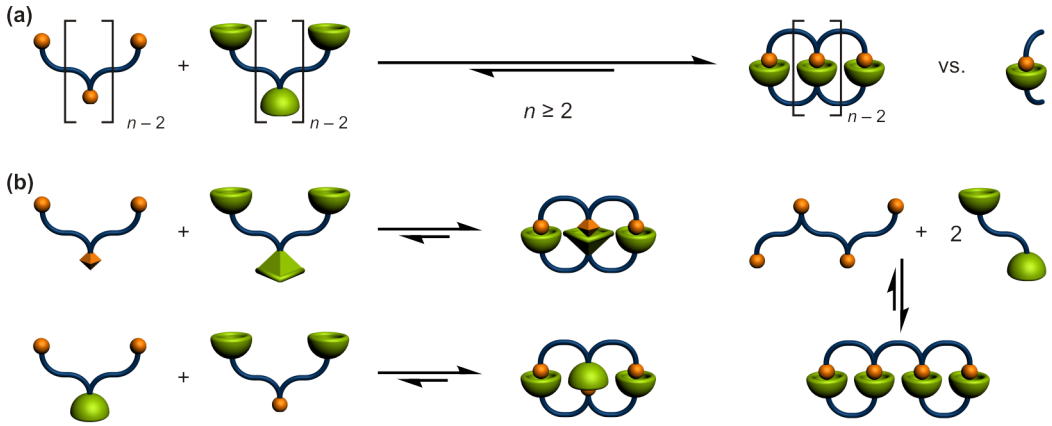

Figure 2.11. **(a)** Formation of a homomultivalent complex from an *n*-valent guest and an *n*-valent host ($n \geq 2$). The formation of the *n*-valent assembly is usually favoured over monovalent complexes. The binding sites of host and guest need to be complementary to each other, but **(b)** different types of binding sites are possible (heteromultivalency) and the number of binding sites in host and guest may differ.

faster is the exchange between both and the quicker and more effective are the error-correction mechanisms in the system. These error-correction mechanisms are especially important when working with more complex higer-valent systems. Both crown ether/ammonium complexes introduced in Section 2.1.1 allow for error correction. This renders both motifs suitable as binding sites in multivalent assemblies.

The "multivalency effect"—that is, the binding enhancement in these systems—can be deconvoluted into statistical and cooperative effects.[5,6,87] Mere statistics render the multivalent interaction favourable over the monovalent one irrespective of possible cooperative effects in the multivalent system. For example, the probability of a monovalent guest to bind to a m-valent host is m-times higher than to bind to a monovalent host.[4,88] This symmetry effect[88–91] is caused by the equivalent binding sites of the host and, hence, also occurs in multivalent systems. These statistical factors have to be determined for quantification of the underlying cooperative effects of the system. The cooperative effects—the effect that one binding event has on subsequent events in an n-valent system—help to elucidate the detailed principles which render the multivalent interaction favourable. Both, cooperative and statistical effects, will be discussed in more detail in Section 2.3.

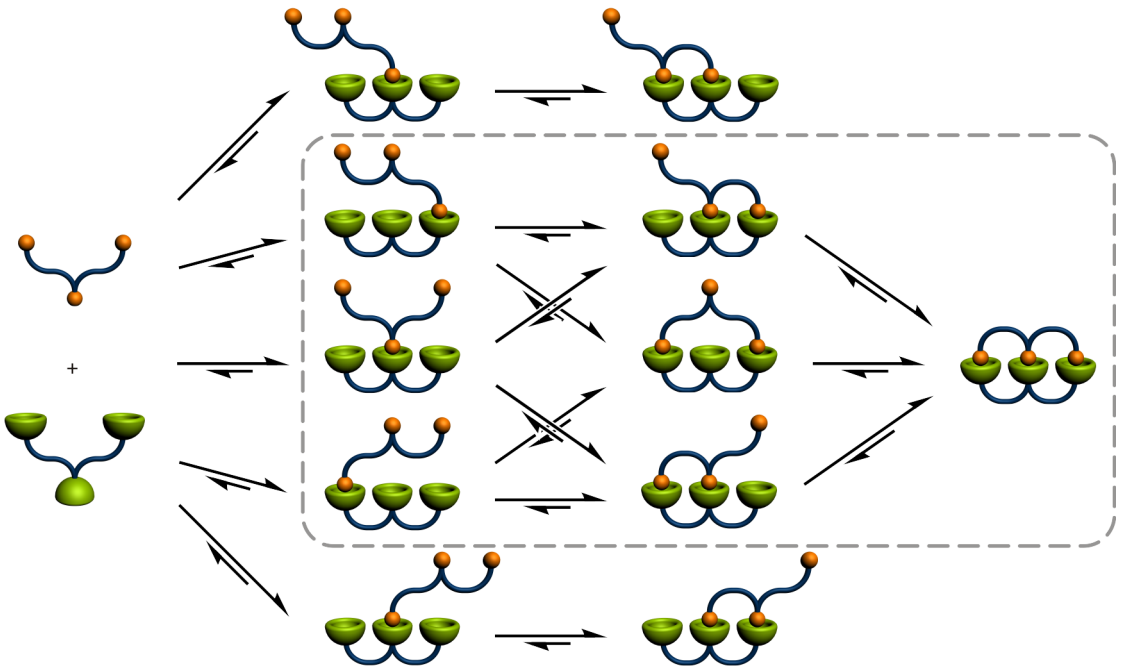

Figure 2.12. Association equilibria of a trivalent complex from its individual components. Rebinding can occur between the bound and the partly bound states (dashed grey box).

Different theories and models try to explain aspects of the cooperative behaviour of multivalent interactions. One of those is the higher local concentration of binding sites in the partly bound states.[92,93] The first binding event between a multivalent host and a multivalent guest brings the other binding sites into closer spacial proximity (Figure 2.12). They are more preorganised with respect to each other in this state. This increases the local concentration of binding sites and makes the following binding events more feasible. These following binding events are intramolecular rather than intermolecular interactions.

Another model explaining the strength of multivalent interactions is strongly related to the local concentration. It refers to the probability of binding site dissociation and re-association between the bound and partly bound states of a multivalent complex (Figure 2.12, grey box). If one binding site of the fully bound multivalent complex dissociates, the spacial proximity (or local concentration) of these recently separated interaction partners makes it very probable for them to re-associate. Thus, the complex is kinetically "trapped" in its bound and partly bound states. This dissociation/re-association phenomenon is called rebinding.[94,95]
Weber and co-workers[95] predicted that rebinding contributes strongly to the stability of complexes with monovalent binding sites which have a low barrier between bound and unbound state. In complexes with a higher barrier, rebinding operates less effectively. This is in line with the better error-correction mechanisms in the former systems. If these findings are transferred to the crown ether/ammonium binding motif discussed in Section 2.1.1, rebinding should contribute to the stability of multivalent [18]crown-6/primary ammonium ion complexes but not very much to the stability of [24]crown-8/secondary ammonium ion pseudorotaxanes.

The spacer is not an "innocent" connecting unit when it comes to the thermodynamics in multivalent systems. Indeed, the length of the spacer can alter the association enthalpy ΔH_{multi} of a multivalent interaction due to steric strain or the lack thereof.[2] If host and guest spacer perfectly match (Figure 2.13, middle), no enthalpic effect is observed. If the spacers of one binding partner are slightly longer or shorter than that of the other, the complex suffers enthalpic strain. Multivalent binding can also be prohibited, if the spacers of one component are too short to bridge the binding sites of the other (Figure 2.13, top) or if the spacers are too long and rigid and cannot fold back (Figure 2.13, bottom right). It depends on the flexibility of the spacer, how large these enthalpic effects are. The more rigid the spacers, the larger the effect of small geometric mismatches.[2,25,96]
In general, a good complementarity of the spacers with respect to their length is fea-

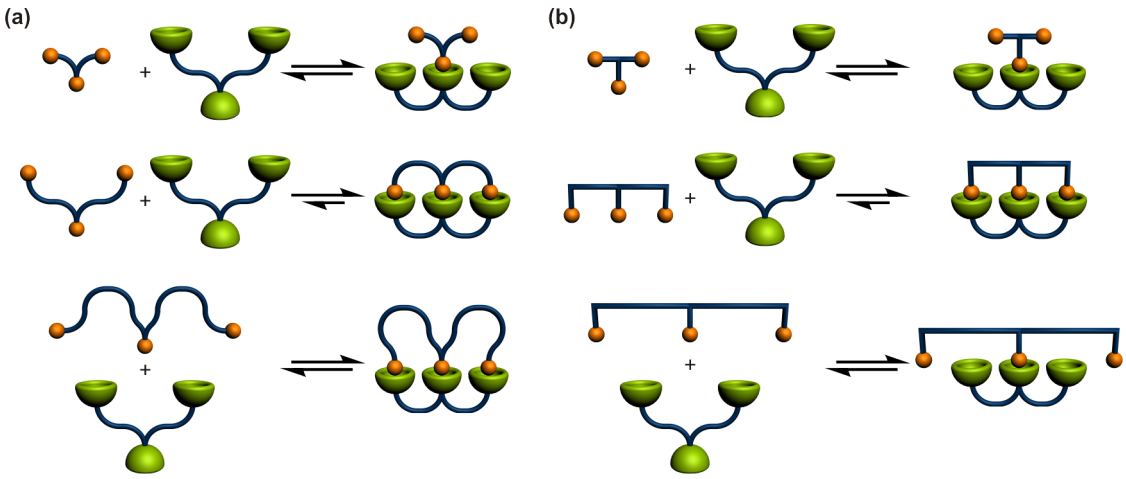

Figure 2.13. The effects of different spacer lengths (too short, optimal, long, from top to bottom) on **(a)** flexible guest spacers and **(b)** rigid guest spacers. If the guest spacer is too short to bridge the binding sites of the host, no multivalent binding occurs irrespective of the spacer flexibility. in the case of a perfect match of host and guest spacer, the rigid guest spacer is supposed to be favourable over the flexible as it suffers less entropic penalty caused by conformational restriction upon binding. Long and flexible guest spacers suffer enthalpic strain and entropic penalty. Long and rigid guest spacers prohibit the multivalent interaction again.

sible. This leads to a good preorganisation of the binding sites in the singly-bound state and, thus, facilitates the following association steps. Moreover, rebinding can operate more efficiently in the case of a good geometric match of the spacers.

Furthermore, the spacer causes one of the major drawbacks of multivalent systems. That is, the association of a multivalent guest to a multivalent host is entropically unfavoured compared to the monovalent interaction, because the spacer structures in the multivalent system suffer a considerable loss of conformational entropy (ΔS_{conf}) upon the first binding event.[92] Whitesides and co-workers[2] elucidated the entropic effects of the spacers on the association behaviour of multivalent systems by making two assumptions: (i) The entropic contributions of the multivalent complex and a monovalent complex are virtually the same except for the conformational entropy of the spacer (Eq. 2.2). (ii) The spacer has no enthalpic effect whatsoever on the multivalent system (Eq. 2.3).

$$\Delta S_{\mathrm{multi}} = \Delta S_{\mathrm{mono}} + \Delta S_{\mathrm{conf}} \tag{2.2}$$

$$\Delta H_{\mathrm{multi}} = n\,\Delta H_{\mathrm{mono}} \tag{2.3}$$

Under these conditions, high valencies are entropically favoured over low valencies. Furthermore, one can conclude that rigid spacer scaffolds are favourable over flexible

ones, because rigid structures suffer of less conformational fixation upon multivalent binding (Figure 2.13). From these considerations, it seems obvious that rigid preorganisation has to be the state of the art. Nevertheless, Mammen et al.[2] also postulate that the adaptability of flexible systems might be advantageous to guarantee an interaction of all binding sites without large enthalpic strain (compare Figure 2.13a & b, bottom).

In line with the arguments of entropic penalty for conformational restriction upon multivalent binding, Anderson and co-workers[24] found that the intramolecular interactions between a hexavalent ligand and a cyclic zinc-porphyrin oligomer are significantly favoured over the interaction with a linear oligomer (Figure 2.14). The preorganisation in the rigid rings leads to a remarkable increase of four orders of magnitude in binding affinity compared to the linear rigid but non-preorganised analogues.

As already hinted by Whitesides and co-workers[2], the impact of spacer flexibility on multivalent interaction is not straightforward. Hunter and co-workers[31] did comprehensive studies on the impact of spacer flexibility on heterodivalent zinc-porphyrin/pyridine complexes and found a flexibility–complementarity dichotomy

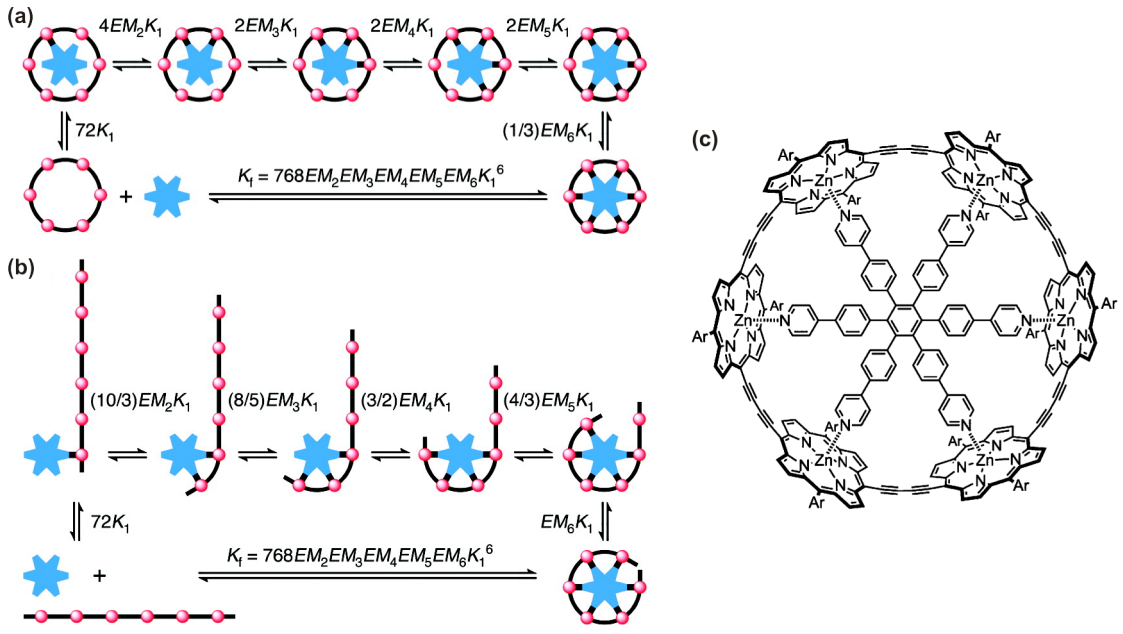

Figure 2.14. Stepwise association mechanism of hexavalent pyridine ligand (blue) **(a)** to a hexameric zinc-porphyrin ring or **(b)** to a linear hexameric zinc-porphyrin oligomer.[24] The effective molarity *EM* is the key value in an intramolecular cyclisation reaction and will be explained further in Section 2.3.2. **(c)** Structure of the hexavalent complex with the cyclic host. The linear zinc-porphyrin oligomer exhibits virtually the same structure.[24]
Adapted with permission from Hogben et al.[24] (© 2011 American Chemical Society).

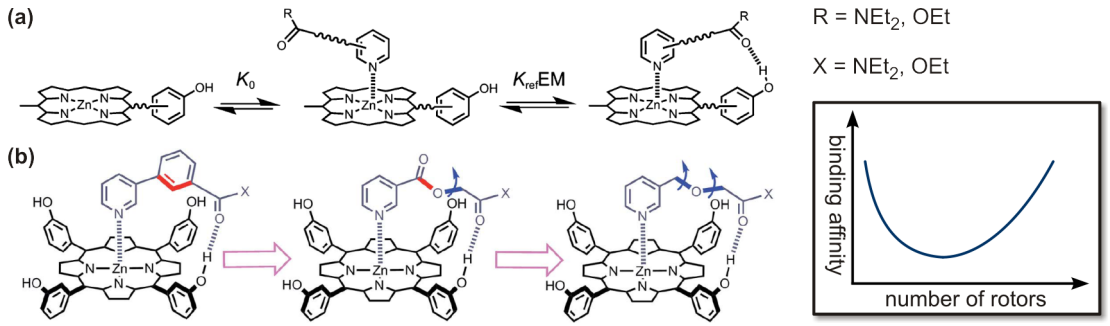

Figure 2.15. **(a)** Stepwise association mechanism of zinc-porphyrin/pyridine complexes with intramolecular hydrogen bonds.[31] **(b)** Zinc-porphyrin/pyridine complexes with varying spacer flexibility: rigid, semi-rigid and flexible (from left to right), the latter two exhibiting one or two additional rotors, respectively. Key rotatable bonds in the spacer are highlighted in blue, restricted rotors are highlighted in red.[31]
Adapted with permission from Sun et al.[31] (© 2015 The Royal Society of Chemistry).

(Figure 2.15). The intramolecular cyclisation step is most favourable in systems with rigid aromatic spacers as expected from entropic considerations. In systems with flexible ether spacers and two more rotational degrees of freedom, the intramolecular association constant is reduced by factor three. Unexpectedly, freezing one of these rotors in semi-rigid ether systems does not lead to an increase of binding affinity but to another decrease by the factor three (Eq. 2.4).

$$EM_{\text{rigid}} = 3\,EM_{\text{flexible}} = 9\,EM_{\text{semi-rigid}} \tag{2.4}$$

The authors conclude that although the penalty for conformational restriction upon binding is lower for the more rigid systems, the flexibility allows for geometric optimisation of the complementarity of the binding partners. Hence, there is a trade off between rigid preorganisation and fit.

More recently, a third spacer effect apart from entropic contributions and enthalpic strain was identified by Schalley and co-workers.[34] They investigated the association thermodynamics of homodivalent crown ether/ammonium pseudorotaxanes with different guest-spacer lengths (Figure 2.16a). In the crystal structure of the best binder, they found evidence that the structure is not only favoured due to the perfect geometric match between the spacers (Figure 2.16b): Secondary π–π interactions between the host's electron rich anthracene unit and the benzylic phenyl groups of the guest stabilise the doubly bonded structure. Longer guest spacers prohibit these favourable interactions. Paulus and co-workers[97] later substantiated these these findings by DFT calculations. Thus, positive secondary spacer–spacer

interactions can considerably contribute to the stability of a multivalent assembly. Spacer–spacer repulsion on the other hand may destabilise a multivalent array.

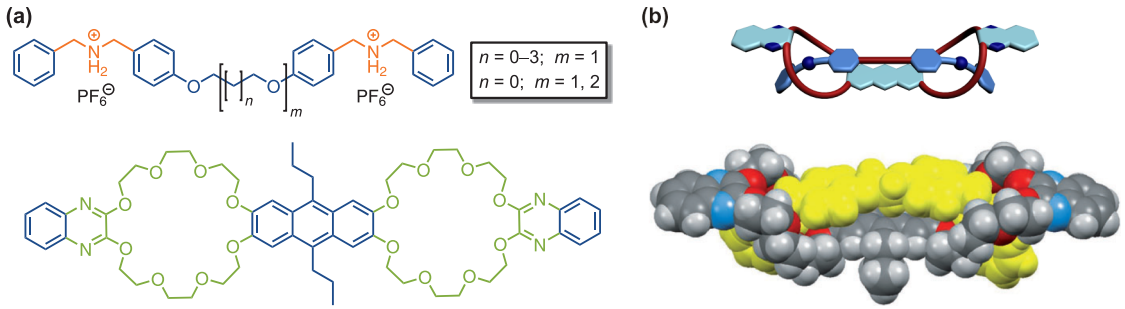

Figure 2.16. **(a)** Structures of guests with different spacer lengths and a divalent crown-ether host from Schalley and co-workers.[34] **(b)** Cartoon of the investigated pseudo[2]rotaxanes and crystal structure of the best binder ($n = 0$; $m = 1$).[34] Cartoon and crystal structure adapted with permission from Fasting et al.[4] (© 2012 Wiley-VCH Verlag GmbH & Co. KGaA, Weinheim).

2.3 Cooperative effects in multivalent systems

As already mentioned in Section 2.2, the "multivalency effect" can be deconvoluted into statistical[88–91] and cooprative effects.[5,6,87] Both of these will be addressed in this section separately. Cooperativity describes the effect that one binding event has on the subsequent events in a structure with more than one interaction site. This cooperative effect can be positive or negative, which translates into an enhanced or diminished following binding event. A system can also be non-cooperative in which case the binding sites do not affect each other. In a multivalent assembly, three types of cooperative effects can occur: allosteric cooperativity, chelate cooperativity and interannular cooperativity.[5,6,87] The latter is quite a special case and very seldomly observed. Allosteric cooperativity, though present in multivalent systems, does not require multivalency. It can already occur in the association of one multivalent component and many monovalent counterparts. Chelate cooperativity is of the greatest interest, if multivalent systems are investigated. It quantifies the likeliness of a partly-bound complex between a multivalent host and a multivalent guest to end up as a fully bound complex rather than as a partly bound complex or as oligomers. Ercolani and Schiaffino[5] as well as Hunter and Anderson[6] wrote comprehensive essays about the three different types of cooperativity and how they are quantified. The main aspects of these are summarised and partly complemented in the following three sections.

2.3.1 Allosteric cooperativity

The simplest example of a system, in which allosteric cooperativity can occur, is a complex of two monovalent hosts and a divalent guest (Figure 2.17). The association equilibria of this complex in Figure 2.17a[5,6] are expressed as products of their microscopic association constants K_1 and K_2 and their statistical factors $K_{\sigma_{a1}}$ and $K_{\sigma_{a2}}$, respectively. The statistical factors[88–91] correct for the previously mentioned symmetry effects in multiply bonded systems (for details, see Section 2.3.5). Thermodynamically speaking, allosteric cooperativity is present, if $K_1 \neq K_2$. If no cooperativity is present, the two microscopic association constants are equal and identical to the monovalent reference association constant K_{mono} (Figure 2.17b).

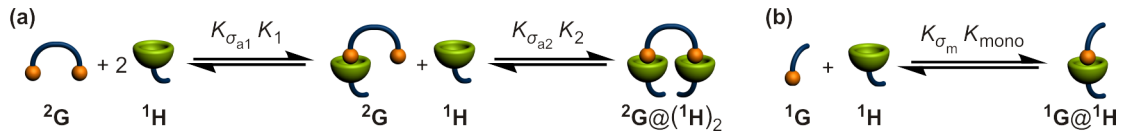

Figure 2.17. (a) Association equilibria of two monovalent hosts **^{1}H** and a divalent guest **^{2}G**.[5] **(b)** Monovalent reference complex **^{1}G@^{1}H** for evaluation of the monovalent association constant K_{mono}. All association constants are corrected by their statistical factors K_σ.

From these considerations, a—by definition—dimensionless cooperativity factor for allosteric cooperativity can be defined:[5]

$$\alpha = \frac{K_1 \cdot K_2}{(K_{\text{mono}})^2} \,. \tag{2.5}$$

K_{mono} can be separately determined from a monovalent reference compound (Figure 2.17b). Alternatively, it is often approximated that $K_1 \approx K_{\text{mono}}$.[5,6] This, however, implies that the two connected unoccupied binding sites of **^{2}G** do not affect each other. If this is inserted into Eq. 2.5, the cooperativity factor can also be written as:[6]

$$\alpha' = \frac{K_1 \cdot K_2}{(K_1)^2} = \frac{K_2}{K_1} \,. \tag{2.6}$$

The same rules apply for both dimensionless cooperativity factors: in the case of positive cooperativity, α is larger than 1; in the case of negative cooperativity, it is smaller than 1. If $\alpha = 1$, no cooperativity is present.

As already indicated before, the system depicted in Figure 2.17 is not multivalent. In multivalent systems, allosteric effects can be even more pronounced, because host and guest exhibit individual allosteric effects which add up in the multivalent assembly. Allosteric effects of host and guest can amplify in the multivalent system, if they are of the same sign or compensate each other, if their sign is reversed. Hence, allosteric cooperativity can strongly affect the multivalent interaction and has to be treated with care.

Allosteric cooperativity can cause remarkable effects in biological[86,98] and supramolecular[99–101] systems. The archetypal example of allosteric cooperativity is the binding of four oxygen molecules to hemoglobin.[86,98] Hemoglobin is a tetramer of four proteins each bearing one heme unit. The association of the first oxygen molecule to one of the four heme units induces conformational changes in the tertiary structure of the protein. These steric changes propagate through the protein's quaternary structure to the other binding sites and facilitate the association of

oxygen to the remaining hemes. This propagation of structural changes over large distances was termed allosteric cooperativity (or allostery). More recently, it was recognised that the communication between the remote binding sites does not have to be of steric nature, electronic communication or a change in dynamic properties are possible as well.[87,102–104]

Thordarson and co-workers[99,100] reported a tetratopic host, in which anion binding could be switched "on" allosterically by binding of two cations (Figure 2.18). They investigated the association of chloride anions and calcium cations to the host independently and sequentially. The allosteric cooperativity for two cloride ions binding to the host is strongly negative ($0.01 < \alpha < 0.05$). The association of two calcium cations is less negatively cooperative ($\alpha \approx 0.8$) but not favourable. Sequential addition of calcium and chloride ions to the host, however, leads to an remarkable enhancement of chloride binding ($\alpha \approx 1,500$). Without allosteric activation of the tetratopic host by binding of two cations, anion binding would not have been possible in this system.

That something as small as a proton can induce large allosteric changes in a complex structure, such as a doubly stranded helicate, was recently shown by Yashima and co-workers.[101] They investigated doubly stranded spiroborate helicate with 2,2'-bipyridine spacers and observed contraction of the helicate after addition of acid (Figure 2.19). The bypyridine units change their conformation from *anti* to *syn* to bind a proton in a stable bisdentate manner. This conformational change allosterically translates to the spiroborates and causes the whole helicate to contract. Sequestering of the protons by addition of base causes the bypyridine units to return to their *anti* conformation and thereby reverses the process. Remarkably, the handedness of the helicates is retained upon contraction and expansion.

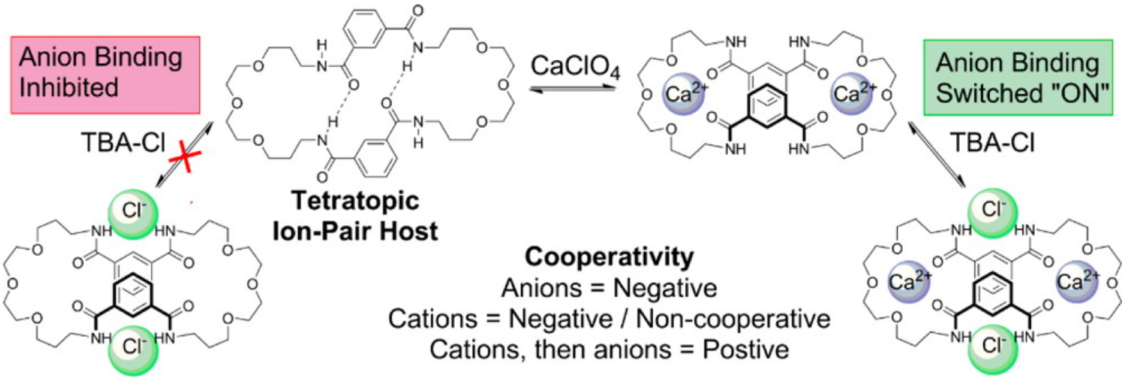

Figure 2.18. Thordarson and co-workers[99,100] allosterically switched "on" the anion binding on a tetratopic host by binding of two cations.
Reprinted with permission from Howe et al.[99] (© 2014 American Chemical Society).

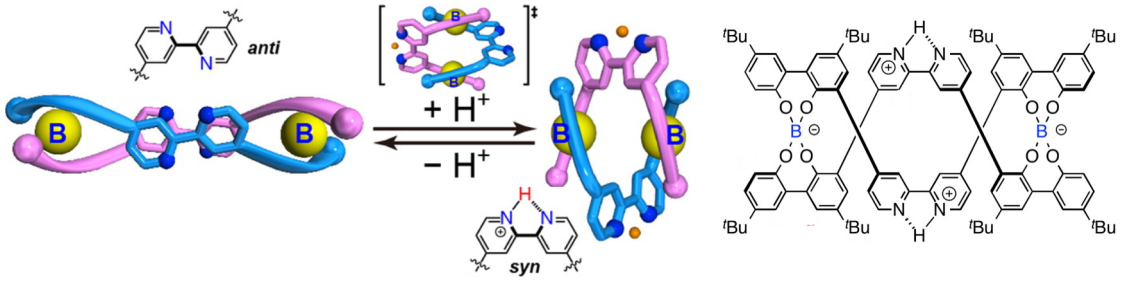

Figure 2.19. Cartoons and structure of a double stranded spiroborate helicate reported by Yashima and co-workers[101] which contracts/expands by addition/removal of protons. Adapted with permission from Suzuki et al.[101] (© 2016 American Chemical Society).

2.3.2 Chelate cooperativity

The cooperative effect that occurs exclusively in multivalent systems is the chelate cooperativity. Hence, the simplest example of a system, in which chelate cooperativity can occur, is a divalent complex ($^{\mathbf{2}}\mathbf{G}@^{\mathbf{2}}\mathbf{H}$). The association equilibria are depicted in Figure 2.20. The host $^{\mathbf{2}}\mathbf{H}$ is present in large excess (Eq. 2.7) so that structures involving more than one divalent guest $^{\mathbf{2}}\mathbf{G}$ can be neglected.

$$[^{\mathbf{2}}\mathbf{H}]_0 \gg [^{\mathbf{2}}\mathbf{G}]_0 \qquad \Rightarrow \qquad [^{\mathbf{2}}\mathbf{H}]_0 \approx [^{\mathbf{2}}\mathbf{H}] \approx c_{\text{total}} \tag{2.7}$$

Furthermore, there shall be no allosteric cooperativity present in the system ($\alpha = 1$). Thus, all microscopic intermolecular association constants are equal to K_{mono}.[5] If the dimensionless intramolecular association constants in the equilibrium (K_{intra} & $(K_{\text{inter}})^{-1}$) shall be expressed as multiples of K_{mono} as well, the bimolecular association constant K_{mono} (unit: M^{-1}) needs to be corrected by a factor with the unit of a concentration: the microscopic effective molarity EM (unit: M).[5,6]

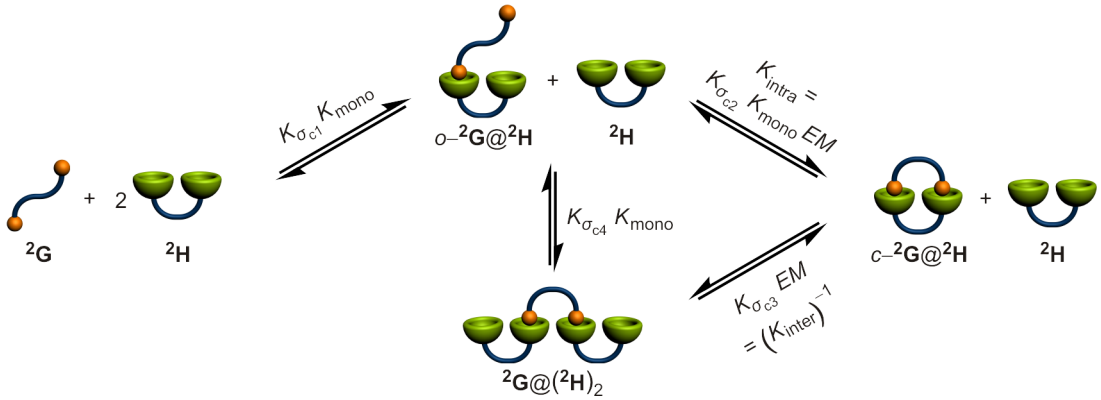

Figure 2.20. Association equilibria of a two divalent hosts $^{\mathbf{2}}\mathbf{H}$ and a divalent guest $^{\mathbf{2}}\mathbf{G}$ assuming $[^{\mathbf{2}}\mathbf{H}]_0 \gg [^{\mathbf{2}}\mathbf{G}]_0$ and $\alpha = 1$.[5] K_{mono} is defined as in Figure 2.17b. All association constants are corrected by their statistical factors K_{σ_c}.

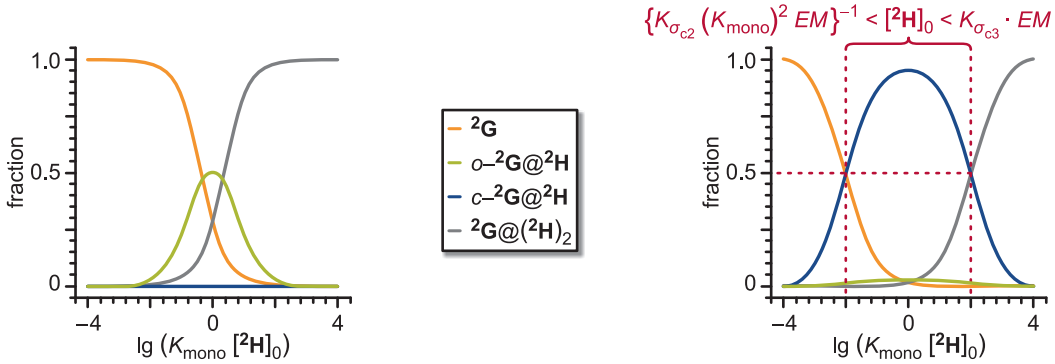

Figure 2.21. Speciation profiles[5,6] for the equilibria shown in Figure 2.20: in the absence of chelate interaction ($K_{\text{intra}} = 0$; left) and in the presence of chelate interaction ($K_{\text{intra}} = 25$; right). The concentration scale is normalized by multiplication with K_{mono}.

Under these conditions, the guest can only adapt four different states: unbound $^{\mathbf{2}}\mathbf{G}$, the singly-bound open 1:1 complex o–$^{\mathbf{2}}\mathbf{G}@^{\mathbf{2}}\mathbf{H}$, the doubly-bound closed 1:1 complex c–$^{\mathbf{2}}\mathbf{G}@^{\mathbf{2}}\mathbf{H}$ and the doubly-bound oligomeric 1:2 complex $^{\mathbf{2}}\mathbf{G}@(^{\mathbf{2}}\mathbf{H})_2$. Speciation profiles for the equilibria shown in Figure 2.20 are given in Figure 2.21: in the absence of any chelate cooperativity ($K_{\text{intra}} = 0$; left), and in the presence of chelate cooperativity ($K_{\text{intra}} = 25$; right). As expected, there is virtually no doubly-bound complex c–$^{\mathbf{2}}\mathbf{G}@^{\mathbf{2}}\mathbf{H}$ (blue line) formed in absence of chelate cooperativity. The open complex o–$^{\mathbf{2}}\mathbf{G}@^{\mathbf{2}}\mathbf{H}$ (green line) is only present as an intermediate until host concentration $[^{\mathbf{2}}\mathbf{H}]_0$ is high enough to allow for oligomer formation ($^{\mathbf{2}}\mathbf{G}@(^{\mathbf{2}}\mathbf{H})_2$, grey line). In contrast to that, the presence of chelate interaction suppresses the intermediate open complex o–$^{\mathbf{2}}\mathbf{G}@^{\mathbf{2}}\mathbf{H}$ and oligomerisation occurs at much higher host concentration $[^{\mathbf{2}}\mathbf{H}]_0$. Most importantly, there is a concentration-dependent "all-or-none" effect observed for the doubly-bound complex c–$^{\mathbf{2}}\mathbf{G}@^{\mathbf{2}}\mathbf{H}$: At medium host concentrations $[^{\mathbf{2}}\mathbf{H}]_0$, the doubly-bound complex c–$^{\mathbf{2}}\mathbf{G}@^{\mathbf{2}}\mathbf{H}$ suppresses all other species. At low or high host concentrations, the unbound guest $^{\mathbf{2}}\mathbf{G}$ (orange line) or oligomers $^{\mathbf{2}}\mathbf{G}@(^{\mathbf{2}}\mathbf{H})_2$ are favoured, respectively.[5,6]

The host concentrations ($[^{\mathbf{2}}\mathbf{H}]_{\text{on}}$ and $[^{\mathbf{2}}\mathbf{H}]_{\text{off}}$), at which the system switches from "none" to "all" (chelate interaction is switched "on") or vice versa, can be calculated from the equilibria in Figure 2.20. The chelate interaction switches "on", if the concentrations of guest $[^{\mathbf{2}}\mathbf{G}]$ and doubly-bound complex $[c$–$^{\mathbf{2}}\mathbf{G}@^{\mathbf{2}}\mathbf{H}]$ are equal (Eqs 2.8 & 2.9).[6]

$$\frac{[c - {}^{\mathbf{2}}\mathbf{G}@^{\mathbf{2}}\mathbf{H}]}{[^{\mathbf{2}}\mathbf{G}]} = K_{\sigma_{c1}} K_{\sigma_{c2}} (K_{\text{mono}})^2 \, EM \, [^{\mathbf{2}}\mathbf{H}]_{\text{on}} = 1 \tag{2.8}$$

$$\Rightarrow \quad [^{\mathbf{2}}\mathbf{H}]_{\text{on}} = \left\{ K_{\sigma_{c1}} K_{\sigma_{c2}} (K_{\text{mono}})^2 \, EM \right\}^{-1} \tag{2.9}$$

Similarly, the system switches back to "nothing", if the concentrations of doubly-bound complex [c–$^{\mathbf{2}}\mathbf{G}@^{\mathbf{2}}\mathbf{H}$] and 1:2 complex [$^{\mathbf{2}}\mathbf{G}@(^{\mathbf{2}}\mathbf{H})_2$] are equal (Eqs 2.10 & 2.11).

$$\frac{[^{\mathbf{2}}\mathbf{G}@^{\mathbf{2}}\mathbf{H}_2]}{[c - {}^{\mathbf{2}}\mathbf{G}@^{\mathbf{2}}\mathbf{H}]} = K_{\text{inter}}\,[^{\mathbf{2}}\mathbf{H}]_{\text{off}} = (K_{\sigma_{\text{c3}}} EM)^{-1}\,[^{\mathbf{2}}\mathbf{H}]_{\text{off}} = 1 \tag{2.10}$$

$$\Rightarrow \quad [^{\mathbf{2}}\mathbf{H}]_{\text{off}} = (K_{\text{inter}})^{-1} = K_{\sigma_{\text{c3}}} EM \tag{2.11}$$

Thus, the microscopic effective molarity (corrected by the statistical factor $K_{\sigma_{\text{c3}}}$) is the threshold concentration of $[^{\mathbf{2}}\mathbf{H}]_0$ at which the oligomers win over the cyclic complexes.[5] This concentration-dependent behaviour of the supramolecular cyclisation is in line with covalent cyclisation reactions. They only work at high dilution conditions as well (Ruggli-Ziegler[105,106] dilution principle).

There are two equally noteworthy approaches to quantify the chelate cooperativity effect of a system in terms of a chelate cooperativity factor. Other definitions, though present in literature,[2] were not used for the studies in this thesis and are therefore not mentioned here. Ercolani and Schiaffino[5] assumed that the critical point in a chelate cooperative system is reached, if the 1:2 complexes $^{\mathbf{2}}\mathbf{G}@(^{\mathbf{2}}\mathbf{H})_2$ win over the cyclic complexes c–$^{\mathbf{2}}\mathbf{G}@^{\mathbf{2}}\mathbf{H}$. This assumption is strongly related to covalent cyclisation reactions[105,106] and the observations from the speciation profiles (Figure 2.21) that chelate interactions are concentration-dependent. Hence, they defined the inverse intermolecular association constant $(K_{\text{inter}})^{-1}$ corrected by the host concentration $[^{\mathbf{2}}\mathbf{H}]_0$ as chelate cooperativity factor β (Eqs 2.12 & 2.13).

$$\beta = \frac{(K_{\text{inter}})^{-1}}{[^{\mathbf{2}}\mathbf{H}]_0} \tag{2.12}$$

$$\Rightarrow \quad \beta = K_{\sigma_{\text{c3}}}\,\frac{EM}{[^{\mathbf{2}}\mathbf{H}]_0} \tag{2.13}$$

Hunter and Anderson[6] on the other hand, considered the ring closing step as the critical point in a chelate cooperative system. That is the point when the doubly-bound complex c–$^{\mathbf{2}}\mathbf{G}@^{\mathbf{2}}\mathbf{H}$ wins over the open singly-bound o–$^{\mathbf{2}}\mathbf{G}@^{\mathbf{2}}\mathbf{H}$. The relation between the two species is given by the intramolecular association constant K_{intra}. Hunter and Anderson corrected K_{intra} by its statistical factor and defined that as their cooperativity factor β' (Eq. 2.14).

$$\beta' = \frac{K_{\text{intra}}}{K_{\sigma_{\text{c2}}}} = K_{\text{mono}}\,EM \tag{2.14}$$

As in the allosteric cooperativity factors, β and β' will be larger than one, if positive cooperativity is present. A value of β or β', which is below one, denotes negative cooperativity. The system is non-cooperative in the case of $\beta = 1$ ($\beta' = 1$).

Both cooperativity factors can also be applied to multivalent systems with n binding sites (Figure 2.11a), assuming that EM is equal for all intramolecular association steps (Eqs 2.15 & 2.16).[5,6]

$$\beta = \frac{2}{n^n} \left(\frac{EM}{[\boldsymbol{n}\mathbf{H}]_0} \right)^{n-1} \tag{2.15}$$

$$\beta' = (K_{\text{mono}})^n \, EM^n \tag{2.16}$$

in the case of β, the factor $2\,n^{-n}$ originates from the combined statistical factors of $n-1$ $(K_{\text{inter}})^{-1}$ in the n-valent system.

Remarkable examples for systems, in which chelate cooperativity effectively operates, have already been mentioned in Section 2.2. In most of these[24,31] and other[107,108] examples, chelate cooperativity is not quantified by β or β', but the effective molarity EM is given alone. EM accounts for the ease of the intramolecular ring closure in a chelate system. Anderson's[24] zinc-porhyrin wheels exhibit effective molarities of up to $EM_{\text{cyc}} = 10^3$ M for association of the hexameric guest Figure 2.14. Higher supramolecular effective molarities have not been reported so far. The linear porphyrin oligomers only express effective molarities around $EM_{\text{lin}} \approx 50$ mM. The effective molarities in Hunter's[31] zinc-porphyrin systems with intermolecular hydrogen bonds (Figure 2.15) are stronger in the complexes with rigid aromatic spacers ($380\,\text{mM} < EM_{\text{rigid}} < 500\,\text{mM}$) than in those with flexible ether linkers ($120\,\text{mM} < EM_{\text{flexible}} < 160\,\text{mM}$). Schalley and co-workers[34] reported effective molarities of up to $EM = 130$ mM in their divalent pseudorotaxanes (Figure 2.16).

Another intriguing example of chelate cooperativity "at work" are the H-bonded duplexes by Hunter and co-workers (Figure 2.22).[32,33] They investigated the association of complementary oligomers and found that hydrogen bond formation is cooperative along the chain despite the flexible backbone. Actually, varying the flexibility of the backbone does hardly affect the chelate cooperativity. The moderate effective molarities ($EM = 14$ mM) for the intramolecular interactions effectively zip up the oligomers into duplexes not unlike the assembly of a DNA double stand. Chelate cooperativity factors of $\beta' = 5$ indicate that each H-bond is 80 % populated in the duplex. The stability of the duplex increases by one order of magnitude for each H-bonding group added two the chain.

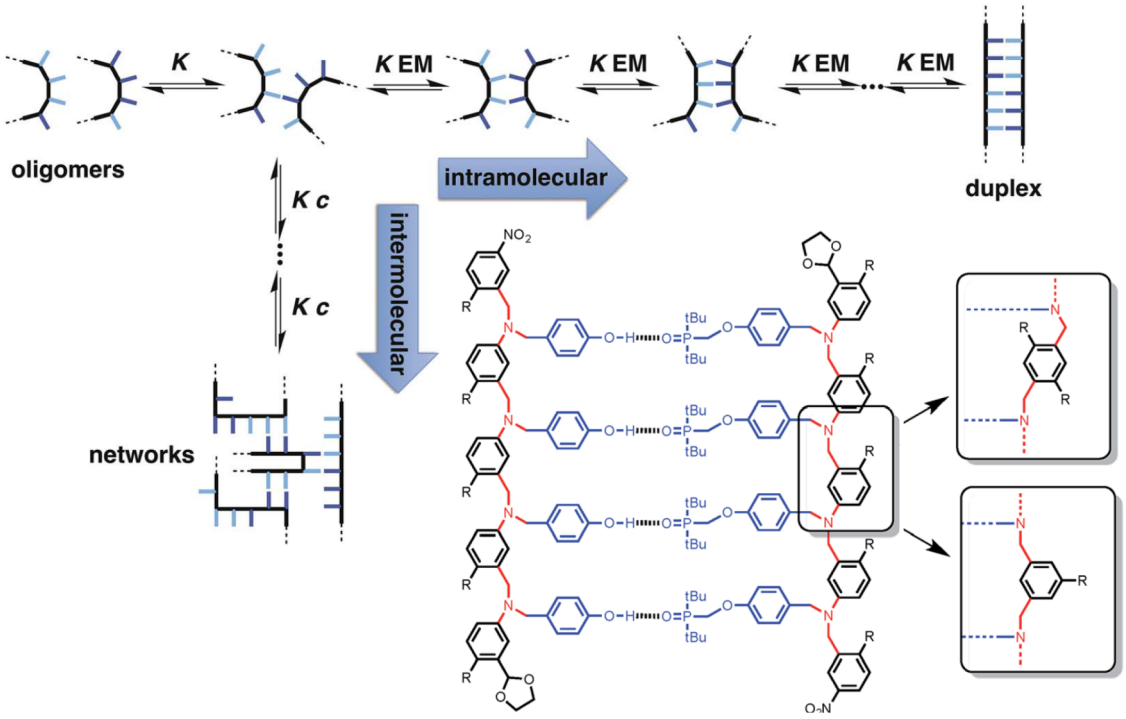

Figure 2.22. Top left: Recognition-directed duplex formation between two complementary oligomers competes with uncontrolled assembly of networks. K is the monovalent association constant. c is the operating concentration. Bottom right: Chemical structure of a antiparallel tetrameric duplex. Three different backbone modules are shown (R = 2-ethylhexoxy).[32,33] Adapted with permissions from Stross et al.[32,33] (© 2016 The Royal Society of Chemistry).

2.3.3 Interannular cooperativity

Interannular cooperativity arises from the interplay of two or more chelating interactions on one multivalent component. The interactions affect each other in an allosteric fashion. A simple example for such a system is the association of two divalent hosts $^{2}\mathbf{H}$ and a tetravalent guest $^{4}\mathbf{G}$ in which one pair of binding sites can freely rotate with respect to the other (Figure 2.23a). $^{2}\mathbf{H}$ is present in medium excess so that assemblies with more than one guest $^{4}\mathbf{G}$ as well as oligomers can be neglected. Furthermore, allosteric cooperativity is excluded ($\alpha = 1$).[5] The association equilibria for formation of $^{4}\mathbf{G}@(^{2}\mathbf{H})_2$ under these conditions are depicted in Figure 2.23a. The association of the first $^{2}\mathbf{H}$ to $^{4}\mathbf{G}$ freezes its internal rotor and, hence, facilitates association of the second $^{2}\mathbf{H}$. Thus, the system is cooperative ($EM_2 > EM_1$). Since the association of the first $^{2}\mathbf{H}$ does not affect the binding sites of the guest, Ercolani and Schiaffino[5] clearly distinguish this interannular cooperativity from allosteric cooperativity.

The cooperative effects in these interannular systems can be quantified by comparing the two microscopic effective molarities of the interannular system EM_1 and EM_2 with the effective molarity EM of a divalent reference system $^{2}\mathbf{G}@^{2}\mathbf{H}$ (Figure 2.23b). The cooperativity factor γ is defined in Eq. 2.17.[5]

$$\gamma = \frac{EM_1\, EM_2}{EM^2} \tag{2.17}$$

In conformity with the other factors, γ will be larger than one, if positive cooperativity is present. $\gamma < 1$ denotes negative cooperativity. The system is non-cooperative in the case of $\gamma = 1$. Although there were systems reported in literature[109–111] (Scheme 2.4) in which interannular cooperativity could operate, the effect has not been experimentally investigated so far.[5]

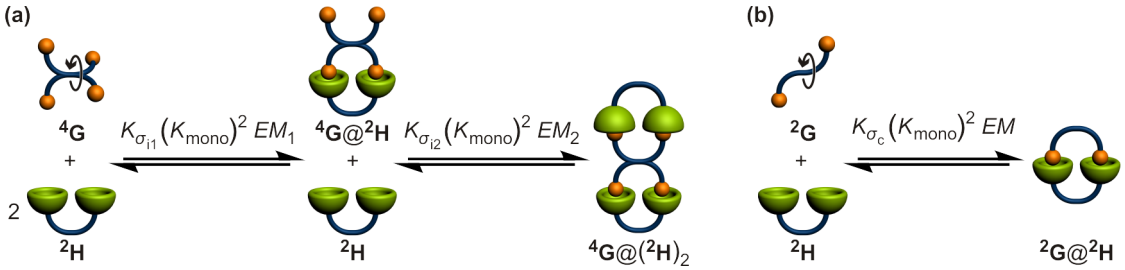

Figure 2.23. **(a)** Association equilibria of two divalent hosts $^{2}\mathbf{H}$ and a tetravalent guest $^{4}\mathbf{G}$ with free internal rotation, assuming $[^{2}\mathbf{H}]_0 \gg [^{4}\mathbf{G}]_0$ and $\alpha = 1$.[5] **(b)** Association equilibria of the divalent host $^{2}\mathbf{H}$ to a divalent model guest $^{2}\mathbf{G}$ for evaluation of the reference EM.[5] This model system is identical to the one in Figure 2.20. K_{mono} is defined as in Figure 2.17b. All association constants are corrected by their statistical factors K_σ.

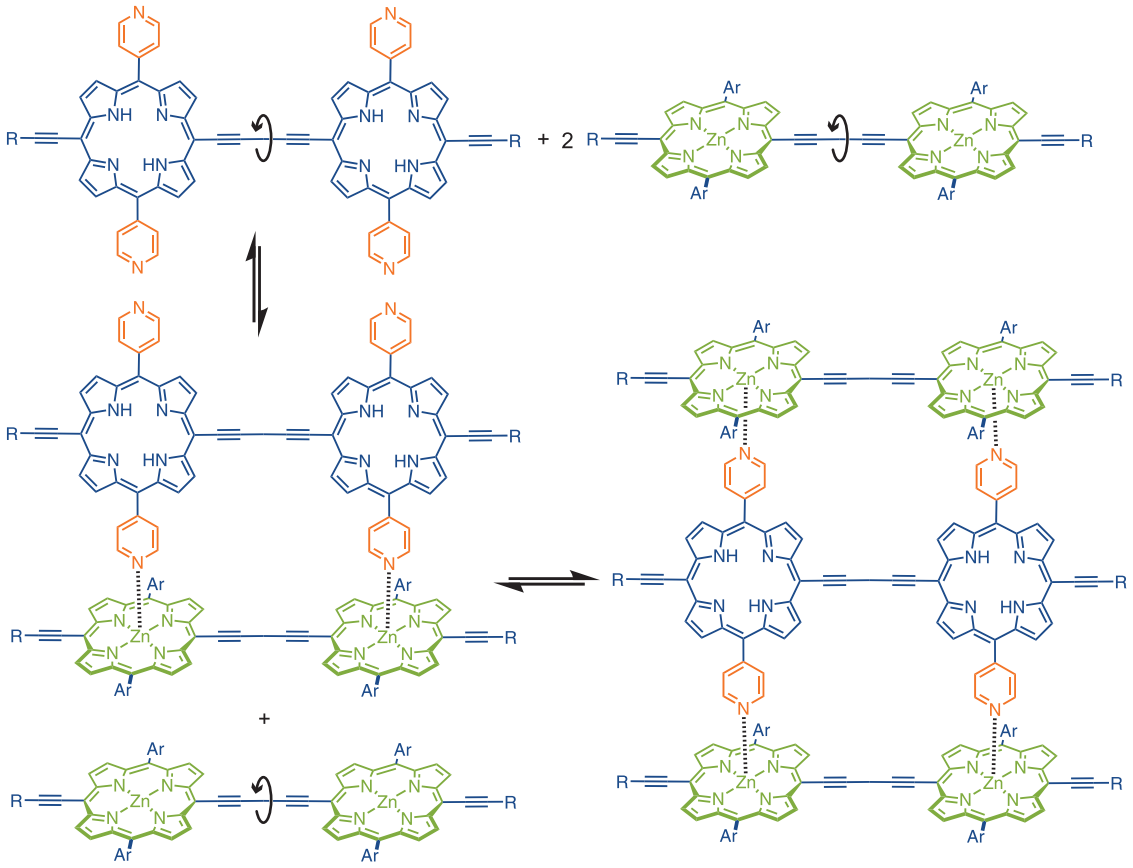

Scheme 2.4. Example of a system of a tetrapyridylporphyrin dimer (≡ **^{4}G**) and two metalloporphyrin dimers (≡ **^{2}H**) by Wilson and Anderson[109] in which interannular cooperativity could operate.

2.3.4 The *double mutant cycle* analysis

The key variable for quantifying the cooperative effects in chelate and interannular systems is the effective molarity *EM*. From the theoretical considerations in the previous two sections, one might conclude that *EM* can be easily measured by comparing the association constant of the cooperative system with that of a monovalent system and correcting that value for the statistical factors (in accordance with the approach for the allosteric cooperativity factor α (Eq. 2.5)). However, it is not as simple as that. Allosteric cooperativity was neglected in all equilibria in Sections 2.3.2 and 2.3.3 for the ease of the theoretical description. When real systems are analysed, this assumption is not valid any more. They are most certainly affected by allosteric effects in host and guest. Hence, the allosteric cooperativities of host and guest have to be determined prior to analysis of *EM* and the association constant of the multivalent system has to be corrected for these allosteric effects. In other words, one needs to dissect out *EM* from the

overall binding constant of the multivalent complex. The most common technique to tackle that task is the double mutant cycle (DMC) analysis. First introduced by Fersht and co-workers,[112] the DMC analysis was later well established for the quantification of *EM* in supramolecular systems by Hunter and co-workers,[31,107,108] Diederich and co-workers,[113] and Schalley and co-workers.[34,114,115]

The double mutant cycle of a divalent system is given in Figure 2.24 (left). It consists of the divalent complex $\mathbf{^2G@^2H}$ (**a**), two monovalent complexes $\mathbf{^1G@^1H}$ (2 **d**), and two mutations $\mathbf{^2G@(^1H)_2}$ and $\mathbf{(^1G)_2@^2H}$ (**b** & **c**, respectively). The latter two are needed to account for the allosteric effects of host and guest. The name double mutant cycle originates from the fact, that **a** and 2 **d** can be transformed into each other by two consecutive mutations 1 and 2. This can either be done via the mutants **b** or **c**. Mutation 1 (**a** ⇳ **b** or **c** ⇳ 2 **d**) corresponds to cutting the host spacer, mutation 2 (**a** ⇳ **c** or **b** ⇳ 2 **d**) corresponds to cutting the guest spacer. Comparison of **b** and 2 **d** quantifies the allosteric cooperativity of the guest (Eq. 2.18, compare Eq. 2.5), comparison of **c** and 2 **d** quantifies the allosteric cooperativity of the host (Eq. 2.19), respectively.

$$\alpha_{\mathbf{^2G}} = \frac{K^{\mathrm{b}}}{(K^{\mathrm{d}})^2} = \frac{K_1^{\mathrm{b}} \cdot K_2^{\mathrm{b}}}{(K^{\mathrm{d}})^2} \tag{2.18}$$

$$\alpha_{\mathbf{^2H}} = \frac{K^{\mathrm{c}}}{(K^{\mathrm{d}})^2} = \frac{K_1^{\mathrm{c}} \cdot K_2^{\mathrm{c}}}{(K^{\mathrm{d}})^2} \tag{2.19}$$

Relating all four mutants **a** – 2 **d** to each other, hence, eliminates all allosteric effects and only the chelate cooperativity (*EM*) remains (Eq. 2.20).

$$K = \frac{K^{\mathrm{a}} \cdot (K^{\mathrm{d}})^2}{K^{\mathrm{b}} \cdot K^{\mathrm{c}}} \sim EM \tag{2.20}$$

$$= \frac{K^{\mathrm{a}}}{\alpha_{\mathbf{^2G}} \cdot \alpha_{\mathbf{^2H}} \cdot (K^{\mathrm{d}})^2} \sim EM \tag{2.21}$$

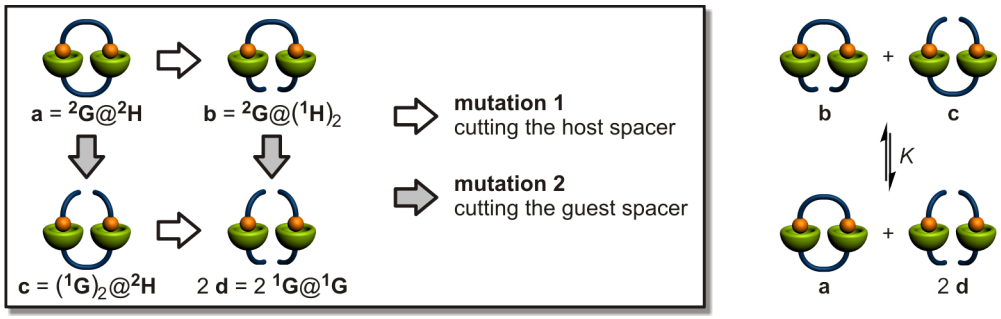

Figure 2.24. **(a)** Double mutant cycle for quantifying the effective molarity *EM* in the divalent complex $\mathbf{^2G@^2H}$. **(b)** Equilibrium between the mutants **b** and **c** and **a** and 2 **d**.

Equation 2.21 shows that the DMC approach is in compliance with the approach for the allosteric cooperativity factor α (Eq. 2.5): The association constant of the divalent system K^{a} is compared with the monovalent reference system K^{d}. As allosteric effects can occur in the divalent system, this relation is corrected for the allosteric effects of divalent guest $\alpha_{\mathbf{G}}^{\mathbf{2}}$ and divalent host $\alpha_{\mathbf{H}}^{\mathbf{2}}$.

The relation of all four mutants (Eq. 2.20) is chemically speaking the equilibrium

$$\mathbf{b} + \mathbf{c} \rightleftharpoons \mathbf{a} + 2\,\mathbf{d}\,.$$

In the case of positive chelate cooperativity, **a** and 2 **d** are primarily formed (Figure 2.24, right). If negative chelate cooperativity is present in the system, **b** and **c** are favoured. In the case of no chelate cooperativity, a statistical distribution of all four mutants exists. K can be experimentally determined by measuring the association constants of the four mutants K^{a} – K^{d}.

From their stepwise binding mechanisms (compare figures 2.17 & 2.20) the association constants of the four mutants **a** – 2 **d** (K^{a} – K^{d}) can also be written as multiples of K_{mono} ($\alpha = 1$ is assumed).

$$K^{\mathrm{a}} = K_{\sigma_{\mathrm{c}1}}\,K_{\sigma_{\mathrm{c}2}} \cdot (K_{\mathrm{mono}})^2 \cdot EM \tag{2.22}$$

$$K^{\mathrm{b}} = K_1^{\mathrm{b}} \cdot K_2^{\mathrm{b}} = K_{\sigma_{\mathrm{a}1}}\,K_{\sigma_{\mathrm{a}2}} \cdot (K_{\mathrm{mono}})^2 \tag{2.23}$$

$$K^{\mathrm{c}} = K_1^{\mathrm{c}} \cdot K_2^{\mathrm{c}} = K_{\sigma_{\mathrm{a}3}}\,K_{\sigma_{\mathrm{a}4}} \cdot (K_{\mathrm{mono}})^2 \tag{2.24}$$

$$(K^{\mathrm{d}})^2 = (K_{\sigma_{\mathrm{m}}}\,K_{\mathrm{mono}})^2 \tag{2.25}$$

If these are inserted into K (Eq. 2.20), EM can be calculated from the four measured association constants K^{a} – K^{d} (Eq. 2.28).

$$K = \frac{K^{\mathrm{a}} \cdot (K^{\mathrm{d}})^2}{K^{\mathrm{b}} \cdot K^{\mathrm{c}}} = \frac{K_{\sigma_{\mathrm{c}1}}\,K_{\sigma_{\mathrm{c}2}}\,(K_{\mathrm{mono}})^2\,EM \cdot (K_{\sigma_{\mathrm{m}}}\,K_{\mathrm{mono}})^2}{K_{\sigma_{\mathrm{a}1}}\,K_{\sigma_{\mathrm{a}2}}\,(K_{\mathrm{mono}})^2 \cdot K_{\sigma_{\mathrm{a}3}}\,K_{\sigma_{\mathrm{a}4}}\,(K_{\mathrm{mono}})^2} \tag{2.26}$$

$$= \frac{K_{\sigma_{\mathrm{c}1}}\,K_{\sigma_{\mathrm{c}2}} \cdot (K_{\sigma_{\mathrm{m}}})^2}{K_{\sigma_{\mathrm{a}1}}\,K_{\sigma_{\mathrm{a}2}} \cdot K_{\sigma_{\mathrm{a}3}}\,K_{\sigma_{\mathrm{a}4}}} \cdot EM \tag{2.27}$$

$$\Rightarrow\ EM = \frac{K_{\sigma_{\mathrm{a}1}}\,K_{\sigma_{\mathrm{a}2}} \cdot K_{\sigma_{\mathrm{a}3}}\,K_{\sigma_{\mathrm{a}4}}}{K_{\sigma_{\mathrm{c}1}}\,K_{\sigma_{\mathrm{c}2}} \cdot (K_{\sigma_{\mathrm{m}}})^2} \cdot \frac{K^{\mathrm{a}} \cdot (K^{\mathrm{d}})^2}{K^{\mathrm{b}} \cdot K^{\mathrm{c}}} \tag{2.28}$$

From Eq. 2.28 it becomes obvious, that the statistical factors, which were not very much considered so far, strongly affect the relationship between K and EM. Section 2.3.5 tackles the task to determine the statistical factors for all systems discussed so far (Sections 2.3.1–2.3.4).

Additionally, the DMC can be used to calculate the free energy contribution $\Delta\Delta G^0$ of the ring closing step in the divalent complex to its overall free energy ΔG^0_a (Eq. 2.29).

$$\Delta\Delta G^0 = \Delta G^0_a - \Delta G^0_b - \Delta G^0_c + 2\,\Delta G^0_d \tag{2.29}$$

The value of $\Delta\Delta G^0$ is not corrected for the statistical factors of the association equilibria. Corresponding to that, this analysis can also be performed for the enthalpic and entropic contributions of the ring closing step, $\Delta\Delta H^0$ and $\Delta(T\,\Delta S^0)$, respectively (Eqs 2.30 & 2.31).

$$\Delta\Delta H^0 = \Delta H^0_a - \Delta H^0_b - \Delta H^0_c + 2\,\Delta H^0_d \tag{2.30}$$

$$\Delta(T\,\Delta S^0) = T\,\Delta S^0_a - T\,\Delta S^0_b - T\,\Delta S^0_c + 2\,(T\,\Delta S^0_d) \tag{2.31}$$

There are various titration techniques which would allow for measuring the association constants of the four mutants of the DMC. In this thesis, isothermal titration calorimetry is the method of choice, as it delivers the association constant K, the Gibbs free energy ΔG, the enthalpy ΔH and the entropy ΔS in a single experiment. Hence, four simple ITC experiments can exploit the full potential of the DMC. Further details about the calorimeter and data evaluation of titration curves are given in Section 2.4.

2.3.5 Statistical factors

As indicated above, the statistical factors K_σ need to be determined for evaluating the cooperative effects in a system (Sections 2.3.1–2.3.4; Figures 2.17–2.24). Ercolani and co-workers[88] summarised different methods to determine K_σ and outlined two major ones: the direct count method[88,90] and Benson's symmetry number method.[89] Both methods are used to determine the K_σ in the various systems exhibiting cooperative effects to demonstrate that both approaches are equally valid. For small systems, the direct count method is probably the simpler one.[88,90]

2.3.5.1 Direct count method

The direct count method determines the K_σ values by dividing the number of possible product arrangements (so-called microspecies; n_{products}) by the number of reactant arrangements ($n_{\text{reactants}}$; Eq. 2.32). The results are displayed in Figure 2.25.

$$K_\sigma = \frac{n_{\text{products}}}{n_{\text{reactants}}} \tag{2.32}$$

For determining the number of microspecies, for example for a divalent guest binding to two monovalent hosts or vice versa, the binding sites of the divalent component—although chemically identical—have to be considered as distinguishable, e.g. left and right (Figure 2.25b & c). The monovalent component can bind to either the left or the right binding site of the divalent component. Thereby, two microspecies are created as products. In the next step, the second monovalent component can bind to the free binding site of the 1:1 complex. However, no matter to which of the two 1:1 microspecies the monovalent component binds, the 1:2 product microspecies will be the same. The reactants represent one microspecies, as there is only one "chemically plausible"[88] way to arrange them. In a two step association mechanism, the reactant, which is still unbound, is not considered in the number of micropecies any more.

In the case of a divalent guest binding to a divalent host, the binding sites of both components have to be considered distinguishable (e.g. orange, red (guest) and left, right (host); Figure 2.25a). Accordingly, the guest in the interannular system has four distinguishable binding sites (yellow, orange, red and violet) and the host two (green and dark green, Figure 2.25e). It becomes obvious, that with increasing complexity of the systems, the direct count method is likely to produce errors. Benson's symmetry number method,[89] however, is often more reliable even for complex systems[88] such as Anderson's[24] porphyrin wheels.

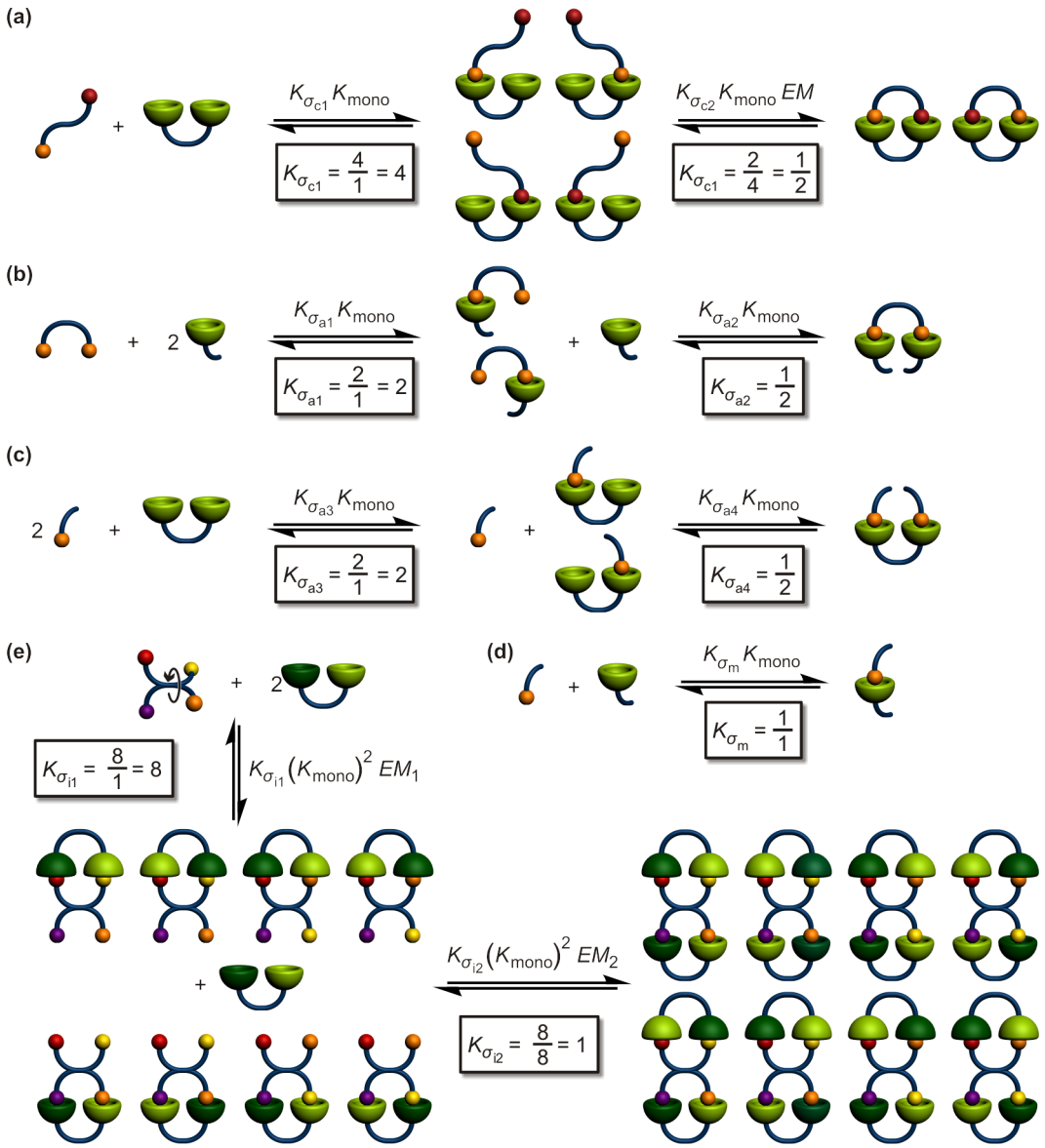

Figure 2.25. Schematic representation of the binding equilibria of the complexes of the double mutant cycle (Figure 2.24) and the interannular system (Figure 2.23). For all binding processes the possible microspecies are displayed for determining the corresponding K_σ with the direct count method. Results match the values[5,6] from literature.

2.3.5.2 Benson's symmetry number method

In Benson's[89] approach, the statistical factors K_σ are calculated from the product of all reactant symmetry numbers $\sigma^i_{\text{reactants}}$ divided by the product of all product symmetry numbers $\sigma^i_{\text{products}}$ (Eq. 2.33).[88,89]

$$K_\sigma = \frac{\prod_i \sigma^i_{\text{reactants}}}{\prod_i \sigma^i_{\text{products}}} \tag{2.33}$$

$$\sigma^i = \sigma^i_{\text{ext}} \cdot \sigma^i_{\text{int}} \tag{2.34}$$

The symmetry numbers σ^i are a product of external and internal symmetry numbers (Eq. 2.34). The external symmetry numbers σ^i_{ext} are derived from the point groups of the unbound, partly bound and fully bound states of the stepwise association processes (Figure 2.26).[88,89] Some examples of point groups and their corresponding symmetry numbers are given in Table 2.2. The internal symmetry numbers σ^i_{int} arise from internal rotations around single bonds; in other words different possible conformers. These conformational changes however, are fast compared to the time scale of the association processes. Therefore, they can be systematically neglected.[88] Neglecting the σ^i_{int} has the advantage of reducing possible errors. The sheer number of possible conformers in supramolecular systems could give rise to numerous errors in σ^i_{int}, if only one conformer is not taken into account.

The tetravalent guest of the interannular system (Figure 2.26e), however, represents a special case. In this case, the possibility to freely rotate one pair of binding sites with respect to the other increases the number of possible host–guest interactions (compare Figure 2.25e). Hence, this internal rotational flexibility of the guest needs to expressed by an internal symmetry number σ_{int}. The possible 180° rotation translates into an internal C_2 axis, thus, $\sigma_{\text{int}} = 2$.

All results of the symmetry number method are depicted in Figure 2.26.

Table 2.2. External symmetry numbers σ_{ext} for various point groups.[88]

point group	σ_{ext}
C_1, C_i, C_s, $C_{\infty v}$	1
$D_{\infty h}$	2
C_n, C_{nv}, C_{nh}	n
D_n, D_{nv}, D_{nh}	$2n$
S_n (n even)	$\frac{n}{2}$

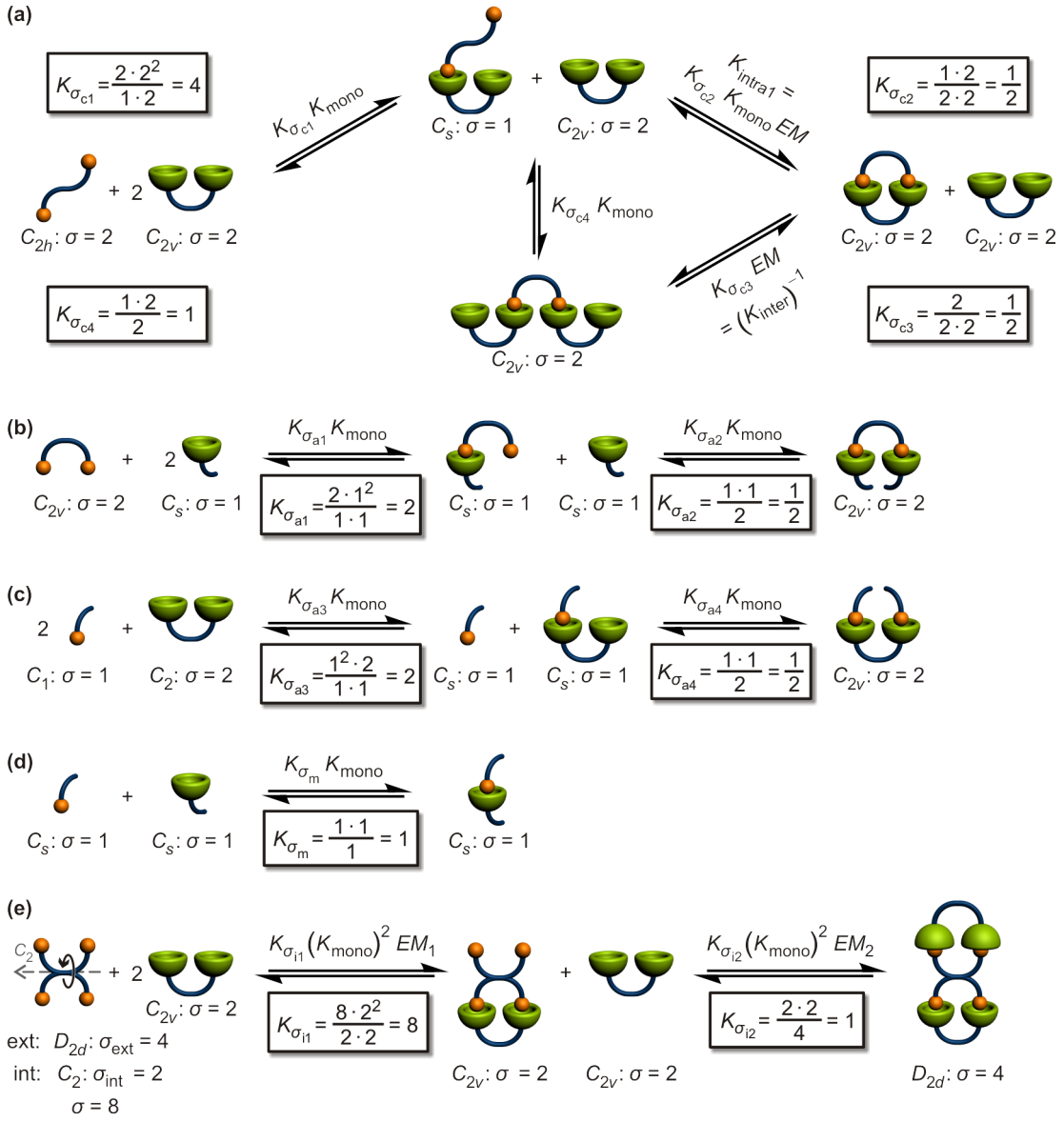

Figure 2.26. Schematic representation of the binding equilibria of the complexes of the double mutant cycle (Figure 2.24) and the interannular system (Figure 2.23). For all states, the point groups and symmetry numbers are displayed and the corresponding K_σ determined by Benson's symmetry number method. Results match the values[5,6] from literature.

The calculated statistical factors K_σ from Figures 2.25 and 2.26 can now be inserted into Equation 2.28 to complete the DMC analysis of the divalent complex $^{\mathbf{2}}\mathbf{G}@^{\mathbf{2}}\mathbf{H}$ (Eq. 2.36).

$$EM = \frac{K_{\sigma_{a1}} K_{\sigma_{a2}} \cdot K_{\sigma_{a3}} K_{\sigma_{a4}}}{K_{\sigma_{c1}} K_{\sigma_{c2}} \cdot (K_{\sigma_m})^2} \cdot \frac{K^a \cdot (K^d)^2}{K^b \cdot K^c} = \frac{2 \cdot \frac{1}{2} \cdot 2 \cdot \frac{1}{2}}{4 \cdot \frac{1}{2} \cdot (1)^2} \cdot \frac{K^a \cdot (K^d)^2}{K^b \cdot K^c} \tag{2.35}$$

$$= \frac{1}{2} \cdot \frac{K^a \cdot (K^d)^2}{K^b \cdot K^c} = \frac{1}{2} K \tag{2.36}$$

2.4 Isothermal titration calorimetry

The association constants of the individual complexes used to quantify cooperative effects in the systems need to be determined for that analysis. The method of choice in this thesis is isothermal titration calorimetry (ITC). The power of ITC lies in the fact that one single ITC measurement delivers the association stoichiometry n, the association constant K, the Gibbs free energy ΔG, the enthalpy ΔH and the entropy ΔS of the analysed system.[116,117] Association constants of up to $K = 10^9\ \mathrm{M}^{-1}$ can be measured.[118] Furthermore, it can be applied to a broad field of physicochemical association processes, because most of them cause a heat change. ITC, as a calorimetric technique, is able to measure this heat change occurring during an association reaction directly and non-invasively. However, the drawback of ITC lies exactly there as well. ITC provides no information about the underlying processes causing the measured heat changes at the molecular level. Hence, ITC needs to be combined with techniques giving structural information about the of the investigated systems (NMR, MS, etc. or DFT, MD).[119] Due to these versatile advantages, ITC has become a routine method for determining thermodynamic data in many biomolecular[119,120] and supramolecular[34,83,114,116] systems.

An ITC consists of a twin-calorimeter set-up of a a sample cell and a reference cell (Figure 2.27). A thermal event in the sample cell—that is a change in the sample temperature T_s—is always detected in dependence on the signal from the reference

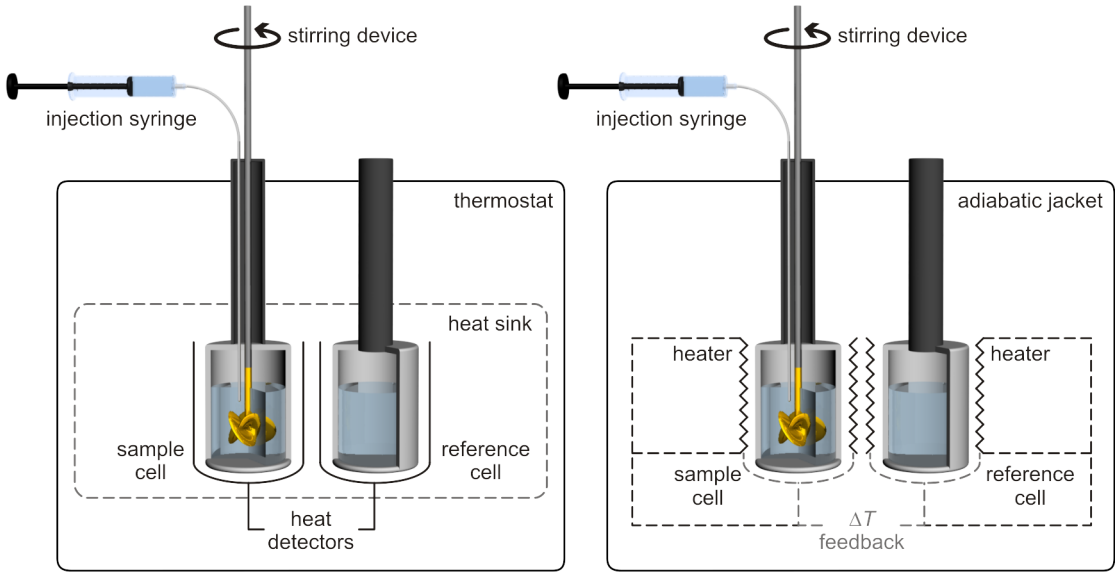

Figure 2.27. ITC instrument design. Schematic representations of a heat conduction calorimeter (left) and a differential power compensation calorimeter (right).[119]

cell (T_r). This is expressed in the heat-balance equation of a twin calorimeter (Eq. 2.37).[121]

$$\frac{\mathrm{d}\,Q_\mathrm{s}}{\mathrm{d}\,t} = k \cdot (T_\mathrm{s} - T_\mathrm{r}) + C \cdot \frac{\mathrm{d}\,T_\mathrm{s}}{\mathrm{d}\,t} = \Phi + C \cdot \frac{\mathrm{d}\,T_\mathrm{s}}{\mathrm{d}\,t} \tag{2.37}$$

The rate of heat production of the sample $\mathrm{d}\,Q_\mathrm{s}/\mathrm{d}\,t$ equals the sum of the heat exchange with the surrounding Φ and the product of the heat capacity of the sample C and the change of the sample temperature over time $\mathrm{d}\,T_\mathrm{s}/\mathrm{d}\,t$. The heat exchange with the surrounding Φ is the product of the heat transfer coefficient k and the temperature difference of sample and reference cell ($T_\mathrm{s} - T_\mathrm{r}$).[121] As the name suggests, an ITC calorimeter set-up is operated under isothermal conditions. From this follows that[121]

$$C \cdot \frac{\mathrm{d}\,T_\mathrm{s}}{\mathrm{d}\,t} = 0\,. \tag{2.38}$$

This simplifies the heat balance equation to[121]

$$\frac{\mathrm{d}\,Q_\mathrm{s}}{\mathrm{d}\,t} = \Phi\,. \tag{2.39}$$

Two types of isothermal titration calorimeters are available on the market: the heat conduction calorimeter and the differential power compensation calorimeter (Figure 2.27, left and right, respectively).[119]
The latter does not operate at isothermal conditions, technically speaking, but applies a constant thermal gradient to sample and reference cell by heaters. Any heat event in the sample cell is measured as a differential temperature signal between sample and reference cell. This temperature difference between the two cells is detected by the calorimeter and the cell feedback adjusts the power supply on sample and reference heaters to compensate the temperature difference. An exothermic event in the sample cell causes a negative feedback, because less power is applied to the sample cell than to the reference cell. An endothermic event in sample cell produces a positive feedback, accordingly. The cells are constantly kept at the same temperature and, hence, the differential power compensation calorimeter operates at "pseudo"-isothermal conditions. The advantage of this calorimeter type is its fast response to thermal events.[119,121]

In the heat conduction calorimeter (Figure 2.27, left), every thermal event in the sample cell is exchanged with the surrounding heat sink, thereby generating real isothermic conditions. The heat evolved or absorbed by the sample cell upon a

thermochemical event is directly measured as the heat flow from or into the sample cell by heat detectors (thermoelectric modules). That signal is always corrected for the heat flow measured at the reference cell. Hence, an exothermic event causes a positive signal in this type of calorimeter, because the heat flow from the sample to the surrounding heat sink is positive. An endothermic event causes a negative signal, accordingly.[119,121] The instrument used in the research for this thesis is a heat conduction calorimeter.

In a typical ITC experiment, the sample cell contains a solution of one of the interacting components (usually the host). The reference cell contains blank solvent. A more concentrated solution of the second interaction partner (the guest) is titrated into the sample cell. After each addition of guest solution, the following host–guest-complex formation generates a thermal event. This creates a deflection of the heat flow signal from the baseline. An appropriate time delay between the titration steps is chosen to allow for re-equilibration of the heat flow (Figure 2.28a). The heat evolved or absorbed by the reaction is calculated by integration of the deflections of heat flow from the baseline. Plotting all of these heat values against the molar ratio of host and guest in the cell results in the binding isotherm (Figure 2.28b).[119]

In the case of a bimolecular association process of a host **H** and a guest **G** to a host–guest complex **G@H** ($n = 1$)

$$\mathbf{G} + \mathbf{H} \rightleftharpoons \mathbf{G@H},$$

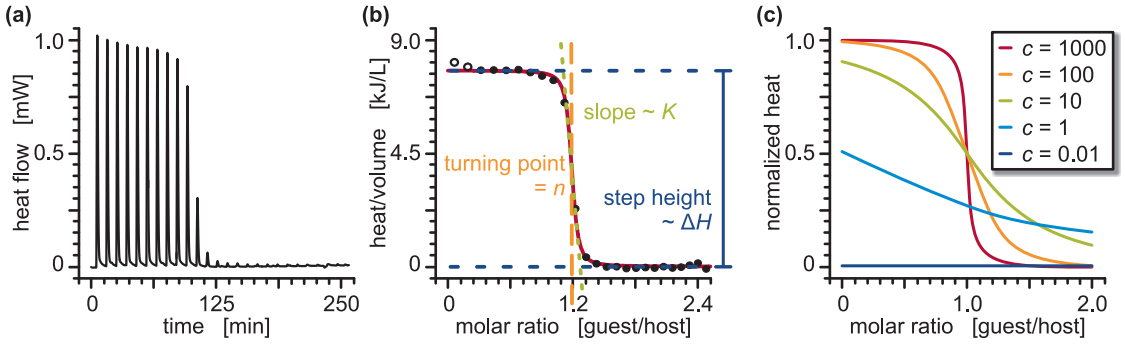

Figure 2.28. **(a)** Typical titration curve of an exothermic association measured at a heat conduction calorimeter. **(b)** Binding isotherm for the reaction in (a) created by plotting the integrated peaks against the molar ratio in the sample cell. Orange, green, and blue marks indicate how the thermodynamic parameters n, K, ΔH are obtained from the isotherm. **(c)** Typical representations of Wiseman[122,123] isotherms ($c = K_a \cdot [\mathbf{H}]_t$; $n = 1$).

the isotherm—that is the heat change of the sample over the time dependent guest concentration $\mathrm{d}\,Q_\mathrm{s}/\mathrm{d}\,[\mathbf{G}]_t$—can be described by the following equation (the so-called Wiseman isotherm):[122,123]

$$\frac{\mathrm{d}\,Q_\mathrm{s}}{\mathrm{d}\,[\mathbf{G}]_t} = \frac{\Delta H^0 \cdot V_0}{2} \cdot \left(1 + \frac{1 - \frac{[\mathbf{G}]_t}{[\mathbf{H}]_t} - (K_\mathrm{a}\,[\mathbf{H}]_t)^{-1}}{\sqrt{\left(1 + \frac{[\mathbf{G}]_t}{[\mathbf{H}]_t} + (K_\mathrm{a}\,[\mathbf{H}]_t)^{-1}\right)^{-1} - 4\,\frac{[\mathbf{G}]_t}{[\mathbf{H}]_t}}} \right) \tag{2.40}$$

V_0 is the effective volume of the calorimeter cell. ΔH^0 is the reaction enthalpy and K_a the association constant. $[\mathbf{H}]_t$ is the host concentration in the cell at a certain time t of the experiment. Non-linear curve fitting of the isotherm according to Equation 2.40 results in the thermodynamic parameters n, K_a and ΔH (Figure 2.28b): n corresponding to the x-value of the inflection point of the isotherm (orange), K to the slope of the isotherm at the inflection point (green) and ΔH corresponds to the step height of the isotherm (blue).[122,123] The other thermodynamic parameters of the association process can be derived by

$$\Delta G^0 = -R\,T \cdot \ln K_\mathrm{a} \tag{2.41}$$

$$= \Delta H^0 - T \cdot \Delta S^0\,. \tag{2.42}$$

How reliable these values are, is strongly dependent on the shape of the isotherm. The factor on which the curve shape depends on is

$$c = n \cdot K_\mathrm{a} \cdot [\mathbf{H}]_t\,. \tag{2.43}$$

As this was first reported by Wiseman, this factor is called Wiseman's "c" parameter (Eq. 2.43).[122,123] Isotherms for different c-values are depicted in Figure 2.28c. Step-like curve shapes ($c \geq 1000$) give very accurate results for ΔH, but the error in K is large. The other extreme, simply concave isotherms ($1 \leq c \leq 10$) still give reliable results for K (errors of $\pm 10\,\%$), but the error in ΔH is large. Slightly sigmoidal curve shapes are optimal for complete data analysis ($10 \leq c \leq 1000$). Since the association constant K and the stoichiometry n of a system cannot be changed, the only possibility to improve a too low or too high c-value is to increase or reduce the host concentration $[\mathbf{H}]$ in the sample cell, respectively.[122,123]

As mentioned above, ITC is a versatile technique which is applied in various fields.[34,83,114,116,119,120] Different examples of supramolecular systems, in which ITC revealed insights into their thermochemistry, were already mentioned in Sec-

tions 2.1.2 and 2.2. De Simone and co-workers[83] measured association constants of different cucurbiturils and hydrophobic guests in water (Figure 2.9). Schalley and co-workers[34] determined the association constants of mono- and divalent pseudorotaxanes in organic solvents (Figure 2.16).

Recently, Nau and co-workers[124] reported the versatile use of cucurbiturils (CB7 and CB8) as hosts for different steroids (Figure 2.29). They observed remarkable size selectivity. Curcurbiturils are biocompatible and the investigated steroid complexes are stable in water, buffers, artificial gastric acid, and in blood serum. Thus, cucurbiturils may be used to increase the bioavailability of steroidal drugs. In other words, curcurbiturils show potential for drug delivery. The thermodynamic analysis, on which this study is based, was again mostly done by ITC. DFT calculations supplement the analysis of size selectivity demonstrating again the power of combined experimental and computational analysis.

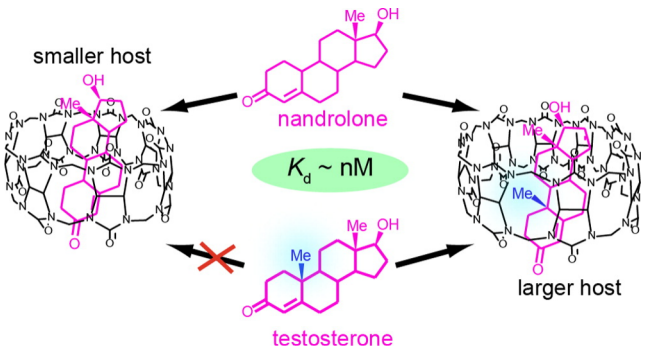

Figure 2.29. Schematic representation of the size-selective binding of steroids to CB7 (left) and CB8 (right). Association constants of up to $K \geq 10^8\ M^{-1}$ were determined by ITC. Size-selectivity was investigated by ITC, DFT and other techniques.[124]
Adapted with permission from Lazar et al.[124] (© 2016 American Chemical Society)

3 Published work

3.1 Theoretical and experimental investigation of crown/ammonium complexes in solution

Andreas J. Achazi, Larissa K. S. von Krbek, Christoph A. Schalley, and Beate Paulus

J. Comput. Chem. **2016**, *37*(1), 18–24.

Submitted on 22 December 2014, first published on 13 April 2015 in the *Journal of Computational Chemistry*. For copyright reasons, the article[125] (Appendix A.1) is not included in the online version of this thesis.

An electronic version of the article is available (DOI: 10.1002/jcc.23914).

3.1.1 Project summary

To elucidate the cooperative effects in multivalent systems, it is mandatory to gain a thorough understanding of the monovalent binding motif first. In this thesis, these binding motifs are crown ether/ammonium binding sites composed of a [18]crown-6 crown ether derivative and a primary ammonium salt or a [24]crown-8 crown ether derivative and a secondary ammonium salt. Since the thermodynamic analysis of cooperative effects in this work is often complemented by density functional theory (DFT) calculations, the association of the used binding motifs needs to be well understood from a computational point of view as well. Ion pairing in the ammonium salts render the association processes in the monovalent binding motifs complicated (compare Section 2.1.3). Thus, they cannot be described by a simple 1:1 model.[42,44] That complexity in the association mechanisms made it necessary to develop a new DFT method. The simplest—and, therefore, most suitable for development of a new DFT approach—monovalent binding motif in this thesis is the [18]crown-6/primary ammonium ion motif (Figure 3.1).

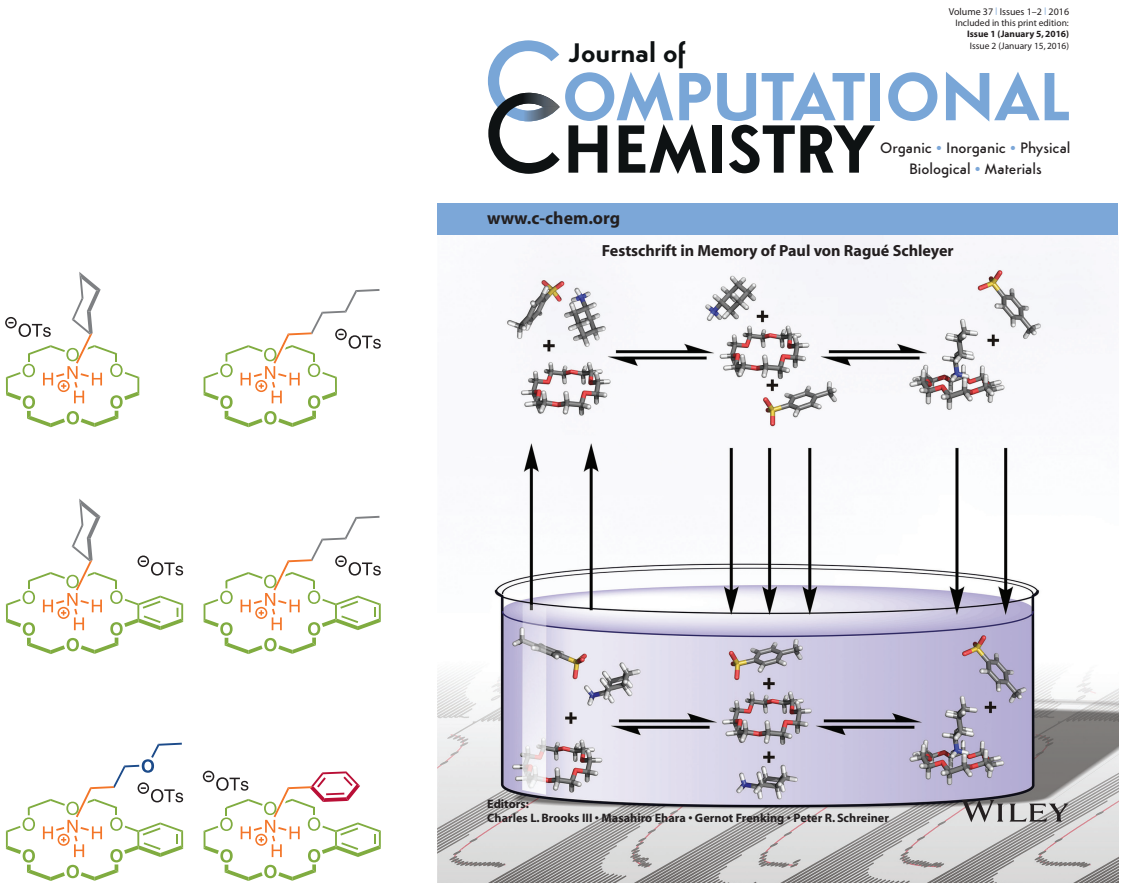

Figure 3.1. Chemical structures of monovalent [18]crown-6 crown ether/primary ammonium complexes under investigation (left). Inside cover of *J. Comput. Chem.* **2016**, *37*(1) elucidating the developed DFT approach (right). The guest ion pair needs to dissociate prior to host complexation. Solvation effects $\delta G_{\mathrm{se}}^{T}$ of all states (indicated by upright arrows) need to be taken into account as well.
Inside cover reprinted with permission from Achazi et al.[125] (© 2015 Wiley Periodicals, Inc).

Hence, we calculated and measured the Gibbs energies of association between primary alkyl ammonium ions and [18]crown-6 crown-ether derivatives in solution (Figure 3.1, left). Experiments conducted by isothermal titration calorimetry (ITC) revealed strong solvent-dependent ion-pair effects in chloroform/methanol mixtures. Two counterbalancing effects of the methanol fraction were revealed: On the one hand, methanol as a good hydrogen bond donor and acceptor competes with hydrogen bond formation between the crown ethers and the ammonium ions. Higher methanol content in the solvent mixture should, therefore, decrease the association strengths. On the other hand, methanol promotes ion pair separation of the ammonium salts in solution by better solvation of both, the ammonium ion and the tosylate counterion. This is advantageous for the association of the

ammonium ion to the crown ether as well as for a good solvation of the counterion after complex formation. Thus, methanol also facilitates complex formation. To which extend these two counterbalancing effect cancel each other depends on the structural details of the ammonium ions and crown ethers.
Calculations were performed with density functional theory (DFT) including Grimme's dispersion correction D3(BJ). The translational, rotational and vibrational contributions to the Gibbs energy of association $\Delta G^T_{\mathrm{sol}}$ were taken into account by a rigid-rotor-harmonic-oscillator approximation with a free-rotor approximation for low lying vibrational modes. We applied the continuum solvation model COSMO-RS to take solvation effects δG^T_{se} into account. A good agreement of theory and experiment is only achieved, when solvation and the effects of the counterions are explicitly taken into account (Figure 3.1, right): The guests' ion pairs need to be separated prior to crown ether/ammonium interaction and solvation energies for all states have to be considered as well.

We thereby found a suitable theoretical method for the evaluation of the host–guest interaction in crown ether/ammonium complexes as well as for the observed ion pair effects. That was the necessary first step, to move on to the analysis of cooperative effects in divalent [18]crown-6/ammonium systems (Sections 3.2 & 3.4).

3.1.2 Author contributions

Syntheses of single components and complexes were done by myself. Furthermore, I conducted the solvent dependent thermodynamic studies of the complex formation by ITC. Andreas J. Achazi did the computations and developed the new DFT approach to calculate the complexes in solution. Andreas J. Achazi and I discussed the results, he worked on the general concept and we wrote the manuscript together with main contributions coming from Andreas J. Achazi. All authors contributed to the final version of the manuscript.

3.2 Allosteric and chelate cooperativity in divalent crown ether/ammonium complexes with strong binding enhancement

Larissa K. S. von Krbek, Andreas J. Achazi, Marthe Solleder, Marcus Weber, Beate Paulus, and Christoph A. Schalley

Chem.—Eur. J. **2016**, *22*(43), 15475–15484.

Submitted on 29 June 2016, first published on 13 September 2016 in *Chemistry—A European Journal*. For copyright reasons, the article[126] (Appendix A.2) is not included in the online version of this thesis.

An electronic version of the article is available (DOI: 10.1002/chem.201603098).

3.2.1 Project summary

In the following project, the monovalent binding motifs studied in Section 3.1 were combined into two virtually identical divalent crown ether/ammonium complexes $\mathbf{G_O}$@**H** and $\mathbf{G_C}$@**H** (Figure 3.2) which only differ by two isoelectronic groups in the flexible guest spacers. As the binding sites are linked in these systems—that is, they are divalent—, cooperative effects can occur: allosteric cooperativity as well as chelate cooperativity.
Both systems exhibit flexible guest spacers, which are expected to be disadvantageous for divalent binding due to conformational restriction in the doubly-bound state.[2,19–21] Thus, we anticipated the systems to exhibit moderate association strengths and mediocre chelate cooperativities. However, $\mathbf{G_O}$@**H** and $\mathbf{G_C}$@**H** are synthetically easily accessible and exhibit a moderate molecular size. Both arguments render these complexes good candidates for a joint analysis of their association mechanisms by ITC, DFT, and molecular dynamics (MD).

We investigated the solvent dependent association thermodynamics of the complexes $\mathbf{G_O}$@**H** and $\mathbf{G_C}$@**H** by ITC and quantified the two occurring cooperative effects. Allosteric and chelate cooperativity were determined by comparison of the divalent complexes with the corresponding 2:1 and 1:2 complexes with monovalent analogues in double mutant cycle (DMC) analyses. Both analyses were complemented with DFT calculations including implicit solvent on the one hand and large-scale MD

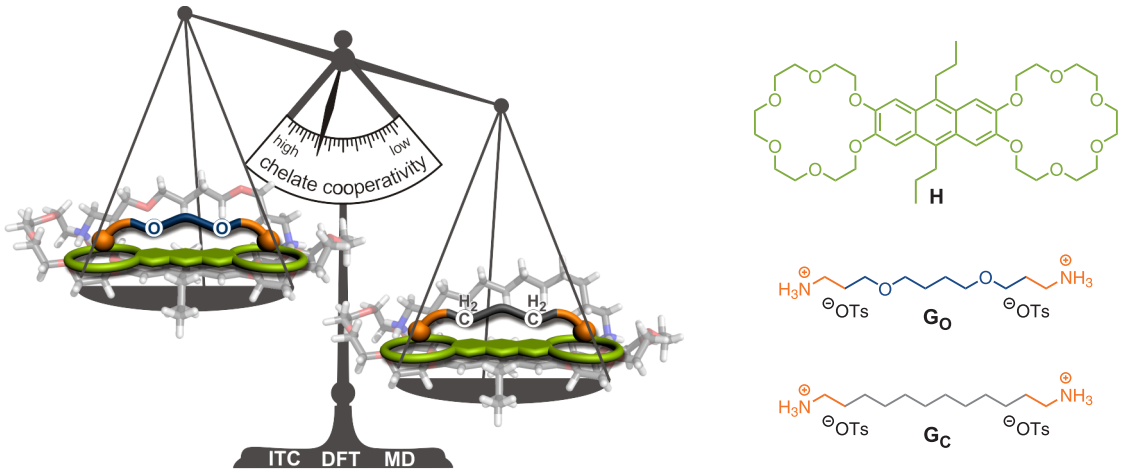

Figure 3.2. Graphical abstract showing schematic representations and DFT calculated structures of the two divalent crown ether/ammonium complexes under investigation; chemical structures are added for clarity. $\mathbf{G_C}$ exhibits significantly higher chelate cooperativity than $\mathbf{G_O}$ despite their virtually identical spacer structures.
Adapted with permission from von Krbek et al.[126] (© 2016 Wiley-VCH Verlag GmbH & Co. KGaA, Weinheim).

simulations with explicit solvent molecules on the other.

ITC measurements revealed high association constants for both complexes. The slight structural change from the ether guest spacer ($\mathbf{G_O}$) to the alkyl guest spacer ($\mathbf{G_C}$) causes up to one order of magnitude stronger binding ($K = 4 \cdot 10^5$ M^{-1} and $K = 3 \cdot 10^6$ M^{-1}, respectively). Our approach elucidated a delicate interplay between ion-pairing effects and interference of protic solvent causing solvent-dependent association strengths similar to those in their monovalent counterparts (Section 3.1). A chloroform/methanol mixture close to 1:1 (v/v) is ideal for high association constants in these systems. Higher or lower methanol fractions cause the association constants to drop significantly.

Negative allosteric cooperativities in host and guests were assigned to charge-charge repulsion and polarisability of the host's π-system as well as to ion-pairing effects in the case of the guests. Intramolecular hydrogen bonds in $\mathbf{G_O}$ rationalise its more negative allosteric cooperativity (Figure 3.3a).

Nevertheless, the complexes exhibit strong chelate cooperativities. Chelate cooperativities of $\mathbf{G_C}$ exceed those of $\mathbf{G_O}$ by up to one order of magnitude ($\beta'_{\mathbf{G_C}} = 150$ and $\beta'_{\mathbf{G_O}} = 10$,[1] respectively). MD simulations could attribute this difference mainly to the intramolecular hydrogen bonds which are present in unbound $\mathbf{G_O}$ (Figure 3.3). They facilitate a coiled unbound structure which has to unfold prior to binding

[1] Note that β' in this publication corresponds to the Ercolani-β [5] whereas β corresponds to the Hunter-β' [6] in Section 2.3.2.

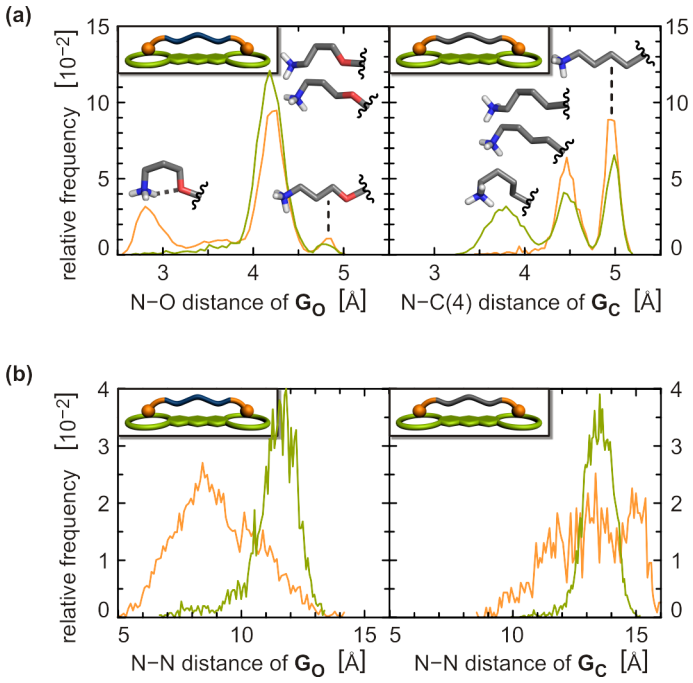

Figure 3.3. **(a)** N–O and N–C(4) distances during the MD simulations of $\mathbf{G_O}$ (left) and $\mathbf{G_C}$ (right) of unbound (orange) and bound guest (green). Maxima were assigned to structures with none, one or two gauche conformations between atoms N and O/C(4).[127] **(b)** N–N distances during the simulation of $\mathbf{G_O}$ (left) and $\mathbf{G_C}$ (right) of unbound (orange) and bound guest (green).
Adapted with permission from von Krbek et al.[126] (© 2016 Wiley-VCH Verlag GmbH & Co. KGaA, Weinheim).

to **H**. In contrast, unbound $\mathbf{G_C}$ prefers a mostly stretched conformation which facilitates association to **H** and rationalises $\mathbf{G_C}$'s higher chelate cooperativity.

By the comprehensive investigation of these relatively simple divalent [18]crown-6/ammonium complexes, we gained detailed insight into the association mechanisms of divalent crown ether/ammonium systems. That enabled us to proceed with the analysis of more complex di- and trivalent [24]crown-8/ammonium pseudorotaxanes (Section 3.3).

3.2.2 Author contributions

Syntheses of single components and complexes were done by myself. Furthermore, I conducted the NMR and MS analysis of the complexes as well as the solvent dependent thermodynamic studies of the complex formation by ITC. I quantified the cooperative effects of the systems including application of the DMC to the new systems and calculation of the statistical factors of all associations processes by

Benson's symmetry number method,[88,89] double checking the results by the direct count method.[88,90] Andreas J. Achazi did the DFT computations and adjusted his new DFT approach (Section 3.1) for calculating singly and doubly charged species in solution. Marthe Solleder worked on the MD simulations. Andreas J. Achazi, Marthe Solleder and I discussed the results. Andreas J. Achazi and I worked on the general concept. Andreas J. Achazi, Marthe Solleder and I wrote the manuscript together with main contributions coming from my side. All authors contributed to the final version of the manuscript.

3.3 Thermodynamic analysis of allosteric and chelate cooperativity in di- and trivalent ammonium/crown-ether pseudorotaxanes

Karol Nowosinski, Larissa K. S. von Krbek, Nora L. Traulsen, and Christoph A. Schalley

Org. Lett. **2015**, *17*(20), 5076–5079.

Submitted on 08 September 2015, first published on 06 October 2015 in *Organic Letters*. For copyright reasons, the article[128] (Appendix A.3) is not included in the online version of this thesis.

An electronic version of the article is available (DOI: 10.1021/acs.orglett.5b02592).

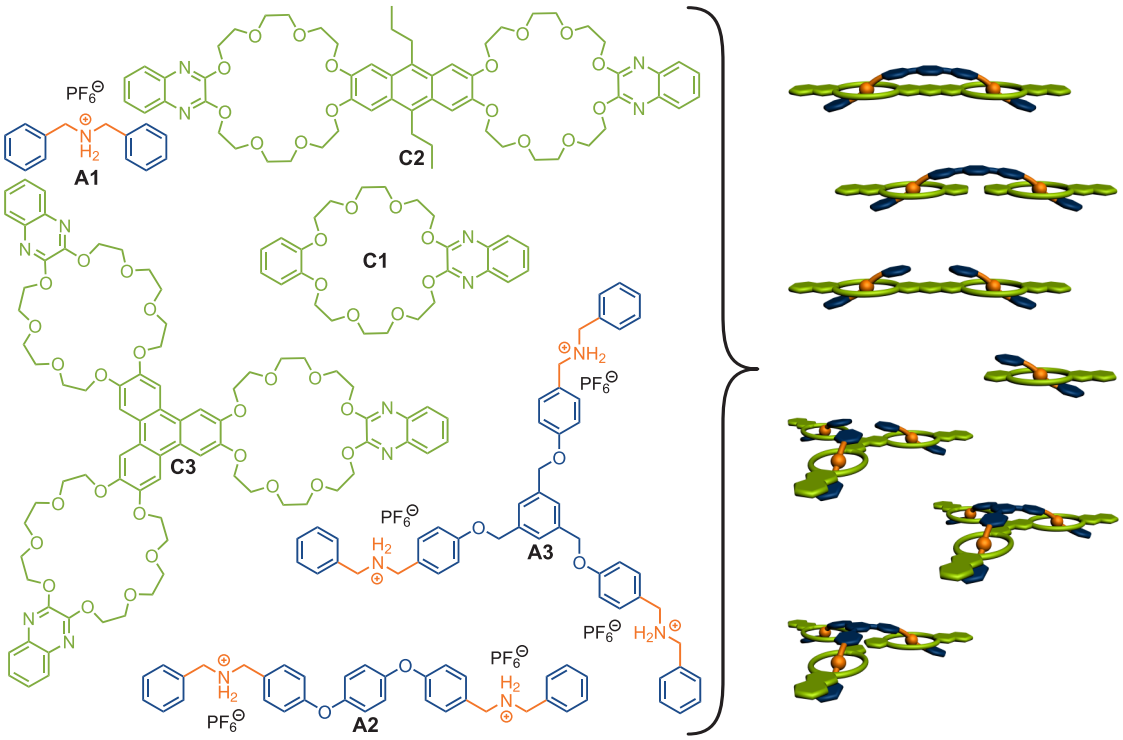

Figure 3.4. Schematic representation of the self-assembly of mono-, di-, and trivalent building blocks under investigation.[128]

3.3.1 Project summary

After the cooperative effects in divalent [18]crown-6/ammonium complexes were quantified, interpreted and explained with help of DFT and MD computations (Section 3.2), the same experimental approach was transferred to di- and trivalent [24]crown-8/ammonium pseudorotaxanes (Figure 3.4).

Our detailed thermodynamic analysis by ITC experiments combined with the DMC approach revealed an interesting interplay of cooperative effects in the [24]crown-8/ammonium pseudorotaxanes. Di- and trivalent ammonium guests **A2** and **A3** exhibit positive allosteric cooperativities whereas di- and trivalent crown-ether hosts **C2** and **C3** reveal negative allosteric cooperativties. In **A2@C2**, these opposite alosteric effects of host and guest cancel each other out; in **A3@C3**, an overall negative allosteric effect remains. Nevertheless, the chelate cooperativities of both multivalent assemblies **A2@C2** and **A3@C3** are positive.
Positive allosteric cooperativities in the guests were attributed to cooperative ion-pair effects in their unbound states. The guests' arms fold around the PF_6^- counterions in unpolar solvents (Figure 3.5) and these arrangements have to break upon the first binding event. The subsequent binding events are, hence, facilitated compared to the first one as the ion-pair coil is already weakened or diminished in **A3** and **A2**, respectively. The di- and trivalent crown ethers **C2** and **C3** are structurally similar to the earlier studied host **H** and, therefore, we ascribe their negative allosteric cooperativities to the polarisation of their π-systems as well.
Positive chelate cooperativities of multivalent assemblies **A2@C2** and **A3@C3** indicate their efficient design with careful consideration of both complementary preorganisation and adaptability.

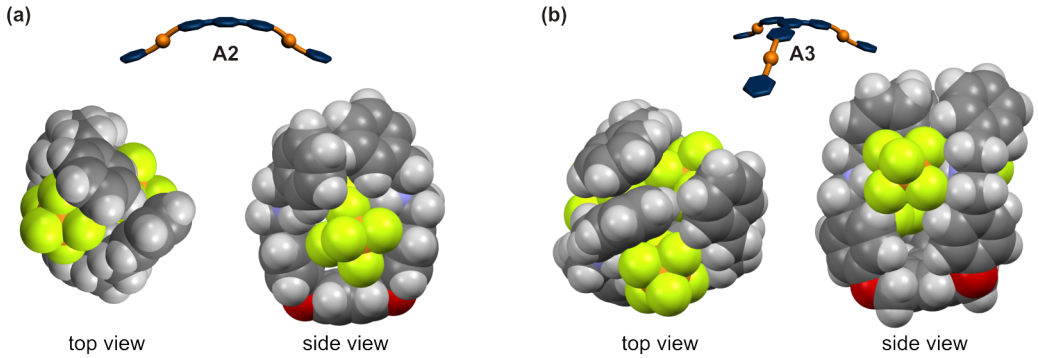

Figure 3.5. MM2 force-field-optimised structures of the di- and trivalent guest salts **A2** and **A3** folded through ion-pairing effects.[128]
Adapted with permission from Nowosinski et al.[128] (© 2015 American Chemical Society).

We hereby demonstrated the applicability of our approach to analyse divalent crown ether/ammonium complexes (Section 3.2) to more complex structures.

3.3.2 Author contributions

Syntheses of single components and pseudorotaxanes were done by Karol Nowosinski. Furthermore, he conducted the NMR and MS analysis of the pseudorotaxanes. Karol Nowosinski and Nora L. Traulsen performed the ITC measurements with main contributions coming from his side. Nora L. Traulsen and I interpreted the ITC data with main contributions coming from my side. I determined the statistical factors of the associations processes of mono-, di-, and trivalent pseudorotaxanes by Benson's symmetry number method.[88,89] I double checked the results by the direct count method[88,90] in discussion with Karol Nowosinski and Nora L. Traulsen. Karol Nowosinski and I performed the DMC analysis and quantification of both cooperative effects. Karol Nowosinski and I discussed the results and worked on the general concept together with main contributions coming from his side. Karol Nowosinski wrote the manuscript in collaboration with me. All authors contributed to the final version of the manuscript.

3.4 The delicate balance of preorganisation and adaptability in multiply bonded host–guest complexes

Larissa K. S. von Krbek, Andreas J. Achazi, Stefan Schoder, Marius Gaedke, Tobias Biberger, Beate Paulus, and Christoph A. Schalley

Chem.—Eur. J. **2017**, *23*(12), 2877–2883.

Submitted on 01 November 2016, first published on 31 January 2017 in *Chemistry—A European Journal*. For copyright reasons, the article[129] (Appendix A.4) is not included in the online version of this thesis.

An electronic version of the article is available (DOI: 10.1002/chem.201605092).

3.4.1 Project summary

The investigation of cooperative effects in di- and trivalent crown ether/ammonium assemblies as described in Sections 3.2 and 3.3 was complemented by a broad screening of cooperative effects in complexes with varying guest spacer lengths and flexibilities (Figure 3.6). According to the principle of preorganisation, widely used

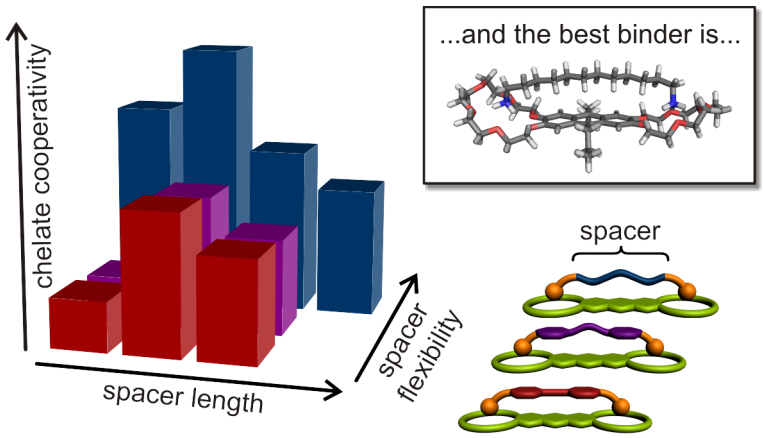

Figure 3.6. Graphical summary of the publication's main results. Chelate cooperativities of complexes consisting of a divalent crown ether host (green) and various guests with different spacer lengths and spacer flexibilities (blue, violet, red) were investigated (chemical structures are depicted in Chart 3.1). If bound to a rigid host structure, adaptability of the guest is more important than preorganisation to reach high chelate cooperativities.
Reprinted with permission from von Krbek et al.[129] (© 2017 Wiley-VCH Verlag GmbH & Co. KGaA, Weinheim).

in supramolecular chemistry,[2,17–19] the more rigid guest structures are expected to exhibit higher chelate cooperativities. They supposedly suffer of less entropic penalty due to conformational restrictions of the guest spacer in the doubly-bound state.[20,21] However, these rigid structures are sensible to slight mismatches which can reduce chelate cooperativity significantly. In natural systems, flexible building blocks are predominantly found which exhibit a certain adaptability to cope with possible mismatches and generate reliable systems with high affinities.[25] With our study we aimed to elucidate the balance between preorganisation and adaptability.

We chose our known rigid host system **H** (Section 3.2) and analysed its association to a variety of divalent guests **GX** exhibiting different spacer lengths and flexibilities by ITC (Figure 3.6 & Chart 3.1). The chelate cooperativities were determined by comparison with the corresponding 2:1 and 1:2 complexes with monovalent analogues in DMC analyses. We again used DFT calculations as a powerful tool for the interpretation of experimental results.
Long guest spacers show one order of magnitude smaller chelate cooperativities compared to guest spacers which exhibit the "ideal" length for bridging the distance between the host's binding sites. Unexpectedly, the more rigid systems are not

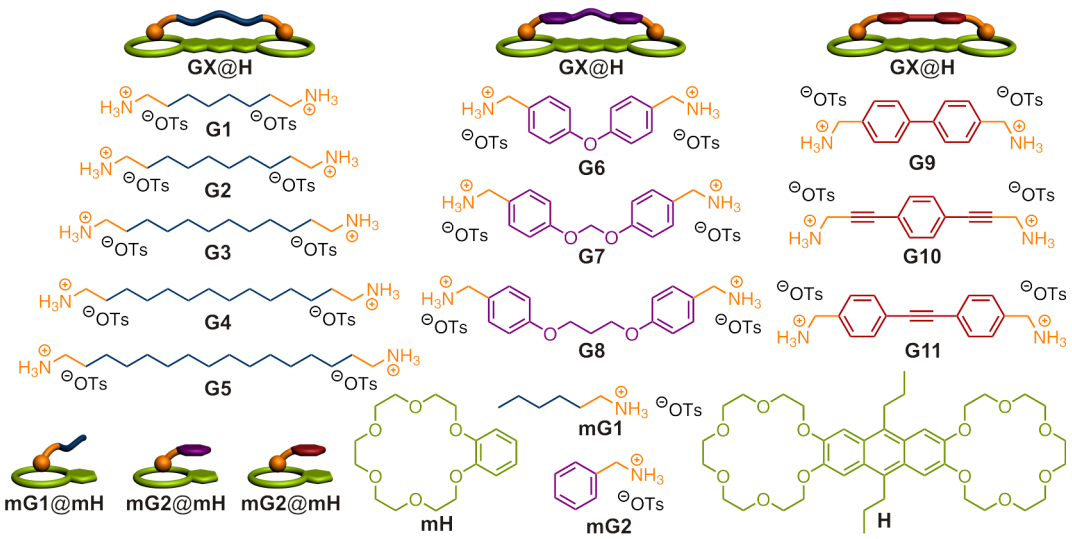

Chart 3.1. Divalent host **H**, divalent guests **GX** and their complexes **GX@H** under investigation. Divalent guests **GX** exhibit spacers of different lengths and degrees of flexibility between their ammonium binding sites. The different degrees of flexibility are colour coded: flexible = blue, "semi-rigid" = violet, rigid = red. Monovalent reference compounds **mGX**, **mH** and their complexes **mGX@mH** are crucial for quantification of cooperative effects in divalent complexes **GX@H**. Note that **mG2** is the monovalent reference compound for "semi-rigid" as well as rigid divalent guests.
Reprinted with permission from von Krbek et al.[129] (© 2017 Wiley-VCH Verlag GmbH & Co. KGaA, Weinheim).

preferred over the flexible ones. Quite the contrary, flexible guests express chelate cooperativities which exceed those of the more rigid structures by one order of magnitude. The ability of flexible spacers to correct for small geometric mismatches between host and guest seems to overcome the expected penalty for conformational restriction upon binding. Indeed, residual enthalpies and entropies of the complexes indicate, that secondary spacer–spacer interactions in the complexes have a higher positive impact in terms of enthalpy on chelate cooperativities than entropic penalty has a negative impact due to conformational restriction.
A delicate balance between preorganisation and adaptability seems to be at play when multiply bonded structures are concerned. The concepts of preorganisation still hold true (e.g. Figure 2.14, Section 2.2),[2,17–19,24] but flexible systems have been underestimated so far. We believe that flexible linkers are more likely to give good results when searching for the best multivalent ligand for a multivalent receptor.

The quantification of cooperative effects and the analysis of their origin in such systems provided insight into the details of multivalent binding (Sections 3.2 – 3.4). These insights can be generalised in form of a multivalency "toolkit":

- Complementarity of host and guest is crucial.
- In case of the lack of complementarity, flexible systems can mimic complementarity by adapting to the interaction partner.
- Maximum spacer–spacer interactions should be pursued whenever possible.

This toolkit will help in designing and synthesising other optimised pseudorotaxanes, supramolecular structures inheriting function and multiply threaded molecular machines in the future. In the following sections, it is described how we used our multivalency toolkit to tune the function of a supramolecular photoswitch (Section 3.5) and to design more complex supramolecular assemblies (Section 3.6).

3.4.2 Author contributions

Syntheses of single components were done by Stefan Schoder, Marius Gaedke, Tobias Biberger, Tuğrul Kaynak, Florian Korinth and myself. The contributions of Tuğrul Kaynak and Florian Korinth were considerably smaller and, therefore, they did not co-author the publication but are mentioned in the acknowledgements. Furthermore, I conducted the self-assembly of the complexes and their NMR and MS analysis. I also performed the thermodynamic studies of the complex formation

by ITC, interpreted the results and quantified the cooperative effects arising in the systems by DMC analysis. Andreas J. Achazi did the DFT computations. Andreas J. Achazi and I discussed the results and worked on the general concept together with main contributions coming from my side. I wrote the manuscript. All authors contributed to the final version of the manuscript.

3.5 Gating the photochromism of an azobenzene by strong host–guest interactions in a divalent pseudo[2]rotaxane

Mirko Lohse, Karol Nowosinski, Nora L. Traulsen, Andreas J. Achazi, Larissa K. S. von Krbek, Beate Paulus, Christoph A. Schalley, and Stefan Hecht

Chem. Commun. **2015**, *51*(48), 9777–9780.

Submitted on 04 April 2015, first published on 01 May 2015 in *Chemical Communications*. For copyright reasons, the article[130] (Appendix A.5) is not included in the online version of this thesis.

An electronic version of the article is available (DOI: 10.1039/C5CC02811F).

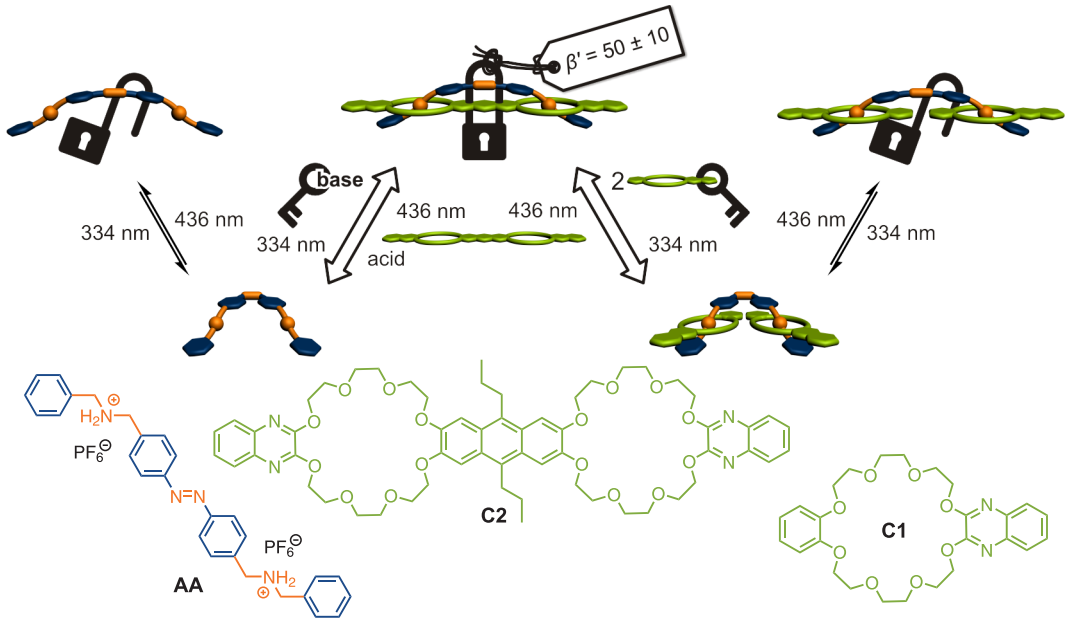

Figure 3.7. The ability of an *E*-configured azobenzene guest **AA** to undergo photoisomerisation is "locked" by the presence of a complementary host **C2**. Addition of base/acid allowed for a weakening/strengthening of the interactions in the divalent pseudo[2]rotaxane complex and hence working as a "key" to "unlock"/"lock" photochromic activity. Formation of a 1:2 [3]pseudorotaxane with **AA** and **C1** demonstrates that specifically the multivalent interaction—more precisely the strong chelate cooperativity—in **AA@C2** "locks" the photochromic activity of **AA**.

3.5.1 Project summary

After thorough analysis of cooperative effects in different di- and trivalent systems (Sections 3.2 – 3.4) we put the acquired knowledge to use and generated a supramolecular inhibitor of an azobenzene photoswitch (Figure 3.7).

In the presence of a complementary host **C2**, the ability of the divalent *E*-configured azobenzene guest **AA** to undergo $E \rightarrow Z$ photoisomerisation was controlled. The photochromic activity of **AA** could be switched "on" by weakening of the supramolecular interaction to **C2** by addition of base or a stronger competing solvent. The former method turned out to be the more effective one to switch "on" photochromic activity, as the supramolecular interaction is not only weakened in this case but completely annihilated (compare Section 2.1.1). Addition of acid switched the supramolecular interaction "on" and, hence, switched "off" $E \rightarrow Z$ photoisomerisation of **AA**. The 1:2 complex of **AA** and two monovalent hosts **C1** showed usual photochromic activity thereby demonstrating that the multivalent interaction in the divalent pseudo[2]rotaxane **AA@C2** is causing the inhibition of photochromic activity of **AA**. DMC analysis of **AA@C2** could attribute this to a strongly positive chelate cooperativity of $\beta' = 50$.[2]
In this study, we could demonstrate how strong chelate cooperativity can not only increase multivalent binding, but can also efficiently act as a "lock" to the photochromic activity of one of the components in a supramolecular assembly.

These findings might open up new possibilities of using multivalency not only to effectively design functional architecture, but also to tune the function of a system.

3.5.2 Author contributions

Syntheses of single components and pseudorotaxanes were done by Karol Nowosinski and Mirko Lohse. Mirko Lohse performed UV-Vis studies of the pseudorotaxanes and their "on" or "off" switching of photochromic activity. Karol Nowosinski conducted the NMR and MS analysis of the pseudorotaxanes. Karol Nowosinski and Nora L. Traulsen performed the ITC measurements. Nora L. Traulsen and I interpreted the ITC data with main contributions coming from her side. I determined the statistical factors of the associations processes of mono- and divalent pseudorotaxanes by Benson's symmetry number method.[88,89] I double checked the

[2] Note that β' in this publication corresponds to the Ercolani-β [5] whereas β corresponds to the Hunter-β' [6] in Section 2.3.2.

results by the direct count method[88,90] in discussion with Karol Nowosinski and Nora L. Traulsen. Karol Nowosinski, Nora L. Traulsen and I performed the DMC analysis and quantification of both cooperative effects. Andreas J. Achazi did the DFT computations. Karol Nowosinski and Mirko Lohse discussed the results and worked on the general concept and wrote the manuscript. All authors contributed to the final version of the manuscript.

3.6 Discrete multiporphyrin pseudorotaxane assemblies from di- and tetravalent porphyrin building blocks

Mirko Lohse, Larissa K. S. von Krbek, Sebastian Radunz, Suresh Moorthy, Christoph A. Schalley, and Stefan Hecht

Beilstein J. Org. Chem. **2015**, *11*(4), 748–762.

Submitted on 28 February 2015, first published on 2 May 2015 in the *Beilstein Journal of Organic Chemistry*.
An electronic version of the article is available (DOI: 10.3762/bjoc.11.85).

3.6.1 Project summary

The greater objective of this thesis was to use the multivalency toolkit obtained in the course of this thesis to efficiently design more complex supramolecular structures.

In a first attempt towards these complex structures, we created complementary[3] building blocks and used their self-assembly to obtain discrete structures (Figure 3.8). The building blocks were porphyrin-based di- and tetravalent crown-ether hosts **C2'** and **C4'** and secondary ammonium guests **A2'** and **A4'** as well as monovalent analogues (**C1'** and **A1'**) as control compounds. The rigid porphyrin scaffolds were chosen to implement complementarity and directionality into the building blocks. Rotational flexibility between the binding sites and the porphyrin grants correction of possible mismatches. The mixing of an arbitrary host with a guest resulted in the formation of specific multiply threaded 1:1, 1:2 or 1:4 pseudorotaxanes. The formation of these discrete assemblies was shown by NMR in solution and confirmed by mass spectrometry in the gas phase.
We thereby demonstrated effectively the power of multivalent interactions to program multicomponent self-assembly into discrete structures.

[3] Note that the term "preorganisation" in the title refers more to complementarity of hosts and guests than to rigid preorganised systems to which this term was attributed in this thesis.

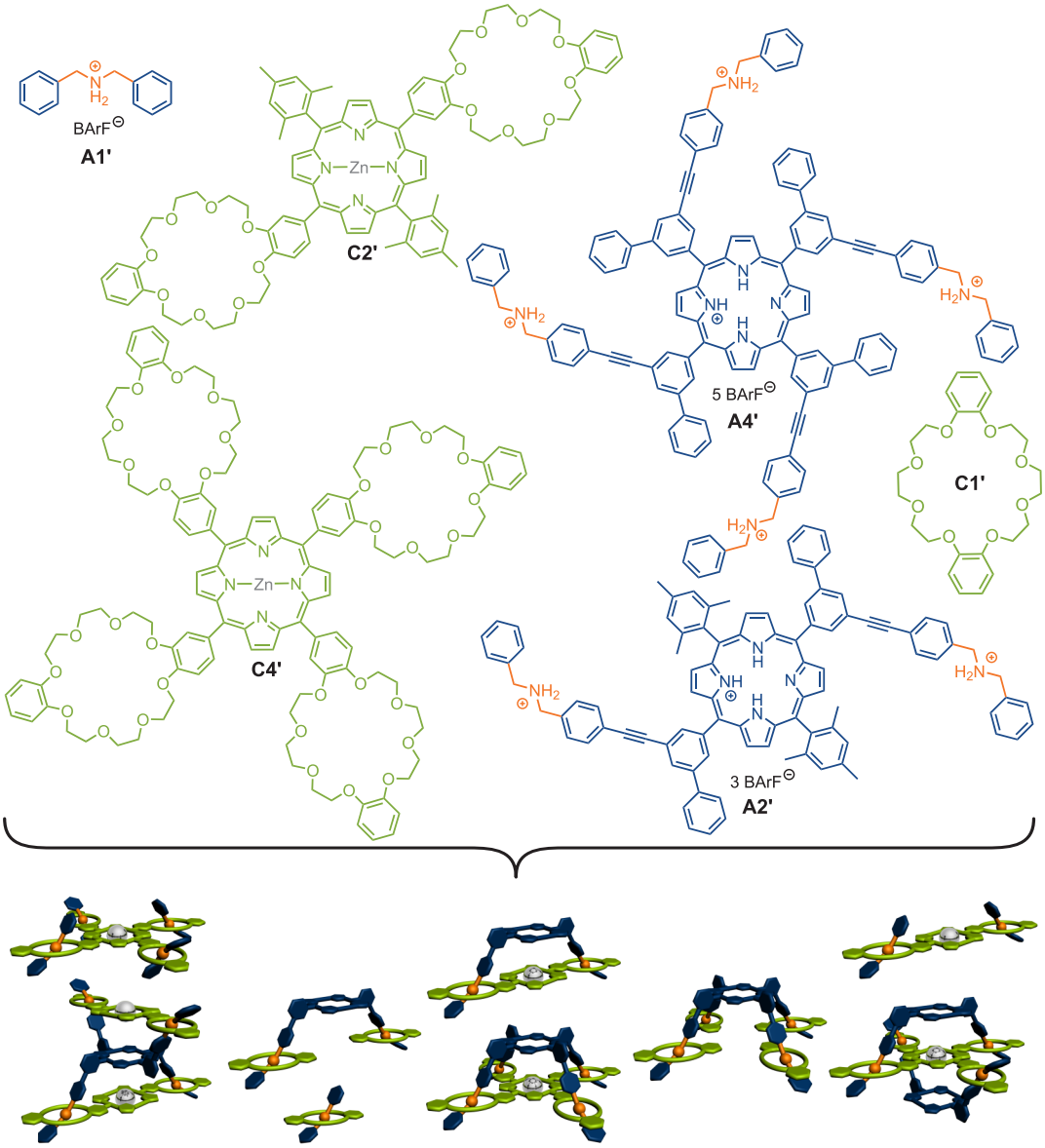

Figure 3.8. Schematic representation of the self-assembly of complementary mono-, di- and tetravalent building blocks into discrete mono, di- and tetravalent porphyrin pseudorotaxanes.[131]

In the future, we will continue to exploit this concept of complementary multivalent binding to program the complex self-assembly of multiple chromophore components into functional supramolecular architecture.

3.6.2 Author contributions

General conception of the project was done by Christoph A. Schalley, Stefan Hecht, Mirko Lohse and myself. Syntheses of single components and pseudorotaxanes were

done by Mirko Lohse and Sebastian Radunz. Suresh Moorthy was the first to synthesise **C4'**. Mirko Lohse later on repeated this synthesis and significantly optimised it. Mirko Lohse performed NMR and UV-Vis studies of the pseudorotaxanes. I did the MS analysis of the discrete assemblies. Christoph A. Schalley, Stefan Hecht, Mirko Lohse and I discussed the results and worked on the general concept of the publication and wrote the manuscript together. All authors contributed to the final version of the manuscript.

4 Conclusion

A thorough analysis of monovalent [18]crown-6/primary ammonium complexes revealed profound insight into solvent and counterion effects in these assemblies. The investigation of the association processes in a range of chloroform/methanol mixtures uncovered the operation of counterbalancing solvent and ion-pairing effects in the crown ether/ammonium complexes: The solvated guest ion pairs need to be separated and the individual ions solvated prior to binding of the ammonium ion to the crown ether. For a reasonable theoretical description of the association processes in solution, both effects—solvation and counterion effects—must be taken into account.

Developing a thorough understanding of the monovalent systems was the necessary first step towards the investigation of cooperative effects in di- and trivalent assemblies and the development of a general "toolkit" for generating multivalent interactions with high binding amplifications. The analysis of divalent [18]crown-6/primary ammonium complexes as well as di- and trivalent [24]crown-8/secondary ammonium pseudorotaxanes revealed a complex interplay of ion-pairing effects, solvent effects and cooperative effects. Further insight into the association mechanisms of the [18]crown-6/primary ammonium complexes was achieved by complementing the experimental analysis by DFT calculations and MD simulations with implicit and explicit solvent, respectively. As in the monovalent model analogues, ion-pairing effects are counterbalanced by the interference of more polar solvents in multivalent systems. Furthermore, these ion-pairing effects bring about two seemingly opposing allosteric effects in the two different ammonium guests. In the case of the primary ammonium guests, ion pairing causes negative allosteric cooperativity, because the separation of the first ion pair strengthens the second which then competes more strongly with the host–guest interaction than the first. In the case of the secondary ammonium salts, their different structure and the less polar solvent system cause the guests to wrap around their counterions. Stepwise disruption of that cluster of ion pairs upon binding to the host renders each binding event less unfavourable—thus, positive allosteric cooperativity is observed. Although the net allosteric effect has

opposite signs in the two cases, the ion-pairing effects causing allostery are of the same nature. The characteristics of the spacer also have a large impact on the cooperative effects of the crown ether/ammonium assemblies. Negative allosteric cooperativities of all hosts are caused by the polarisability of their anthracene and triphenylene scaffolds. Moreover, in the case of the flexible primary ammonium guests, incorporation of oxygen atoms into the guest spacer is counterproductive for high chelate cooperativities. Isoelectronic methylene units, however, give rise to maximum binding energies. Beyond this, spacer length and geometry, spacer–spacer interactions as well as their ability to adapt to a given host structure (flexibility despite complementarity) affect the degree of chelate cooperativity in the divalent and trivalent assemblies.

As the last step towards the objective of obtaining a general toolkit for strong multivalent interactions, we addressed the question, whether rigid, preorganised or flexible and adaptable scaffolds are advantageous. By selectively altering guest spacer lengths and flexibilities, the impact of three factors—adaptability, preorganisation and spacer length—on chelate cooperativity was elucidated. The flexible guests are favoured over the more rigid ones, almost irrespective of their length—too short guest spacers are unfavourable as they cannot bridge the distance between the host's binding sites. Nevertheless, good complementarity in host and guest spacer lengths leads to maximum chelate cooperativities. Furthermore, the cyclisation of our complexes seems to be mainly driven by enthalpy, i.e. secondary spacer–spacer interactions between host and guest. The entropic penalty due to conformational restriction in the doubly-bound state seems to play only a minor role. When high chelate cooperativity is pursued, the ability of a flexible guest to adapt to a complementary rigid host structure seems to be more important than preorganisation and conformational restriction. Flexible spacers can easily compensate for mismatches and result in relatively strainless doubly-bound complexes. That can lead to very high chelate cooperativities. Furthermore, they bear the advantage of being more readily accessible than rigid structures. A delicate balance between preorganisation and adaptability seems to be at play when multiply bonded structures are concerned. The concepts of preorganisation still hold true, but flexible systems have been underestimated so far. We believe that complementary flexible linkers are more likely to give good results when searching for the best multivalent ligand for a multivalent receptor.

In the course of four elaborate studies of cooperativity effects in di- and trivalent crown ether/ammonium assemblies, a precise understanding of the aspects of

preorganisation and adaptability in multivalent systems was gained. These insights can be generalised in form of a multivalency toolkit:

- Complementarity of the association partners is crucial.
- If perfect complementarity is not granted, flexible systems—in sharp contrast to rigid ones—can mimic complementarity by adapting to the interaction partner. Hence, flexible systems are favourable over rigid ones in this case.
- Whenever possible, spacer–spacer interactions should be maximized.

This toolkit will enhance our capability to efficiently design and construct larger supramolecular architectures with multiple building blocks by predicting their properties. Furthermore, expanding the knowledge about multivalent binding processes will help to optimise supramolecular functional structures such as molecular switches, as it provides enhanced control over the non-covalent interactions incorporated in these assemblies.

In a first attempt towards more complex functional structures, we designed a novel molecular switch and various tetravalent pseudorotaxanes using the guiding principles of our multivalency toolkit. The ability of a divalent *E*-configured azobenzene guest to undergo $E \rightarrow Z$ photoisomerisation was succesfully controlled by the multivalent interaction to a complementary host. Furthermore, we used our design rules for self-assembly of discrete di- and tetravalent crown ether/ammonium pseudorotaxanes. Rigid porphyrin building blocks are used to ensure complementarity between hosts and guests and directionality of the interactions. This stiffness is compensated by the rotational flexibility of the attached binding sites with respect to the porphyrin units. That enables our systems not only to form di- and tetravalent 1:1 complexes but also to adapt to quadruply bound 1:2 and 2:1 complexes when mixing hosts and guests with different numbers of binding sites.

The balance between preorganisation and adaptability in these porphyrin systems renders them ideal for an investigation of the so far sparsely reported interannular cooperativity (Figure 4.1a) and for further application towards complex functional structures. They could be used to program the self-assembly of multiple chromophore components into functional supramolecular architectures (Figure 4.1b). The porphyrin units can bind different metal ions which should be sufficiently close to each other in the pseudorotaxane assemblies to allow for metal–metal interaction (compare Figure 2.10, Section 2.2).[36,84,85] Stacking a large number of these metalloporphyrins might enable us to use these stacks as molecular wires. By stoppering these pseudorotaxane stacks to generate rotaxane stacks, acid/base shuttles such as

in the divalent elevator by Liu and co-workers[38] (Figure 2.7, Section 2.1.1) could be generated. These would even allow for stimuli-responsive on/off switching of conductivity in the wires (Figure 4.1c).

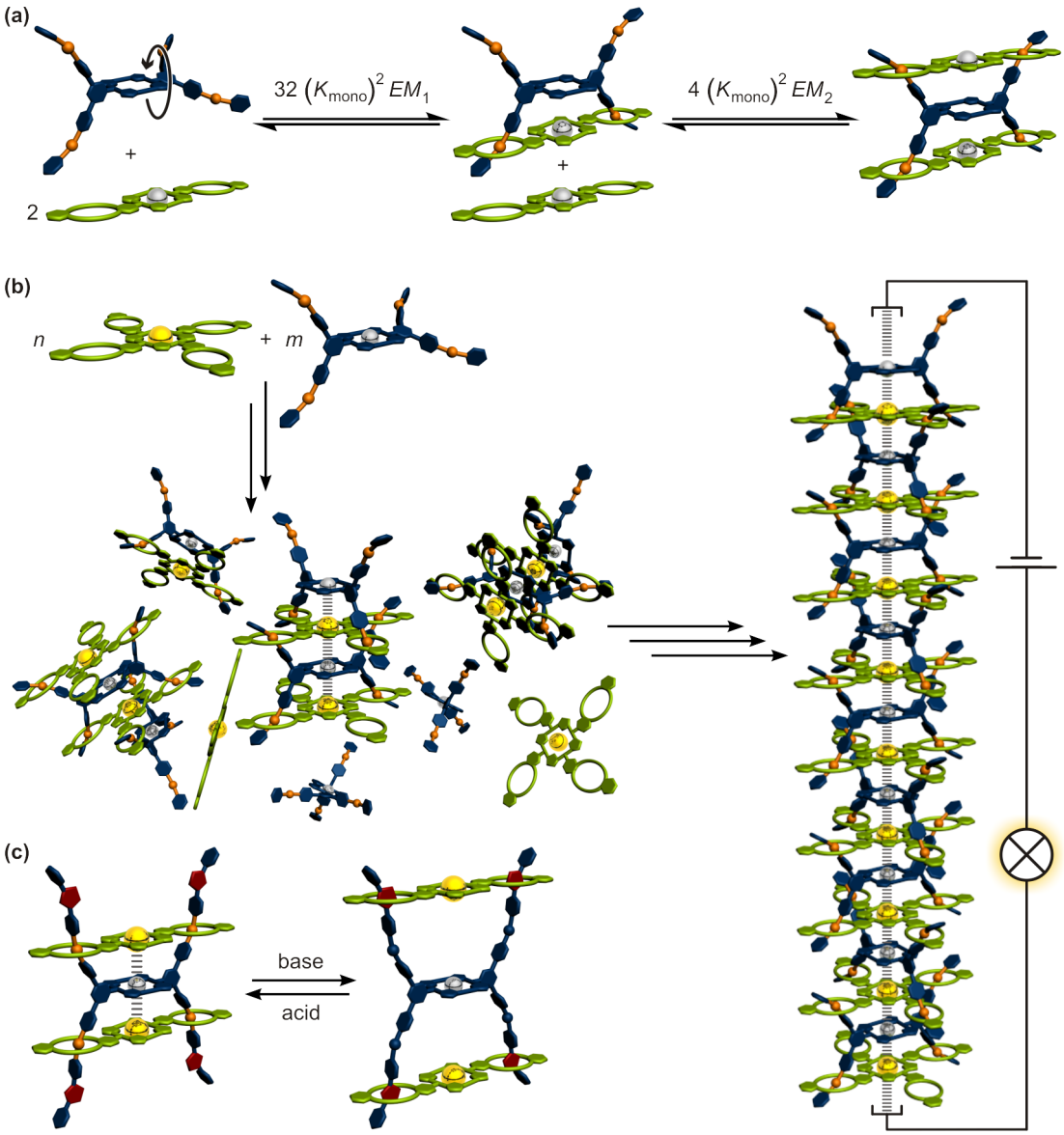

Figure 4.1. **(a)** Analysis of interannular cooperativity in porphyrin based[132] tetravalent pseudorotaxanes. **(b)** Schematic representation of the self-assembly of complementary tetravalent building blocks[132] into supramolecular stacks. With appropriate metal ions the stacks might be conductive and could be used as self-assembled wires. **(c)** Modification of the assembly from pseudorotaxanes to rotaxanes by a suitable stopper[38] can allow for on/off switching of conductivity by addition of acid/base.

Bibliography

[1] Nature Education, [16 September 2016, 14:30 MEZ]. http://www.nature.com/scitable/topicpage/cells-can-replicate-their-dna-precisely-6524830.

[2] M. Mammen, S.-K. Choi, G. M. Whitesides, *Angew. Chem. Int. Ed.* **1998**, *37*, 2754–2794; *Angew. Chem.* **1998**, *110*, 2908–2953.

[3] D. Schwefel, C. Maierhofer, J. G. Beck, S. Seeberger, K. Diederichs, H. M. Möller, W. Welte, V. Wittmann, *J. Am. Chem. Soc.* **2010**, *132*, 8704–8719.

[4] C. Fasting, C. A. Schalley, M. Weber, O. Seitz, S. Hecht, B. Koksch, J. Dernedde, C. Graf, E.-W. Knapp, R. Haag, *Angew. Chem. Int. Ed.* **2012**, *51*, 10472–10498; *Angew. Chem.* **2012**, *124*, 10622–10650.

[5] G. Ercolani, L. Schiaffino, *Angew. Chem. Int. Ed.* **2011**, *50*, 1762–1768; *Angew. Chem.* **2011**, *123*, 1800–1807.

[6] C. A. Hunter, H. L. Anderson, *Angew. Chem. Int. Ed.* **2009**, *48*, 7488–7499; *Angew. Chem.* **2009**, *121*, 7624–7636.

[7] A. Joshi, D. Vance, P. Rai, A. Thiyagarajan, R. S. Kane, *Chem.—Eur. J.* **2008**, *14*, 7738–7747.

[8] S. Jusuf, P. J. Loll, P. H. Axelsen, *J. Am. Chem. Soc.* **2003**, *125*, 3988–3994.

[9] L. L. Kiessling, J. E. Gestwicki, L. E. Strong, *Angew. Chem. Int. Ed.* **2006**, *45*, 2348–2368; *Angew. Chem.* **2006**, *118*, 2408–2429.

[10] A. Mulder, J. Huskens, D. N. Reinhoudt, *Org. Biomol. Chem.* **2004**, *2*, 3409–3424.

[11] J. Huskens, *Curr. Opin. Chem. Biol.* **2006**, *10*, 537–543.

[12] J. D. Badjić, A. Nelson, S. J. Cantrill, W. B. Turnbull, J. F. Stoddart, *Acc. Chem. Res.* **2005**, *38*, 723–732.

[13] J. Hamacek in *Metallofoldamers*, G. Maayan, M. Albrecht (Eds.), John Wiley & Sons, Ltd, Chichester, **2013**, chapter 3, pp. 91–123.

[14] G. M. Whitesides, J. P. Mathias, C. T. Seto, *Science* **1991**, *254*, 1312–1319.

[15] M. M. Safont-Sempere, G. Fernández, F. Würthner, *Chem. Rev.* **2011**, *111*, 5784–5814.

[16] Z. He, W. Jiang, C. A. Schalley, *Chem. Soc. Rev.* **2015**, *44*, 779–789.

[17] D. J. Cram, *Angew. Chem. Int. Ed. Engl.* **1986**, *25*, 1039–1057; *Angew. Chem.* **1986**, *98*, 1041–1060.

[18] D. J. Cram, *Angew. Chem. Int. Ed. Engl.* **1988**, *27*, 1009–1020; *Angew. Chem.* **1988**, *100*, 1041–1052.

[19] V. M. Krishnamurthy, L. A. Estroff, G. M. Whitesides in *Fragment-based Approaches in Drug Discovery*, W. Jahnke, D. A. Erlanson (Eds.), Wiley-VCH Verlag GmbH & Co. KGaA, Weinheim, **2006**, chapter 2, pp. 11–53.

[20] M. Mammen, E. I. Shakhnovich, G. M. Whitesides, *J. Org. Chem.* **1998**, *63*, 3168–3175.

[21] F. Eblinger, H.-J. Schneider, *Angew. Chem. Int. Ed.* **1998**, *37*, 826–829; *Angew. Chem.* **1998**, *110*, 821–824.

[22] H. Adams, E. Chekmeneva, C. A. Hunter, M. C. Misuraca, C. Navarro, S. M. Turega, *J. Am. Chem. Soc.* **2013**, *135*, 1853–1863.

[23] J. K. Sprafke, B. Odell, T. D. W. Claridge, H. L. Anderson, *Angew. Chem. Int. Ed.* **2011**, *50*, 5572–5575; *Angew. Chem.* **2011**, *123*, 5687–5690.

[24] H. J. Hogben, J. K. Sprafke, M. Hoffmann, M. Pawlicki, H. L. Anderson, *J. Am. Chem. Soc.* **2011**, *133*, 20962–20969.

[25] Y. Zhao, *ChemPhysChem* **2013**, *14*, 3878–3885.

[26] S. H. Gellman, *Acc. Chem. Res.* **1998**, *31*, 173–180.

[27] D. J. Hill, M. J. Mio, R. B. Prince, T. S. Hughes, J. S. Moore, *Chem. Rev.* **2001**, *101*, 3893–4012.

[28] M. Huse, J. Kuriyan, *Cell* **2002**, *109*, 275–282.

[29] Z. Zhong, X. Li, Y. Zhao, *J. Am. Chem. Soc.* **2011**, *133*, 8862–8865.

[30] V. M. Krishnamurthy, V. Semetey, P. J. Bracher, N. Shen, G. M. Whitesides, *J. Am. Chem. Soc.* **2007**, *129*, 1312–1320.

[31] H. Sun, C. A. Hunter, E. M. Llamas, *Chem. Sci.* **2015**, *6*, 1444–1453.

[32] A. E. Stross, G. Iadevaia, C. A. Hunter, *Chem. Sci.* **2016**, *7*, 94–101.

[33] A. E. Stross, G. Iadevaia, C. A. Hunter, *Chem. Sci.* **2016**, *7*, 5686–5691.

[34] W. Jiang, K. Nowosinski, N. L. Löw, E. V. Dzyuba, F. Klautzsch, A. Schäfer, J. Huuskonen, K. Rissanen, C. A. Schalley, *J. Am. Chem. Soc.* **2012**, *134*, 1860–1868.

[35] J. D. Badjić, C. M. Ronconi, J. F. Stoddart, V. Balzani, S. Silvi, A. Credi, *J. Am. Chem. Soc.* **2006**, *128*, 1489–1499.

[36] Y. Yamada, M. Okamoto, K. Furukawa, T. Kato, K. Tanaka, *Angew. Chem. Int. Ed.* **2012**, *49*, 709–713; *Angew. Chem.* **2012**, *122*, 733–737.

[37] P. R. Ashton, E. J. T. Chrystal, P. T. Glink, S. Menzer, C. Schiavo, N. Spencer, J. F. Stoddart, P. A. Tasker, A. J. P. White, D. J. Williams, *Chem.—Eur. J.* **1996**, *2*, 709–728.

[38] Z.-J. Zhang, M. Han, H.-Y. Zhang, Y. Liu, *Org. Lett.* **2013**, *15*, 1698–1701.

[39] W. Jiang, D. Sattler, K. Rissanen, C. A. Schalley, *Org. Lett.* **2011**, *13*, 4502–4505.

[40] W. Jiang, H. D. F. Winkler, C. A. Schalley, *J. Am. Chem. Soc.* **2008**, *130*, 13852–13853.

[41] W. Jiang, C. A. Schalley, *Proc. Natl. Acad. Sci. USA* **2009**, *106*, 10425–10429.

[42] H. W. Gibson, J. W. Jones, L. N. Zakharov, A. L. Rheingold, C. Slebodnick, *Chem.—Eur. J.* **2011**, *17*, 3192–3206.

[43] F. Huang, J. W. Jones, C. Slebodnick, H. W. Gibson, *J. Am. Chem. Soc.* **2003**, *125*, 14458–14464.

[44] J. W. Jones, H. W. Gibson, *J. Am. Chem. Soc.* **2003**, *125*, 7001–7004.

[45] T. B. Gasa, J. M. Spruell, W. R. Dichtel, T. J. Sørensen, D. Philp, J. F. Stoddart, P. Kuzmič, *Chem.—Eur. J.* **2009**, *15*, 106–116.

[46] C.-J. Chuang, W.-S. Li, C.-C. Lai, Y.-H. Liu, S.-M. Peng, I. Chao, S.-H. Chiu, *Org. Lett.* **2009**, *11*, 385–388.

[47] J. W. Steed, D. R. Turner, K. Wallace, *Core Concepts in Supramolecular Chemistry and Nanochemistry*, John Wiley & Sons, Ltd, Chichester, **2007**.

[48] K. Ariga, T. Kunitake, *Supramolecular Chemistry – Fundamentals and Applications*, Springer-Verlag, Heidelberg, **2006**.

[49] G. V. Oshovsky, D. N. Reinhoudt, W. Verboom, *Angew. Chem. Int. Ed.* **2007**, *46*, 2366–2393; *Angew. Chem.* **2007**, *119*, 2418–2445.

[50] R. M. Izatt, G. A. Clark, J. D. Lamb, J. E. King, J. J. Christensen, *Thermochim. Acta* **1986**, *97*, 115–126.

[51] R. M. Izatt, K. Pawlak, J. S. Bradshaw, R. L. Bruening, *Chem. Rev.* **1991**, *91*, 1721–2085.

[52] D. J. Cram, J. M. Cram, *Science* **1974**, *183*, 803–809.

[53] C. J. Pedersen, *J. Am. Chem. Soc.* **1967**, *89*, 2495–2496.

[54] C. J. Pedersen, *J. Am. Chem. Soc.* **1967**, *89*, 7017–7036.

[55] B. L. Haymore, J. D. Lamb, R. M. Izatt, J. J. Christensen, *Inorg. Chem.* **1982**, *21*, 1598–1602.

[56] R. M. Izatt, N. E. Izatt, B. E. Rossiter, J. J. Christensen, B. L. Haymore, *Science* **1978**, *199*, 994–996.

[57] R. M. Izatt, J. S. Bradshaw, S. A. Nielsen, J. D. Lamb, J. J. Christensen, D. Sen, *Chem. Rev.* **1985**, *85*, 271–339.

[58] R. M. Izatt, R. E. Terry, D. P. Nelson, Y. Chan, D. J. Eatough, J. S. Bradshaw, L. D. Hansen, J. J. Christensen, *J. Am. Chem. Soc.* **1976**, *98*, 7626–7630.

[59] R. M. Izatt, J. D. Lamb, N. E. Izatt, B. E. Rossiter, J. J. Christensen, B. L. Haymore, *J. Am. Chem. Soc.* **1979**, *101*, 6273–6276.

[60] H. An, J. S. Bradshaw, R. M. Izatt, *Chem. Rev.* **1992**, *92*, 543–572.

[61] G. W. Gokel, W. M. Leevy, M. E. Weber, *Chem. Rev.* **2004**, *104*, 2723–2750.

[62] D. J. Cram, R. C. Helgeson, L. R. Sousa, J. M. Timko, M. Newcomb, P. Moreau, F. de Jong, G. W. Gokel, D. H. Hoffman, L. A. Domeier, S. C. Peacock, K. Madan, L. Kaplan, *Pure Appl. Chem.* **1975**, *43*, 327–349.

[63] W. D. Curtis, D. A. Laidler, J. F. Stoddart, G. H. Jones, *J. Chem. Soc., Chem. Commun.* **1975**, *1975*, 835–837.

[64] V. Balzani, M. Clemente-León, A. Credi, J. N. Lowe, J. D. Badjić, J. F. Stoddart, D. J. Williams, *Chem.—Eur. J.* **2003**, *9*, 5348–5360.

[65] L. Jullien, J.-M. Lehn, *Tetrahedron Lett.* **1988**, *29*, 3803–3806.

[66] T. M. Fyles, T. D. James, A. Pryhitka, M. Zojaji, *J. Org. Chem.* **1993**, *58*, 7456–7468.

[67] N. Voyer, M. Robitaille, *J. Am. Chem. Soc.* **1995**, *117*, 6599–6600.

[68] J. A. A. De Boer, D. N. Reinhoudt, *J. Am. Chem. Soc.* **1985**, *107*, 5347–5351.

[69] M. Newcomb, S. S. Moore, D. J. Cram, *J. Am. Chem. Soc.* **1977**, *99*, 6405–6410.

[70] W. Jiang, A. Schäfer, P. C. Mohr, C. A. Schalley, *J. Am. Chem. Soc.* **2010**, *132*, 2309–2320.

[71] M.-V. Martínez-Díaz, N. Spencer, J. F. Stoddart, *Angew. Chem. Int. Ed. Engl.* **1997**, *36*, 1904–1907; *Angew. Chem.* **1997**, *109*, 1991–1994.

[72] P. R. Ashton, R. Ballardini, V. Balzani, I. Baxter, A. Credi, M. C. T. Fyfe, M. T. Gandolfi, M. Gómez-López, M.-V. Martínez-Díaz, A. Piersanti, N. Spencer, J. F. Stoddart, M. Venturi, A. J. P. White, D. J. Williams, *J. Am. Chem. Soc.* **1998**, *120*, 11932–11942.

[73] F. Coutrot, E. Busseron, *Chem.—Eur. J.* **2008**, *14*, 4784–4787.

[74] J. D. Badjić, V. Balzani, A. Credi, S. Silvi, J. F. Stoddart, *Science* **2004**, *303*, 1845–1849.

[75] M. Schliwa, G. Woehlke, *Nature* **2003**, *422*, 759–765.

[76] F. Coutrot, C. Romuald, E. Busseron, *Org. Lett.* **2008**, *10*, 3741–3744.

[77] Z. Meng, C.-F. Chen, *Chem. Commun.* **2015**, *51*, 8241–8244.

[78] F. Coutrot, *ChemistryOpen* **2015**, *4*, 556–576.

[79] A. Goujon, G. Du, E. Moulin, G. Fuks, M. Maaloum, E. Buhler, N. Giuseppone, *Angew. Chem. Int. Ed.* **2016**, *55*, 703–707; *Angew. Chem.* **2016**, *128*, 713–717.

[80] T. Akai, N. Nakamura, H. Chihara, *J. Chem. Soc., Faraday Trans.* **1993**, *89*, 1339–1343.

[81] R. Gratias, H. Kessler, *J. Phys. Chem. B* **1998**, *102*, 2027–2031.

[82] D. B. Smithrud, E. M. Sanford, I. Chao, S. B. Ferguson, D. R. Carcanague, J. D. Evanseck, K. N. Houk, F. Diederich, *Pure Appl. Chem.* **1990**, *62*, 2227–2236.

[83] F. Biedermann, V. D. Uzunova, O. A. Scherman, W. M. Nau, A. De Simone, *J. Am. Chem. Soc.* **2012**, *134*, 15318–15323.

[84] Y. Yamada, M.-a. Okada, K. Tanaka, *Chem. Commun.* **2013**, *49*, 11053–11055.

[85] Y. Yamada, T. Kato, K. Tanaka, *Chem.—Eur. J.* **2016**, *22*, 12371–12380.

[86] L. Kaufmann, C. A. Schalley in *Analytical Methods in Supramolecular Chemistry 2nd ed.*, *Vol. 1*, C. A. Schalley (Ed.), WILEY-VCH Verlag GmbH & Co. KGaA, Weinheim, **2012**, pp. 1–26.

[87] A. Whitty, *Nat. Chem. Biol.* **2008**, *4*, 435–439, In this Commentary, Whitty used the term "configurational cooperativity" instead of "chelate cooperativity".

[88] G. Ercolani, C. Piguet, M. Borkovec, J. Hamacek, *J. Chem. Phys. B* **2007**, *111*, 12195–12203.

[89] S. W. Benson, *J. Am. Chem. Soc.* **1958**, *80*, 5151–5154.

[90] D. M. Bishop, K. J. Laidler, *J. Chem. Phys.* **1965**, *42*, 1688–1691.

[91] G. Ercolani, *J. Am. Chem. Soc.* **2003**, *125*, 16097–16103.

[92] D. J. Diestler, E. W. Knapp, *Phys. Rev. Lett.* **2008**, *100*, 178101.

[93] D. J. Diestler, E. W. Knapp, *J. Chem. Phys. C* **2010**, *114*, 5287–5304.

[94] E. T. Mack, P. W. Snyder, R. Perez-Castillejos, G. M. Whitesides, *J. Am. Chem. Soc.* **2011**, *133*, 11701–11715.

[95] M. Weber, A. Bujotzek, R. Haag, *J. Chem. Phys.* **2012**, *137*, 054111.

[96] R. H. Kramer, J. W. Karpen, *Nature* **1998**, *395*, 710–713.

[97] A. J. Achazi, D. Mollenhauer, B. Paulus, *Beilstein J. Org. Chem.* **2015**, *11*, 687–692.

[98] M. F. Perutz, *Q. Rev. Biophys.* **1989**, *22*, 139–236.

[99] E. N. W. Howe, M. Bhadbhade, P. Thordarson, *J. Am. Chem. Soc.* **2014**, *136*, 7505–7516.

[100] E. N. Howe, G. E. Ball, P. Thordarson, *Supramol. Chem.* **2015**, *27*, 829–839.

[101] Y. Suzuki, T. Nakamura, H. Iida, N. Ousaka, E. Yashima, *J. Am. Chem. Soc.* **2016**, *138*, 4852–4859.

[102] C.-J. Tsai, A. del Sol, R. Nussinov, *Mol. BioSyst.* **2009**, *5*, 207–216.

[103] A. Cooper, D. T. F. Dryden, *Eur. Biophys. J.* **1984**, *11*, 103–109.

[104] V. J. Hilser, E. B. Thompson, *Proc. Natl. Acad. Sci. USA* **2007**, *104*, 8311–8315.

[105] G. Wilke, *Angew. Chem. Int. Ed.* **2003**, *42*, 5000–5008; *Angew. Chem.* **2003**, *115*, 5150–5159.

[106] K. Ziegler, H. Eberle, H. Ohlinger, *Justus Liebigs Ann. Chem.* **1933**, *504*, 94–130.

[107] S. L. Cockroft, C. A. Hunter, *Chem. Soc. Rev.* **2007**, *36*, 172–188.

[108] H. Sun, C. A. Hunter, C. Navarro, S. Turega, *J. Am. Chem. Soc.* **2013**, *135*, 13129–13141.

[109] G. S. Wilson, H. L. Anderson, *Chem. Commun.* **1999**, 1539–1540.

[110] M. Takeuchi, M. Ikeda, A. Sugasaki, S. Shinkai, *Acc. Chem. Res.* **2001**, *34*, 865–873.

[111] G. Ercolani, *Org. Lett.* **2005**, *7*, 803–805.

[112] P. J. Carter, G. Winter, A. J. Wilkinson, A. R. Fersht, *Cell* **1984**, *38*, 835–840.

[113] F. R. Fischer, P. A. Wood, F. H. Allen, F. Diederich, *Proc. Natl. Acad. Sci. USA* **2008**, *105*, 17290–17294.

[114] N. L. Traulsen, C. H.-H. Traulsen, P. M. Deutinger, S. Müller, D. Schmidt, I. Linder, C. A. Schalley, *Org. Biomol. Chem.* **2015**, *13*, 10881–10887.

[115] L. Kaufmann, N. L. Traulsen, A. Springer, H. V. Schröder, T. Mäkelä, K. Rissanen, C. A. Schalley, *Org. Chem. Front.* **2014**, *1*, 521–531.

[116] F. P. Schmidtchen in *Analytical Methods in Supramolecular Chemistry 2nd ed.*, *Vol. 1*, C. A. Schalley (Ed.), WILEY-VCH Verlag GmbH & Co. KGaA, Weinheim, **2012**, pp. 67–104.

[117] J. J. Christensen, R. M. Izatt, L. D. Hansen, J. A. Partridge, *J. Phys. Chem.* **1966**, *70*, 2003–2010.

[118] V. H. Le, R. Buscaglia, J. B. Chaires, E. A. Lewis, *Anal. Biochem.* **2013**, *434*, 233–241.

[119] G. A. Holdgate, *BioTechniques* **2001**, *31*, 164–184.

[120] J. E. Ladbury, B. Z. Chowdhry, *Chem. Biol.* **1996**, *3*, 791–801.

[121] M. E. Brown (Ed.), *Principles and Practice*, Vol. 1 of *Handbook of Thermal Analysis and Calorimetry*, Elsevier Science B.V., Amsterdam, **1998**.

[122] W. B. Turnbull, A. H. Daranas, *J. Am. Chem. Soc.* **2003**, *125*, 14859–14866.

[123] T. Wiseman, S. Williston, J. F. Brandts, L.-N. Lin, *Anal. Biochem.* **1989**, *179*, 131–137.

[124] A. I. Lazar, F. Biedermann, K. R. Mustafina, K. I. Assaf, A. Hennig, W. M. Nau, *J. Am. Chem. Soc.* **2016**, *138*, 13022–13029.

[125] A. J. Achazi, L. K. S. von Krbek, C. A. Schalley, B. Paulus, *J. Comput. Chem.* **2016**, *37*, 18–24.

[126] L. K. S. von Krbek, A. J. Achazi, M. Solleder, M. Weber, B. Paulus, C. A. Schalley, *Chem.—Eur. J.* **2016**, *22*, 15475–15484.

[127] Structures were modeled with *CaChe 5.0* program package, Fujitsu, Krakow/Poland.

[128] K. Nowosinski, L. K. S. von Krbek, N. L. Traulsen, C. A. Schalley, *Org. Lett.* **2015**, *17*, 5076–5079.

[129] L. K. S. von Krbek, A. J. Achazi, S. Schoder, M. Gaedke, T. Biberger, B. Paulus, C. A. Schalley, *Chem.—Eur. J.* **2017**, *23*, 2877–2883.

[130] M. Lohse, K. Nowosinski, N. L. Traulsen, A. J. Achazi, L. K. S. von Krbek, B. Paulus, C. A. Schalley, S. Hecht, *Chem. Commun.* **2015**, *51*, 9777–9780.

[131] M. Lohse, L. K. S. von Krbek, S. Radunz, S. Moorthy, C. A. Schalley, S. Hecht, *Beilstein J. Org. Chem.* **2015**, *11*, 748–762.

[132] M. Lohse, *PhD Thesis*, Humboldt-Universität zu Berlin, **2015**.

Appendix: Publications

A.1 Theoretical and experimental investigation of crown/ammonium complexes in solution

Andreas J. Achazi, Larissa K. S. von Krbek, Christoph A. Schalley, and Beate Paulus

J. Comput. Chem. **2016**, *37*(1), 18–24.

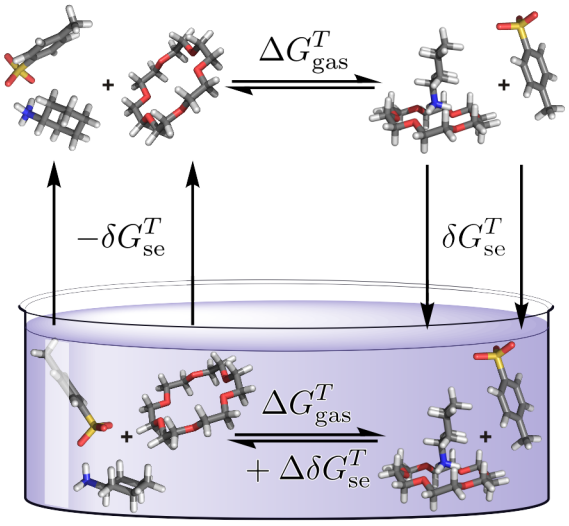

Figure A.2. Graphical abstract.
Reprinted with permission from Achazi et al.[125] (© 2015 Wiley Periodicals, Inc).

Submitted on 22 December 2014, first published on 13 April 2015 in the *Journal of Computational Chemistry*. For copyright reasons, the article is not included in the online version of this thesis.

An electronic version of the article is available (DOI: 10.1002/jcc.23914).

A.2 Allosteric and chelate cooperativity in divalent crown ether/ammonium complexes with strong binding enhancement

Larissa K. S. von Krbek, Andreas J. Achazi, Marthe Solleder, Marcus Weber, Beate Paulus, and Christoph A. Schalley

Chem.—Eur. J. **2016**, *22*(43), 15475–15484.

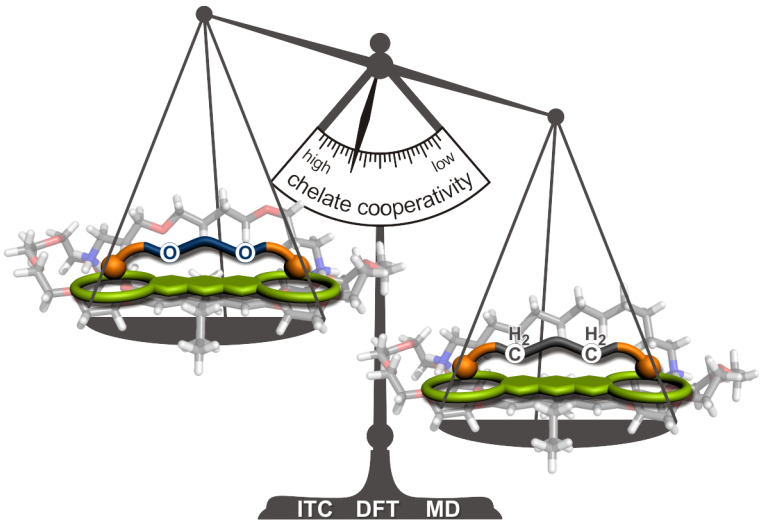

Figure A.3. Graphical abstract.
Reprinted with permission from von Krbek et al.[126] (© 2016 Wiley-VCH Verlag GmbH & Co. KGaA, Weinheim).

Submitted on 29 June 2016, first published on 13 September 2016 in *Chemistry—A European Journal*. For copyright reasons, the article is not included in the online version of this thesis.

An electronic version of the article is available (DOI: 10.1002/chem.201603098).

A.3 Thermodynamic analysis of allosteric and chelate cooperativity in di- and trivalent ammonium/crown-ether pseudorotaxanes

Karol Nowosinski, Larissa K. S. von Krbek, Nora L. Traulsen, and Christoph A. Schalley

Org. Lett. **2015**, *17*(20), 5076–5079.

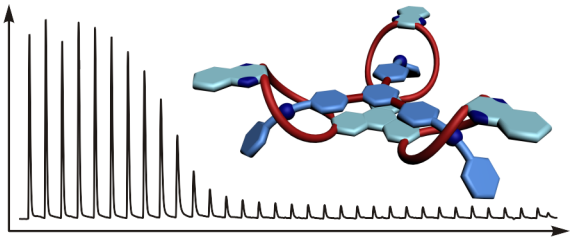

Figure A.4. Graphical abstract.
Reprinted with permission from Nowosinski et al.[128] (© 2015 American Chemical Society).

Submitted on 08 September 2015, first published on 06 October 2015 in *Organic Letters*. For copyright reasons, the article is not included in the online version of this thesis.

An electronic version of the article is available (DOI: 10.1021/acs.orglett.5b02592).

A.4 The delicate balance of preorganisation and adaptability in multiply bonded host–guest complexes

Larissa K. S. von Krbek, Andreas J. Achazi, Stefan Schoder, Marius Gaedke, Tobias Biberger, Beate Paulus, and Christoph A. Schalley

Chem.—Eur. J. **2017**, *23*(12), 2877–2883.

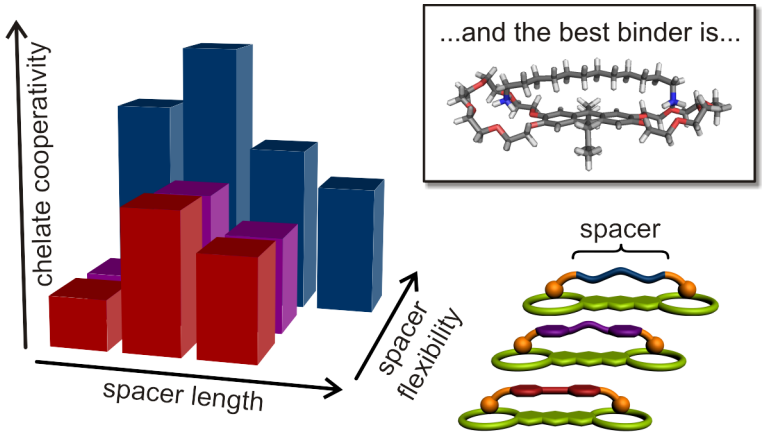

Figure A.5. Graphical abstract.
Reprinted with permission from von Krbek et al.[129] (© 2017 Wiley-VCH Verlag GmbH & Co. KGaA, Weinheim).

Submitted on 01 November 2016, first published on 31 January 2017 in *Chemistry—A European Journal*. For copyright reasons, the article is not included in the online version of this thesis.

An electronic version of the article is available (DOI: 10.1002/chem.201605092).

A.5 Gating the photochromism of an azobenzene by strong host–guest interactions in a divalent pseudo[2]rotaxane

Mirko Lohse, Karol Nowosinski, Nora L. Traulsen, Andreas J. Achazi, Larissa K. S. von Krbek, Beate Paulus, Christoph A. Schalley, and Stefan Hecht

Chem. Commun. **2015**, *51*(48), 9777–9780.

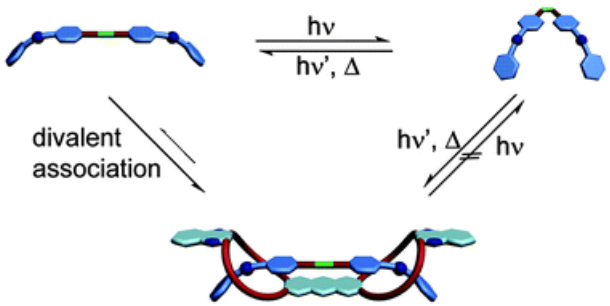

Figure A.6. Graphical abstract.
Reprinted with permission from Lohse et al.[130] (© 2015 The Royal Society of Chemistry).

Submitted on 04 April 2015, first published on 01 May 2015 in *Chemical Communications*. For copyright reasons, the article is not included in the online version of this thesis.

An electronic version of the article is available (DOI: 10.1039/C5CC02811F).

A.6 Discrete multiporphyrin pseudorotaxane assemblies from di- and tetravalent porphyrin building blocks

Mirko Lohse, Larissa K. S. von Krbek, Sebastian Radunz, Suresh Moorthy, Christoph A. Schalley, and Stefan Hecht

Beilstein J. Org. Chem. **2015**, *11*(4), 748–762.

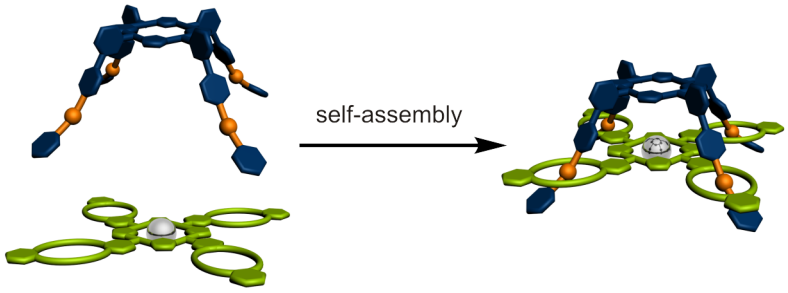

Figure A.7. Graphical abstract.
Reprinted with permission from Lohse et al.[131] (© 2015 Lohse et al.; licensee Beilstein-Institut).

Submitted on 28 February 2015, first published on 2 May 2015 in the *Beilstein Journal of Organic Chemistry*.

An electronic version of the article is available (DOI: 10.3762/bjoc.11.85).

BEILSTEIN JOURNAL OF ORGANIC CHEMISTRY

Discrete multiporphyrin pseudorotaxane assemblies from di- and tetravalent porphyrin building blocks

Mirko Lohse[1], Larissa K. S. von Krbek[2], Sebastian Radunz[1], Suresh Moorthy[2], Christoph A. Schalley[*2] and Stefan Hecht[*1]

Full Research Paper

Open Access

Address:
[1]Department of Chemistry, Humboldt-Universität zu Berlin, Brook-Taylor-Str. 2, 12489 Berlin, Germany. Fax: +49 (0)30 2093-6940; Tel: +49 (0)30 2093-7308 and [2]Institut für Chemie und Biochemie, Freie Universität Berlin, Takustraße 3, 14195 Berlin, Germany. Fax: +49(0)308385-5366; Tel: +49(0)308385-2639

Email:
Christoph A. Schalley[*] - christoph@schalley-lab.de; Stefan Hecht[*] - sh@chemie.hu-berlin.de

* Corresponding author

Keywords:
crown ethers; multicomponent assembly; multivalency; porphyrins; pseudorotaxanes

Beilstein J. Org. Chem. **2015,** *11,* 748–762.
doi:10.3762/bjoc.11.85

Received: 28 February 2015
Accepted: 29 April 2015
Published: 12 May 2015

This article is part of the Thematic Series "Multivalency as a chemical organization and action principle".

Guest Editor: R. Haag

Abstract

Two pairs of divalent and tetravalent porphyrin building blocks carrying the complementary supramolecular crown ether/secondary ammonium ion binding motif have been synthesized and their derived pseudorotaxanes have been studied by a combination of NMR spectroscopy in solution and ESI mass spectrometry in the gas phase. By simple mixing of the components the formation of discrete dimeric and trimeric (metallo)porphyrin complexes predominates, in accordance to binding stoichiometry, while the amount of alternative structures can be neglected. Our results illustrate the power of multivalency to program the multicomponent self-assembly of specific entities into discrete functional nanostructures.

Introduction

Supramolecular chemistry [1], the chemistry “beyond the molecule“ [2], has immensely reshaped the concepts of chemistry by putting the intermolecular interaction into the focus. Different fields of chemistry, from materials [3-6] and analytical sciences [7-12] to life science [13-17] have benefited from the development of the basic concepts of molecular recognition, templation [18], self-assembly [19], or self-sorting [20,21], just to name a few. More recently, multivalent binding [22-24] and cooperativity [25,26] have attracted significant attention mediated in particular by the desire to understand biological phenomena, such as virus docking to cells [27], toxin inhibition [28], or leucocyte recruitment in inflammation processes of the endothelium [29]. Multivalency has also inspired synthetic supramolecular architecture as it not only contributes to binding enhancement, but also helps to exert control over complex formation. For example, “molecular elevators” have been

constructed by Stoddart et al. [30,31] and giant porphyrin wheels were prepared by Anderson and co-workers [32,33], both using a multivalent template strategy.

The crown ether/secondary ammonium ion binding motif [34] is a powerful tool to create well-defined pseudorotaxane structures [35-39], which have also served as precursors in rotaxane syntheses [40-42] thus providing access to interlocked, mechanically bound molecules. Based on these structures, functional supramolecular architectures such as molecular switches and motors [43-45] as well as artificial muscles [46-50], have been synthesized.

Due to their four-fold symmetry, porphyrins are excellent candidates to extend these concepts to tetravalent supramolecules. Beyond being a mere spacer and scaffold connecting the binding sites, porphyrins also offer interesting physical and optical properties [51,52]. Therefore, they have played a pivotal role in supramolecular chemistry [53-66], for example as potential candidates for artificial light-harvesting systems [67-73].

Here, we report the synthesis of two new porphyrin-based di- and tetravalent ammonium guest molecules **A2** and **A4** and their complementary porphyrin-based di- and tetravalent crown ether hosts **C2** and **C4** (Figure 1). The selection of these building blocks is based on force-field calculations, which suggest a good geometric fit between the crown ether hosts and the ammonium ion guests. The two monovalent building blocks **A1** and **C1** serve as control compounds. Based on this

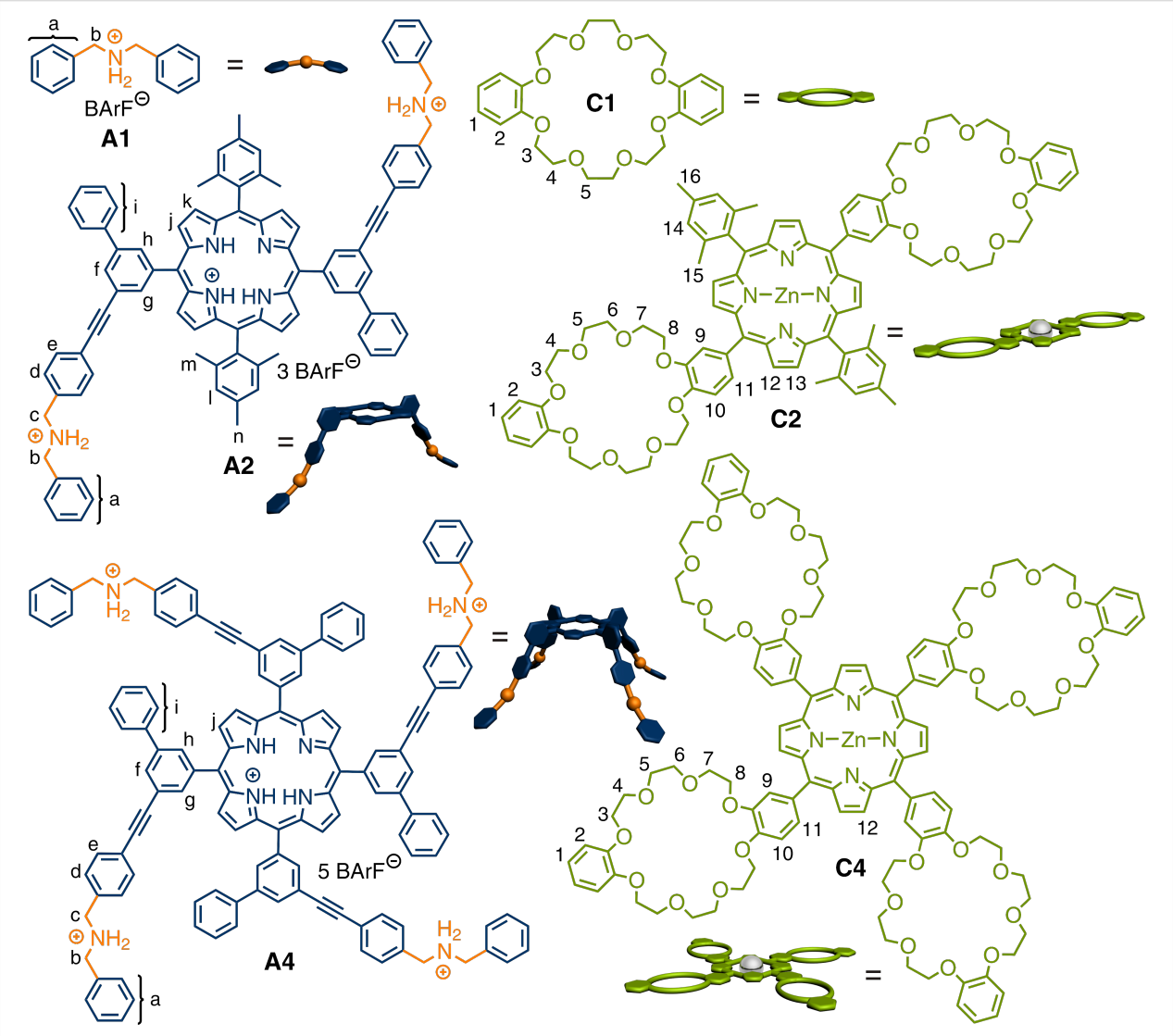

Figure 1: Mono-, di-, and tetravalent axles **A1**, **A2** and **A4** and mono-, di-, and tetravalent hosts **C1**, **C2** and **C4**. Numbers and letters are assigned to specific H atoms as discussed later in the main text.

"toolbox", which can be expanded in the future with other functional building blocks, the formation of specific multiply threaded pseudorotaxanes was achieved, thereby demonstrating the ability to program complex multicomponent self-assembly [74,75].

Results and Discussion

Synthesis

The synthesis of the two ammonium-substituted porphyrins **A2** and **A4** was performed convergent by first preparing two different (zinc)porphyrin cores **1** and **2** (Scheme 1), which are

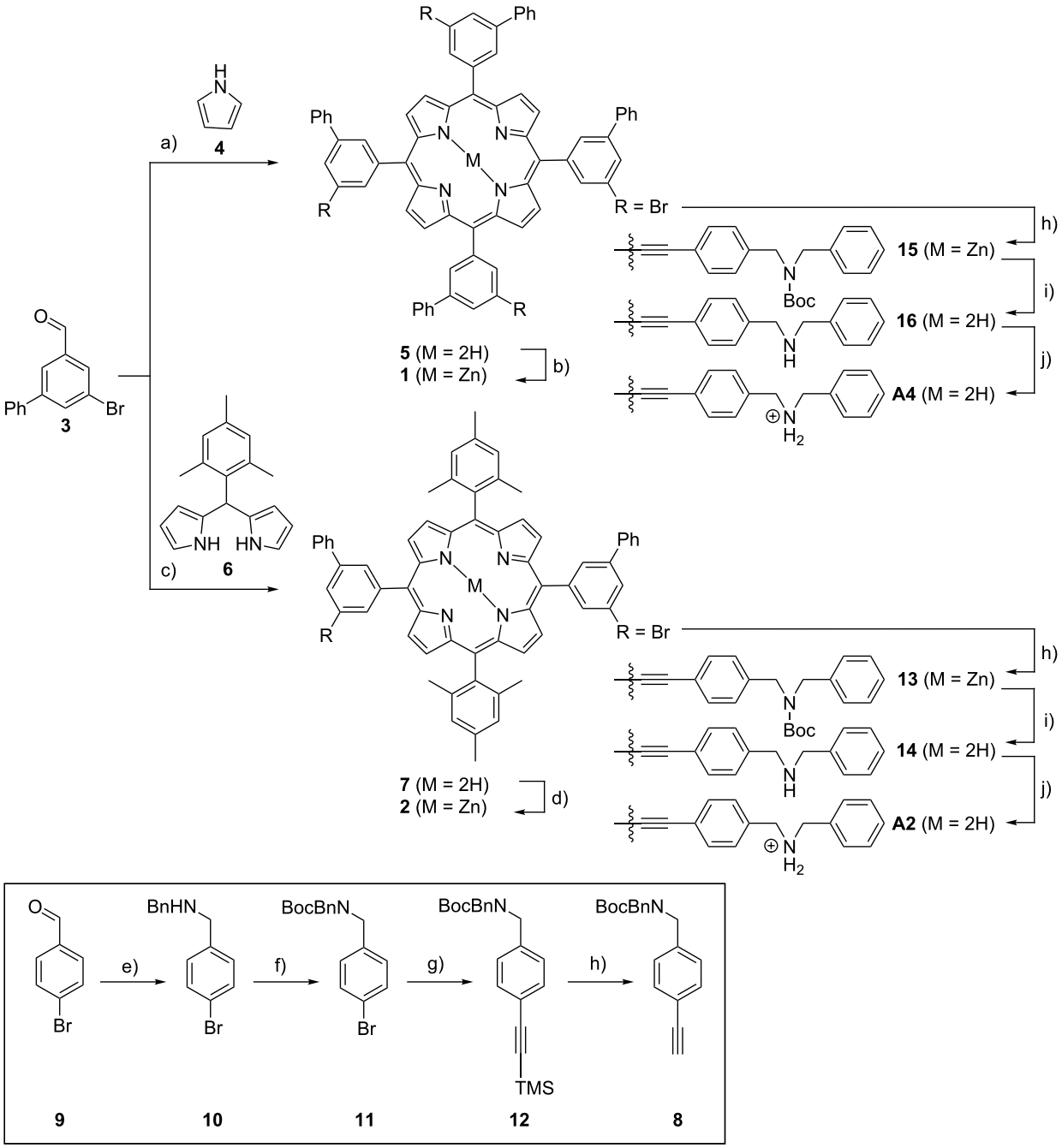

Scheme 1: Overview of the synthesis of the guests **A2** and **A4**. a) Pyrrole (**4**), $BF_3{\cdot}Et_2O$, DDQ, $CHCl_3$, rt; b) $Zn(OAc)_2$, $CHCl_3$/MeOH, rt; c) dipyrromethane **6**, $BF_3{\cdot}Et_2O$, DDQ, $CHCl_3$, rt; d) $Zn(OAc)_2$, $CHCl_3$/MeOH, rt; e) 1. benzylamine, trimethyl orthoformate, rt, 2. $NaBH_4$, THF/MeOH, rt; f) Boc_2O, triethylamine, CH_2Cl_2, rt; g) 1. ethynyltrimethylsilane, CuI, PPh_3, $Pd(PPh_3)_4$, TEA, toluene, 80 °C, 2. KOH, THF, rt; h) precursor **8**, CuI, PPh_3, $Pd(PPh_3)_4$, TEA, toluene, 80 °C; i) TFA, CH_2Cl_2, rt; j) 1. HCl, MeOH/$CHCl_3$, rt, 2. NaBArF, MeOH.

equipped with two and four bromine atoms in the *m*-position of the *meso*-phenyl substituents, respectively, for further functionalization. Zinc porphyrins **1** and **2** have been synthesized following standard protocols for symmetrical [76] A_4 and *trans*-disubstituted [77] A_2B_2 *meso*-functionalized porphyrins. The tetrabrominated core **1** was synthesized from aldehyde **3** and pyrrole (**4**) to form the free base porphyrin **5**, which is subsequently converted into its zinc complex **1**. On the other hand the difunctional core **2** was obtained through the condensation of aldehyde **3** with mesityldipyrromethane (**6**) followed by metalation of the intermediately formed free base porphyrin **7** to give its respective zinc complex **2**. In the next step, axle precursor **8** was synthesized by reductive amination of 4-bromobenzaldehyde (**9**) and benzylamine yielding amine **10**, which was subsequently Boc-protected, then reacted with trimethylsilylacetylene in a Sonogashira cross-coupling followed by desilylation. Finally, the porphyrin cores **1** and **2** were combined with axle precursor **8** in another two and four-fold Sonogashira cross-coupling reaction. After deprotection of the termini of the attached axles with trifluoroacetic acid (TFA), protonation of the free amines with HCl, and anion exchange with sodium tetrakis(3,5-bis(trifluoromethyl)phenyl)borate (NaBArF), the target compounds **A2** and **A4** were obtained. The weakly coordinating BArF counter-ion has been used to overcome solubility problems in organic solvents. It should be noted that the porphyrin is demetalated to yield the free base porphyrin during the deprotection of the Boc group. Furthermore, NMR integration of signals corresponding to the BArF protons relative to those corresponding to the macrocycle indicates that the porphyrin core is protonated (three BArF anions per divalent guest **A2**; five BArF anions per tetravalent guest **A4**). Based on the assumption that protonation of the porphyrin core, which is rather remote to the primary binding sites, does not influence the association strongly, no selective deprotonation of the porphyrin core has been attempted.

The preparation of the corresponding crown ether hosts (Scheme 2) involved an initial Williamson ether synthesis in which catechol (**17**) was first extended with 2-[2-(2-chloroethoxy)ethoxy]ethanol to diol **18**, which was then converted in dibromide **19** by an Appel reaction. Macrocyclization of **19** with 3,4-dihydroxybenzaldehyde under "pseudo high-

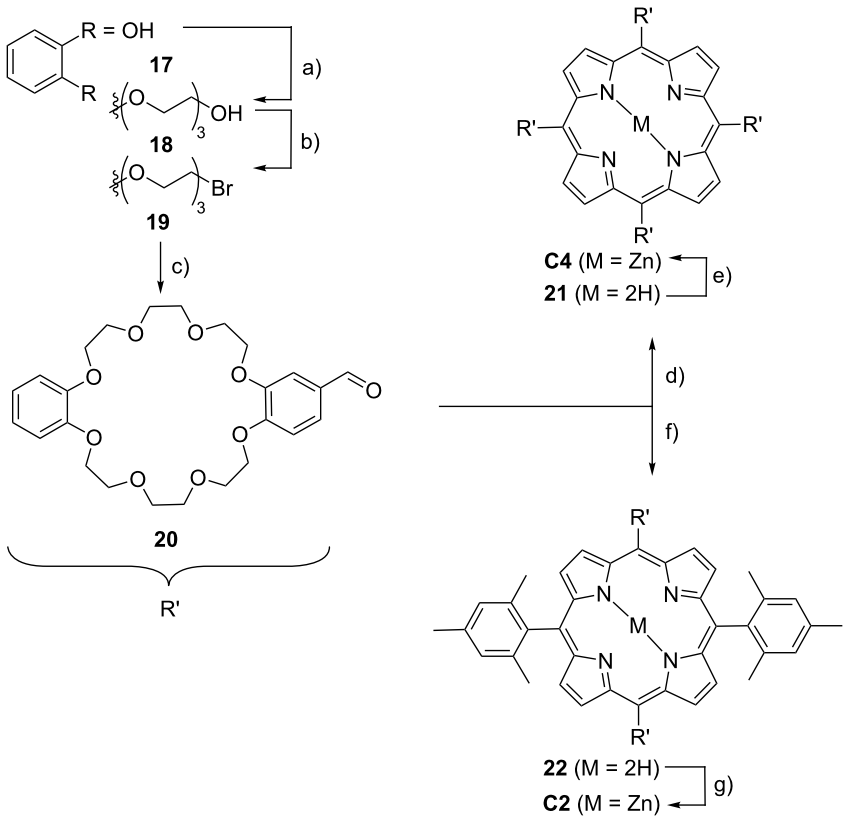

Scheme 2: Synthesis of crown ether hosts **C4** and **C2**: a) K_2CO_3, LiBr, **17**, 2-[2-(2-chloroethoxy)ethoxy]ethanol, DMF, 100 °C; b) CBr_4, PPh_3, CH_2Cl_2, rt; c) Cs_2CO_3, 3,4-dihydroxybenzaldehyde, DMF, 85 °C; d) 1. pyrrole (**4**), propionic acid, 140 °C, 2. $Zn(OAc)_2$, MeOH/$CHCl_3$, rt; e) 1. dipyrromethane (**6**), $BF_3{\cdot}Et_2O$, DDQ, $CHCl_3$, rt, 2. $Zn(OAC)_2$, MeOH/$CHCl_3$, rt.

dilution" conditions, i.e., slow addition of the two reactants into a solution of Cs_2CO_3 in DMF at 100 °C provides the corresponding crown ether aldehyde **20**. Porphyrin synthesis using **20** and pyrrole (**4**) following the Lindsey protocol [77] for A_4 porphyrins gives the desired tetravalent porphyrin host as the free base **21**, which is subsequently converted into the desired product **C4** by metalation using zinc(II) acetate. Host **C2** was synthesized according to the above-mentioned standard procedure [76] for *trans*-A_2B_2-porphyrins from **20** and mesityldipyrromethane **6** to form the divalent free base porphyrin **22**. Final zinc insertion provides the desired host **C2**.

For further detailed synthetic procedures and characterization data the reader is referred to Supporting Information File 1.

Formation and characterization of complexes

NMR spectroscopy of simple pseudorotaxanes prepared from crown ether wheels and secondary ammonium axles provides complexation-induced shift data, which can be easily interpreted and yield insight into complexation. Earlier experiences with divalent crown/ammonium pseudorotaxanes however also demonstrated that the NMR spectroscopic approach is often rather limited for more complex structures [78], as very complicated spectra are obtained with typically overlapping signals that prevent further (straightforward) analysis. Another complication, which makes the NMR analysis difficult, is the fact that the di- and tetravalent crown ethers **C2** and **C4** are achiral themselves, but become chiral, when complexed to axle components **A2** and **A4**. Consequently, the signals for all methylene protons of the crown ethers split into two diastereotopic ones not only producing another set of signals, but also more complicated splitting patterns. Furthermore, the crown ethers are connected to the porphyrin core by single bonds, around which they can easily rotate in the non-complexed state. This rotation is, however, fixed upon complexation and two possible orientations of each of the crown ethers on its corresponding axle are possible. One can therefore expect a mixture of stereoisomers to form. In the simplest case, **A2@C2**, two enantiomers and one *meso*-form are expected to exist, which should result in two overlapping sets of signals. For the other three complexes, the situation is even more complicated. Therefore, a straightforward and easy analysis of the NMR spectra will likely be impossible.

In our earlier studies [37,78,79], however, electrospray ionization (ESI) mass spectrometry (MS) turned out to be a perfectly suited method to characterize the complexes present in solution. The formation of unspecific complexes as well as fragmentation upon ionization have been found to be quite limited so that the picture obtained from the mass spectra can be expected to provide realistic insights into the composition of the complexes present in solution. As all stereoisomers have the same elemental composition, their presence as a mixture does not obscure the mass spectrometric results. For these reasons, we describe our NMR spectroscopic data, but focus on ESI–MS of the complexes under study starting with the four possible combinations of **A2** and **A4** with monovalent dibenzo[24]crown-8 **C1** as well as of **C2** and **C4** with monovalent dibenzylammonium **A1** (Figure 2, top), followed by the results obtained for the multivalent 1:1 and 2:1 complexes **A2@C2**, **A2$_2$@C4**, **A4@C2$_2$** and **A4@C4** (Figure 2, bottom).

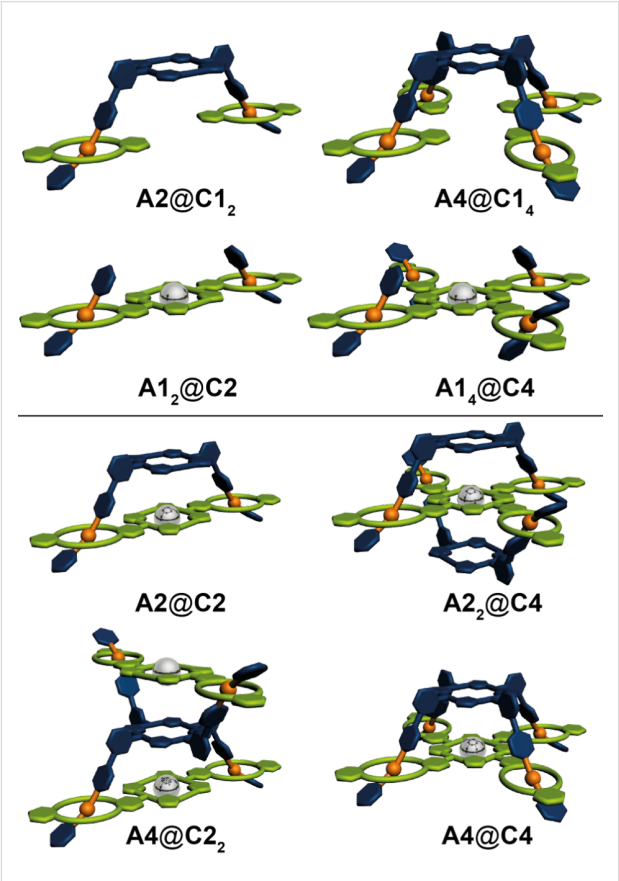

Figure 2: Schematic representation of the host–guests complexes. Top: complexes **A2@C1$_2$**, **A4@C1$_4$**, **A1$_2$@C2** and **A1$_4$@C4**, which are built from one multi- and several monovalent building blocks. Bottom: complexes **A2@C2, A2$_2$@C4, A4@C2$_2$** and **A4@C4**, which are built from di- or tetravalent building blocks.

[3]- and [5]pseudorotaxanes from monovalent building blocks

First the association of **A2** and **A4** with monovalent **C1** as well as **C2** and **C4** with monovalent **A1** was investigated and it can be seen that in all four cases successful complexation with the expected stoichiometry was achieved. For instance, upon addition of **C1** to a 3 mM solution of **A2** (Figure 3a) a continuous complexation, indicated by the appearance of a new set of signals due to slow exchange rates on the NMR-time scale,

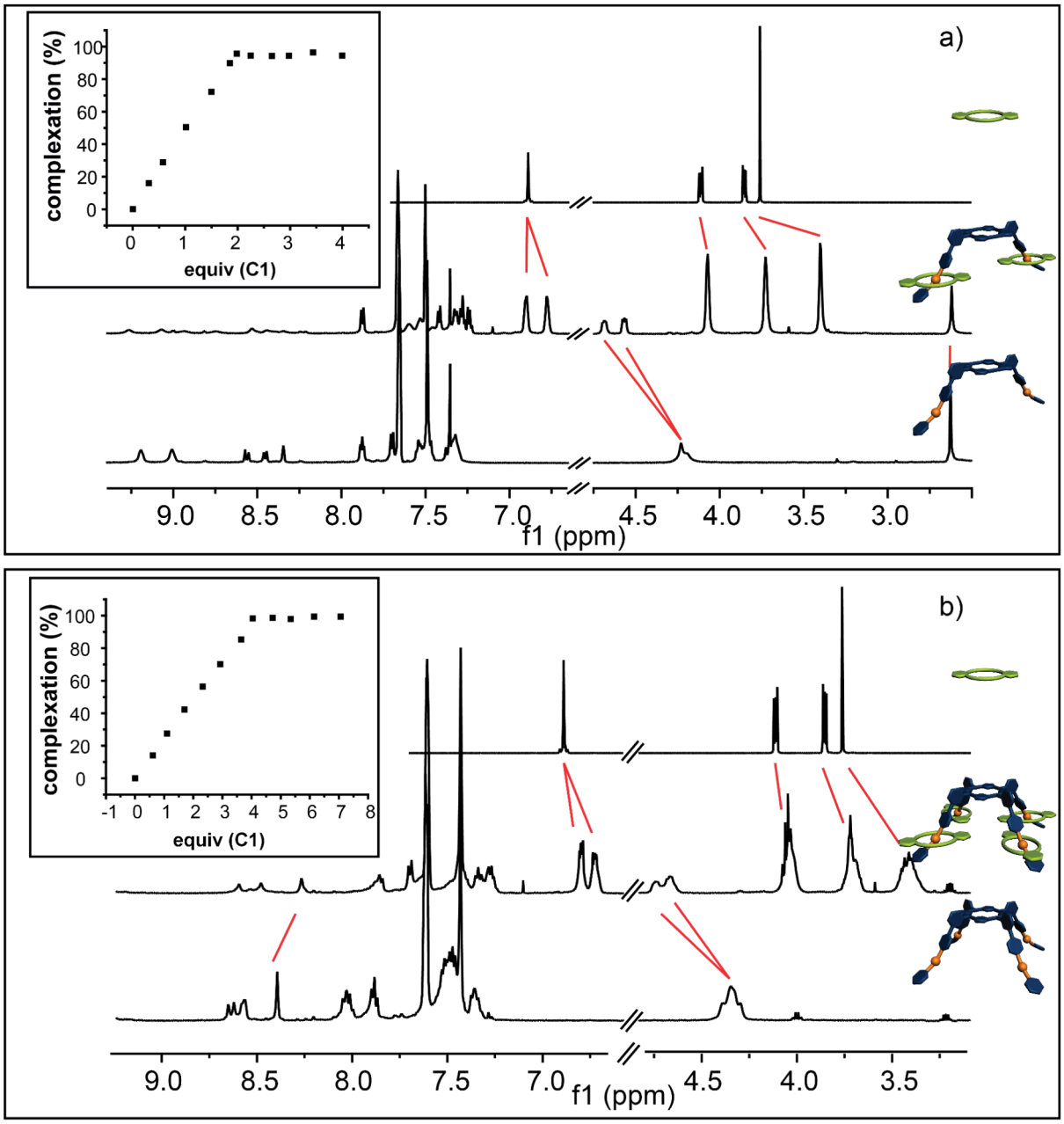

Figure 3: ^{1}H NMR (500 MHz, 298 K, CD_2Cl_2, 3 mM) of a) **C1** (top), **A2@C1$_2$** (middle) and **A2** (bottom); b) **C1** (top), **A4@C1$_4$** (middle) and **A4** (bottom) showing clear evidence of the complexation. The red lines indicate the shift of the proton signals upon addition. The inserts show the titration curve of each complexation with the expected ratio of the complex formed.

could be observed. Upon association the benzyl signals $H^{b/c}$ shift downfield by approximately +0.3 ppm and split into two separate pair of signals, which is typical for a complexation of **C1** with a dibenzylammonium moiety [36]. The aromatic signals of **C1** $H^{1/2}$ shift slightly upfield by −0.1 ppm and split as well. The signals of the crown ether region shift upfield by −0.05, −0.14, and −0.38 ppm due to complexation. An overstoichiometric addition of **C1** results in no further association (see Figure 3a, inset), clearly proving the desired host–guest ratio in the supramolecular structure. Similar results are obtained for the other [3]- and [5]pseudorotaxanes (Figure 3b and Figure 4a,b). However, it should be noted that despite extensive titration experiments (see Supporting Information File 1 for details) a detailed analysis of the binding constants of these systems cannot be obtained as the binding constants are too high for a NMR-based method.

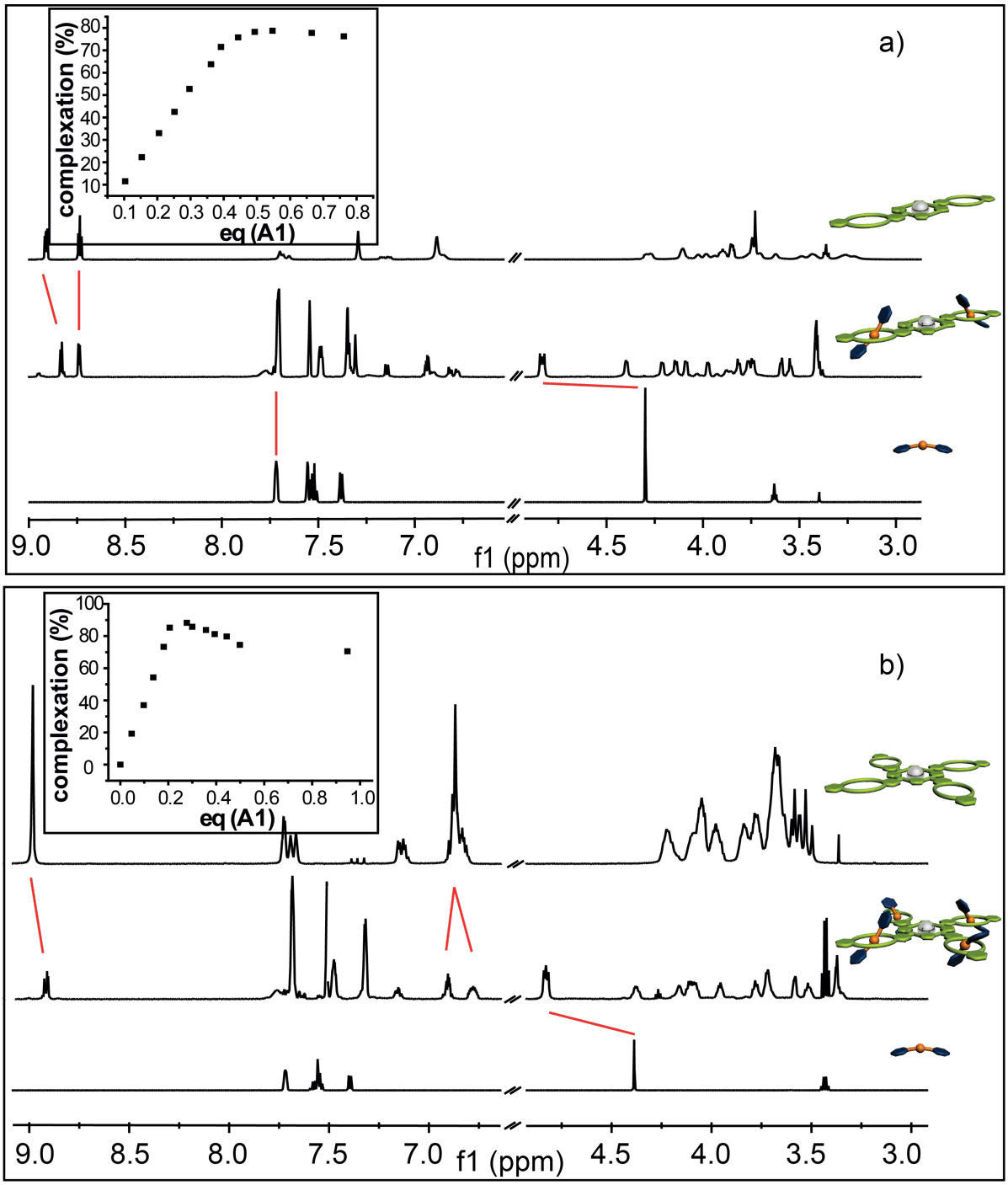

Figure 4: ^{1}H NMR (500 MHz, 298 K, CD_2Cl_2, 3 mM) of a) **C2** (top), **A1$_2$@C2** (middle) and **A1** (bottom) and b) **C4** (top), **A1$_4$@C4** (middle) and **A1** (bottom) showing clear evidence of the complexation. The red lines indicate the shift of the proton signals upon addition. The inserts show the titration curve of each complexation with the expected ratio of the complex formed.

Guests **A2** and **A4** as well as the hosts **C2** and **C4** show typical absorption behavior for porphyrin-based molecules. All four have pronounced absorption maxima at around 420 nm (Soret band) and less intense absorption bands between 500 and 600 nm (Q-bands). However, **A4** shows rather strong aggregation even in the µM concentration regime likely caused by elec-

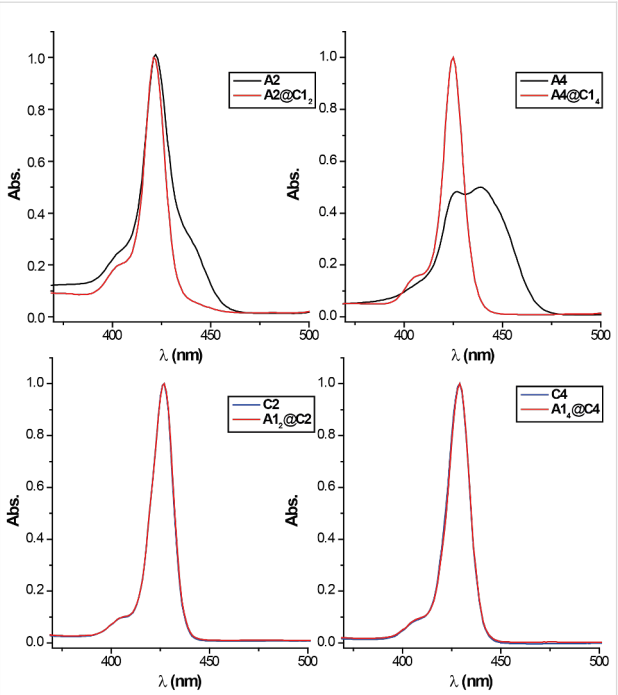

Figure 5: Normalized UV–vis absorption spectra (CH_2Cl_2, 3 μM) of **A2**, **A4**, **C2** and **C4** and their complexes formed with the monovalent building blocks **A1** and **C1** showing no significant batho- or hypsochromic shift. Absorption spectrum of **A4** was normalized to 0.5 because of the strong self-aggregation and the resulting broad Soret band.

trostatic interactions mediated by the closely associated BArF counter-ions that are expected to be significant as rather non-polar solvents are being used. This aggregation results in a broad red-shifted absorption band. Upon complexation this aggregate is broken, resulting in the recovery of a typical sharp Soret band at 420 nm. Note that UV–vis titration shows no significant batho- or hypsochromic shift upon association (Figure 5) of neither di- and tetravalent guests **A2** and **A4** with monovalent host **C1** nor of monovalent guest **A1** to the di- and tetravalent hosts **C2** and **C4**. The lack of such optical signature of the complexation event in the characteristic porphyrin absorption can be explained by the fact that the binding sites are electronically decoupled from the porphyrin core.

The [3]- and [5]pseudorotaxanes with the monovalent building blocks were further investigated by ESI-Q-TOF mass spectrometry. Separate solutions of hosts and guests were prepared (**A1**/**C1**: 4 mM, **A2**/**C2**: 2 mM, **A4**/**C4**: 1 mM all in CH_2Cl_2), and the same aliquots of the individual solutions were combined to obtain equal concentrations of ammonium ion functions and crown ether moieties in each solution. The solutions of the pseudorotaxanes were allowed to equilibrate for 24 hours at room temperature and diluted to 0.2 μM prior to analysis. The respective [3]- or [5]pseudorotaxanes could be detected for all mixtures (Figure 6). In the cases of the 1:2 and 1:4 mixtures of **A2** and **A4** with **C1**, respectively, the respective pseudorotaxanes **A2**@**C1**$_2$ and **A4**@**C1**$_4$ give rise to the second and third most abundant species (Figure 6a,b). One signal represents the desired doubly, respectively quadruply charged pseudorotaxane ([**A2**@**C1**$_2$]$^{2+}$ at m/z 1094 and [**A4**@**C1**$_4$]$^{4+}$ at m/z = 898). In addition, a second set of signals for the triply, respectively five-fold charged species ([**A2**@**C1**$_2$ + H]$^{3+}$ at m/z = 729 and [**A4**@**C1**$_4$ + H]$^{5+}$ at m/z = 719) could be observed. The most abundant species – most probably due to its high ESI response factor – is the one sodium ion containing molecular ion of **C1** ([Na@**C1**]$^{+}$ at m/z 471, see Supporting Information File 1). The spectra of the di- and tetravalent hosts **C2** and **C4** and the monovalent guest **A1** show a more complex signal pattern (Figure 6c,d). In the mixture of divalent crown ether **C2** with **A1** three different species in a statistical distribution of 1:2:1 were detected: the host with two axles [**A1**$_2$@**C2**]$^{2+}$ (m/z = 948), the host with one axle and one sodium ion [Na**A1**@**C2**]$^{2+}$ (m/z = 861) and the host loaded with two sodium ions ([Na$_2$@**C2**]$^{2+}$ m/z = 773). This can be easily explained with the nature of the ESI spray process, which is known to cause the dissociation in multiply charged non-covalently bound complexes. The results of the NMR titrations, however, clearly indicate the doubly bound pseudorotaxane **A1**$_2$@**C2** to be the most prominent species in solution (Figure 4a). The fact that the desired pseudorotaxane **A1**$_2$@**C2** can be detected by mass spectrometry despite the likely dissociation of the multiply charged complex in the ion source shows that this technique gives reasonable results for determining the species present in solution. The 4:1 mixture of **A1** and **C4** gives rise to an even more complex signal pattern (Figure 6d). Due to the four binding sites of **C4**, there are numerous possibilities of **A1** and sodium cations to bind. There are species with three or four guest ions detected with an approximately statistic distribution: [Na$_{(4-x)}$**A1**$_x$@**C4**]$^{4+}$ (x = 1, 2, 3, 4) and [Na$_{(3-y)}$**A1**$_y$@**C4**]$^{3+}$ (y = 1, 2, 3). The desired [5]pseudorotaxane is not very stable at the ionization conditions, but is nevertheless detected ([**A1**$_4$@**C4**]$^{4+}$ at m/z = 737). As explained above, this shows that mass spectrometry gives a reasonable image of the species present in solution, because we already know from NMR titration studies that the [5]pseudorotaxane **A1**$_4$@**C4** is the predominant species in solution (Figure 4b).

To summarize, all four desired [3]- or [5]pseudorotaxanes could be detected by mass spectrometry despite the likeliness of **A1**$_2$@**C2** and **A1**$_4$@**C4** to dissociate upon electrospray ionization. These results show that mass spectrometry should be a well suited method for the investigation of the multivalent pseudorotaxanes under study. These usually show much higher binding constants than the monovalent analogue and should therefore very likely survive the ionization process.

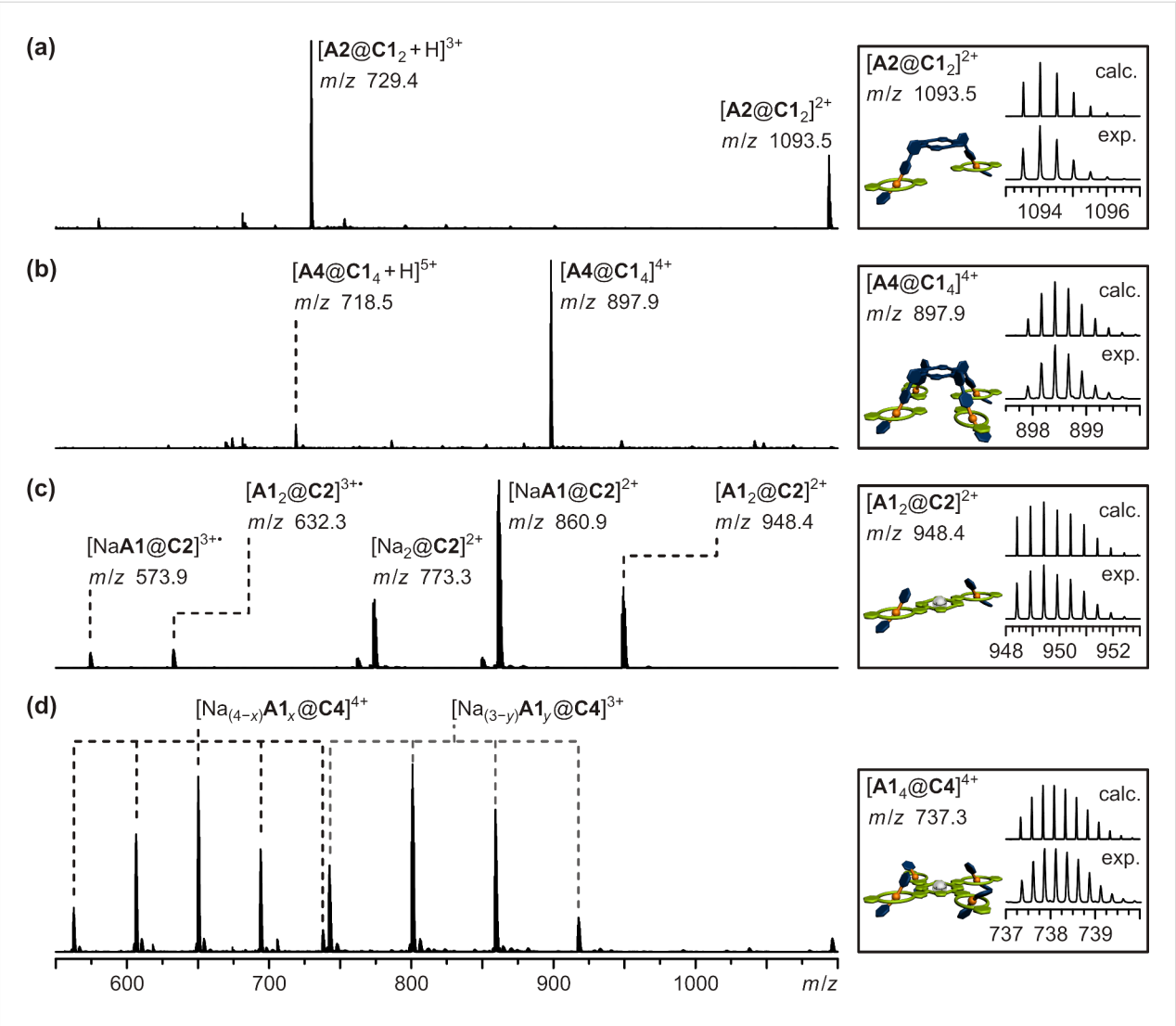

Figure 6: ESI-Q-TOF-MS spectra (CH_2Cl_2, 0.2 μM; left hand side) and respective experimental and calculated isotopic patterns of the desired [3]- or [5]pseudorotaxanes (right hand side): a) 1:2 mixture of **A2** and **C1**, b) 1:4 mixture of **A4** and **C1**, c) 2:1 mixture of **A1** and **C2**, d) 4:1 mixture of **A1** and **C4**. For reasons of clarity not all of the peaks are assigned (see Supporting Information File 1 for details).

[2]- and [3]pseudorotaxanes from di- and tetravalent building blocks

Subsequently, we investigated the di- and tetravalent pseudorotaxanes formed between **A2**, **A4**, **C2**, and **C4**. As already mentioned above, NMR spectroscopy is limited for the given systems because of the numerous isomers that can be formed. However, some general conclusion can be made. In all four cases one can observe a shift of the benzylic protons $H^{b/c}$ down field by approximately 0.5 ppm, which is typical for the threading in a crown ether/secondary ammonium ion binding motif. Furthermore, the signals for the crown ether region broaden significantly, which is in agreement with the assumption that upon complexation the number of signals increases because the methylene protons become diasterotopic and different supramolecular stereoisomers can form. However, based on the present NMR spectroscopy data (Figure 7 and Figure 8) one cannot exclude the formation of polymeric aggregates or only partially threaded structures. For this reason the formed complexes were analyzed in detail using mass spectrometry.

Comparing the absorption of the complexes (Figure 9), one can see that the tetravalent **A4@C4** complex shows the strongest blue shift while the divalent **A4@C2$_2$** shows almost no change in the spectrum (except breaking the **A4** aggregate). The hypsochromic shift indicates a parallel alignment of the porphyrin moieties, which is in good agreement with the hypothesized structure. However, since the observed shifts are rather small the interactions, i.e., exciton coupling, between the two porphyrin chromophores seems to be rather weak.

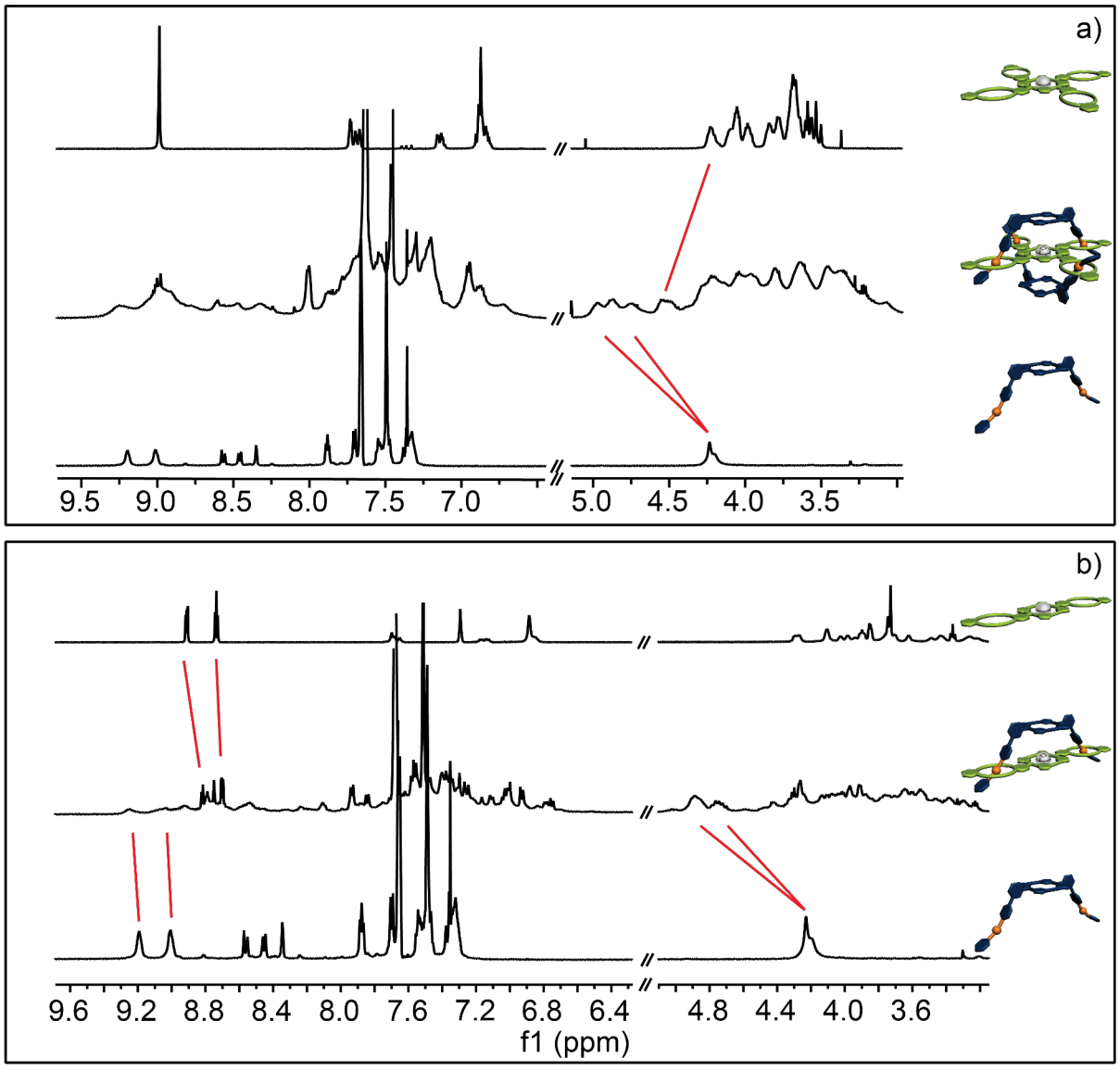

Figure 7: ^{1}H NMR (500 MHz, 298 K, CD_2Cl_2, 1 mM) of a) **C4** (top), **A2$_2$@C4** (middle) and **A2** (bottom); b) **C2** (top), **A2@C2** (middle) and **A2** (bottom). Disappearance and shift of the signals (red lines) suggest complexation. Due to the presence of a complex stereoisomeric mixture only qualitative information of the complexation is possible.

For mass spectrometric analysis (ESI-Q-TOF MS) of the desired pseudorotaxanes separate solutions of hosts and guests were prepared (CH_2Cl_2, **A2**/**C2**: 0.6 mM, **A4**/**C4**: 0.3 mM). They were mixed in the respective 1:1, 1:2, and 2:1 molar ratios and allowed to equilibrate for 14 hours at 6 °C, after which no further changes in the mass spectra were observed and thus equilibrium was reached. The pseudorotaxane solutions were diluted to 0.2 µM prior to analysis. The respective mass spectra are shown in Figure 10. Guest **A2** was combined with host **C2** as well as **C4** in 1:1 and 2:1 ratios, respectively. The expected pseudorotaxanes $[\mathbf{A2@C2}]^{2+}$ (m/z = 1396) and $[\mathbf{A2_2@C4}]^{4+}$ (m/z = 1185) are detected as the major species (Figure 10a,b). A species with only one guest **A2** in host **C4** $[Na_2\mathbf{A2@C4}]^{4+}$ (m/z = 873) could also be detected but with very low intensity. This partly bound species **A2@C4** could in principle allow formation of small oligomers, if present in solution. The fact that no oligomers could be detected and the very small abundance of the signal of the partly bound state $[Na_2\mathbf{A2@C4}]^{4+}$ (m/z = 873) leads to the conclusion, that this partly bound pseudorotaxane is most probably a product of the electrospray ionization process.

In cases of the 1:1 mixture of **A4** and **C4** and the 1:2 mixture of **A4** and **C2** the desired pseudorotaxanes $[\mathbf{A4@C4}]^{4+}$

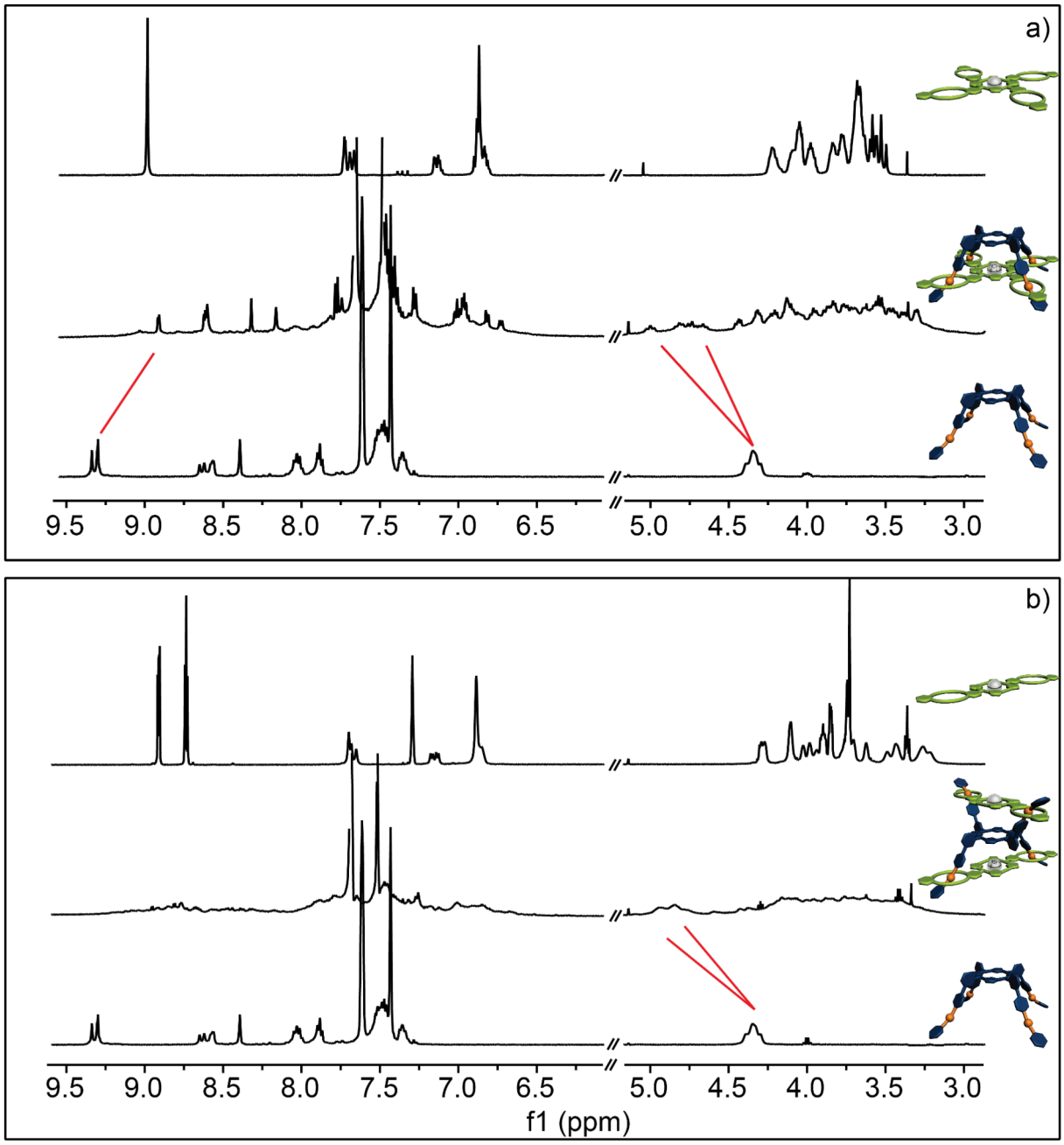

Figure 8: ^{1}H NMR (500 MHz, 298 K, CD_2Cl_2, 1 mM) of a) **C4** (top), **A4@C4** (middle) and **A4** (bottom) and b) **C2** (top), **A4@C2$_2$** (middle) and **A4** (bottom). Disappearance and shift of the signals (red lines) suggest complexation. Due to the presence of a complex stereoisomeric mixture only qualitative information of the complexation is possible.

(m/z = 989) and [**A4@C2**$_2$]$^{4+}$ (m/z = 1200) are the most abundant species and there are again only traces of the possible 1:1 pseudorotaxane [**A4@C2**]$^{4+}$ (m/z = 825) detected (Figure 10c,d). As mentioned above, this is most probably a product of the ionization process. The free hosts **C4** and **C2** are detected in only small amounts or traces. Again, in both cases no oligomers are observed.

In summary, the formation of all desired multivalent pseudorotaxanes of building blocks **A2**, **A4**, **C2**, and **C4** could be verified by mass spectrometry. The defined stoichiometry for the observed pseudorotaxanes in the gas phase ([**A2@C2**]$^{2+}$, [**A2**$_2$**@C4**]$^{4+}$, [**A4@C4**]$^{4+}$, [**A4@C2**$_2$]$^{4+}$), the only slight abundance of partly bound pseudorotaxanes ([Na$_2$**A2@C4**]$^{4+}$, [**A4@C2**]$^{4+}$) and the absence of any oligomeric species gives

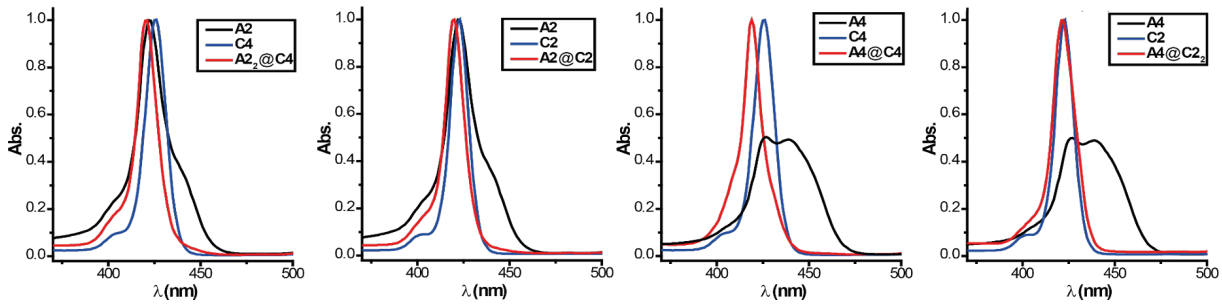

Figure 9: Normalized UV–vis absorption spectra (CH_2Cl_2, 2 μM) of the guests **A2** and **A4** (black), the hosts **C2** and **C4** (blue) and of the mixtures (red), showing a slight hypsochromic shift of the absorption maxima upon complexation.

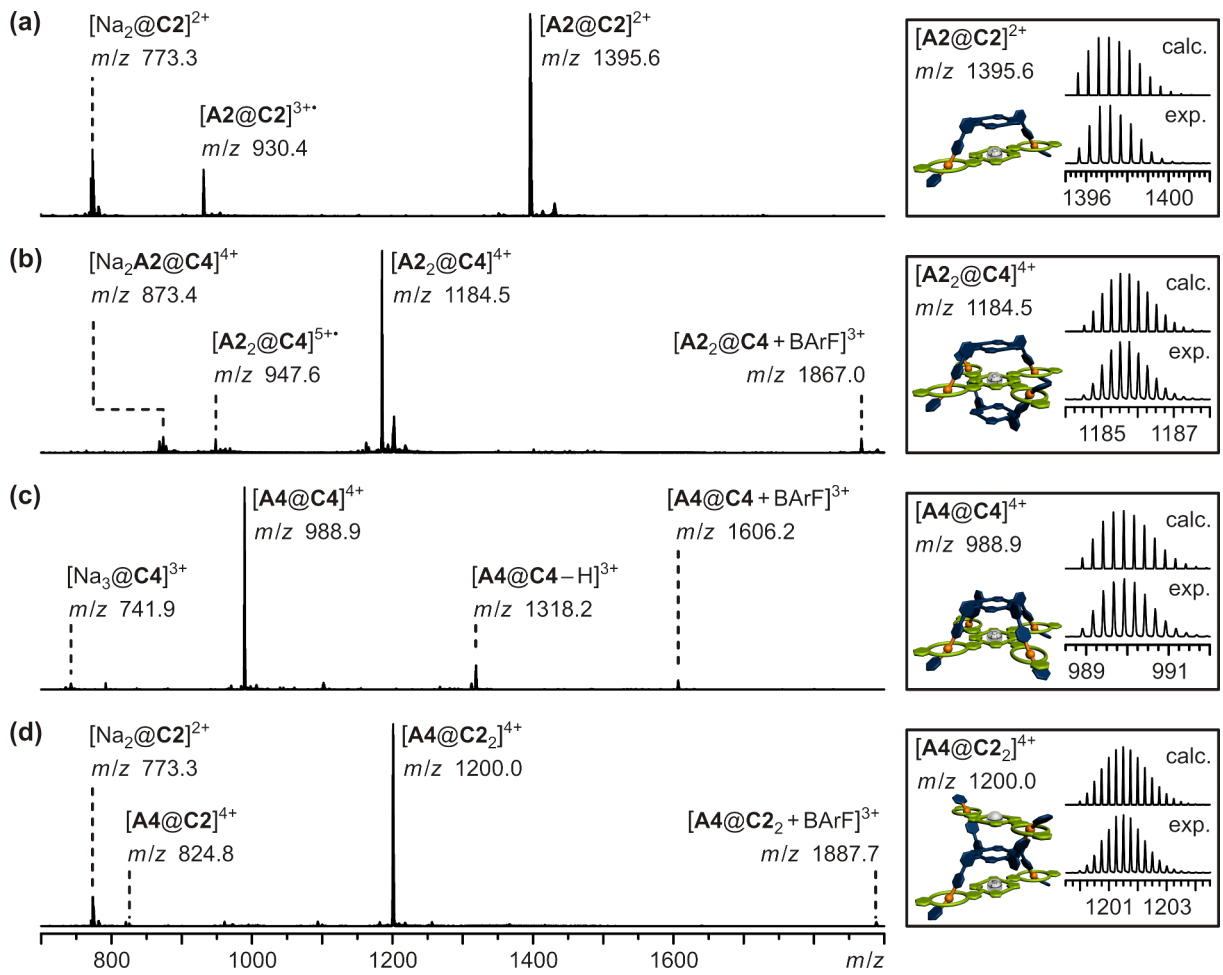

Figure 10: ESI-Q-TOF-MS spectra (CH_2Cl_2, 0.2 μM; left hand side) and respective experimental and calculated isotopic patterns of the desired [2]- or [3]pseudorotaxanes (right hand side): a) 1:1 mixture of **A2** and **C2**, b) 2:1 mixture of **A2** and **C4**, c) 1:1 mixture of **A4** and **C4**, d) 1:2 mixture of **A4** and **C2**.

clear evidence, that this specific binding situation is also present in solution.

Conclusion

The successful synthesis of di- and tetravalent porphyrin-based guests **A2** and **A4** as well as their complementary di- and tetravalent hosts **C2** and **C4** could be achieved. All four molecules show strong binding even to simple monovalent building blocks **A1** and **C1**, respectively, which could be shown by NMR-titration experiments as well as mass spectrometry. Furthermore, the formation of the di- and tetravalent pseudorotaxanes **A2@C2**, $\mathbf{A2_2@C4}$, $\mathbf{A4@C2_2}$, and **A4@C4** could be demonstrated qualitatively by NMR spectroscopy and was investigated in detail by mass spectrometry. Since the association constants in the monovalent cases are already too high to be determined by NMR-titration experiments, currently ongoing work is dealing with the daunting task to quantify the binding constants for the di- and tetravalent multiporphyrin complexes for example using isothermal calorimetry (ITC), in order to analyze the thermodynamics and kinetics of multivalent binding in these architectures in detail. In the future, we will continue to exploit the concept of complementary multivalent binding to program the increasingly complex self-assembly of multiple different chromophore components into functional supramolecular architectures.

Supporting Information

Supporting Information File 1

Detailed synthetic procedures.
[http://www.beilstein-journals.org/bjoc/content/supplementary/1860-5397-11-85-S1.pdf]

Acknowledgements

The authors thank the Deutsche Forschungsgemeinschaft for generous financial support (SFB 765). L.v.K. is grateful to the Studienstiftung des Deutschen Volkes for a Ph.D. fellowship. S.M. acknowledges the Alexander-von-Humboldt foundation for a postdoctoral fellowship.

References

1. Steed, J. W.; Atwood, J. L. *Supramolecular Chemistry;* Wiley: Chichester, UK, 2007.
2. Lehn, J.-M. *Angew. Chem., Int. Ed.* **1988,** *27,* 89–112. doi:10.1002/anie.198800891
3. Desiraju, G. R. *Angew. Chem., Int. Ed.* **2007,** *46,* 8342–8356. doi:10.1002/anie.200700534
4. Hirst, A. R.; Escuder, B.; Miravet, J. F.; Smith, D. K. *Angew. Chem., Int. Ed.* **2008,** *47,* 8002–8018. doi:10.1002/anie.200800022
5. Bhosale, R.; Mišek, J.; Sakai, N.; Matile, S. *Chem. Soc. Rev.* **2010,** *39,* 138–149. doi:10.1039/B906115K
6. Zhao, Y.; Sakai, F.; Su, L.; Liu, Y.; Wei, K.; Chen, G.; Jiang, M. *Adv. Mater.* **2013,** *25,* 5215–5256. doi:10.1002/adma.201302215
7. Cametti, M.; Crousse, B.; Metrangolo, P.; Milani, R.; Resnati, G. *Chem. Soc. Rev.* **2012,** *41,* 31–42. doi:10.1039/C1CS15084G
8. Valeur, B.; Leray, I. *Coord. Chem. Rev.* **2000,** *205,* 3–40. doi:10.1016/S0010-8545(00)00246-0
9. Flink, S.; van Veggel, F. C. J. M.; Reinhoudt, D. N. *J. Phys. Chem. B* **1999,** *103,* 6515–6520. doi:10.1021/jp990014v
10. Beer, P. D.; Gale, P. A. *Angew. Chem., Int. Ed.* **2001,** *40,* 486–516. doi:10.1002/1521-3773(20010202)40:3<486::AID-ANIE486>3.0.CO;2-P
11. Martínez-Máñez, R.; Sancenón, F. *Chem. Rev.* **2003,** *103,* 4419–4476. doi:10.1021/cr010421e
12. Llinares, J. M.; Powell, D.; Bowman-James, K. *Coord. Chem. Rev.* **2003,** *240,* 57–75. doi:10.1016/S0010-8545(03)00019-5
13. Chen, Y.; Liu, Y. *Chem. Soc. Rev.* **2010,** *39,* 495–505. doi:10.1039/B816354P
14. Feiters, M. C.; Rowan, A. E.; Nolte, R. J. M. *Chem. Soc. Rev.* **2000,** *29,* 375–384. doi:10.1039/a804252g
15. Wang, L.; Li, L.-L.; Ma, H. L.; Wang, H. *Chin. Chem. Lett.* **2013,** *24,* 351–358. doi:10.1016/j.cclet.2013.03.018
16. Huskens, J. *Curr. Opin. Chem. Biol.* **2006,** *10,* 537–543. doi:10.1016/j.cbpa.2006.09.007
17. Vigneron, J.-P. *Molecules* **1999,** *4,* 180–203. doi:10.3390/40700180
18. Diederich, F.; Stang, P. J. *Templated Organic Synthesis;* Wiley-VCH: Weinheim, Germany, 2000.
19. Whitesides, G. M.; Mathias, J. P.; Seto, C. T. *Science* **1991,** *254,* 1312–1319. doi:10.1126/science.1962191
20. Safont-Sempere, M. M.; Fernández, G.; Würthner, F. *Chem. Rev.* **2011,** *111,* 5784–5814. doi:10.1021/cr100357h
21. He, Z.; Jiang, W.; Schalley, C. A. *Chem. Soc. Rev.* **2015,** *44,* 779–789. doi:10.1039/C4CS00305E
22. Mammen, M.; Choi, S.-K.; Whitesides, G. M. *Angew. Chem., Int. Ed.* **1998,** *37,* 2754–2794. doi:10.1002/(SICI)1521-3773(19981102)37:20<2754::AID-ANIE2754>3.0.CO;2-3
23. Mulder, A.; Huskens, J.; Reinhoudt, D. N. *Org. Biomol. Chem.* **2004,** *2,* 3409–3424. doi:10.1039/b413971b
24. Fasting, C.; Schalley, C. A.; Weber, M.; Seitz, O.; Hecht, S.; Koksch, B.; Dernedde, J.; Graf, C.; Knapp, E.-W.; Haag, R. *Angew. Chem., Int. Ed.* **2012,** *51,* 10472–10498. doi:10.1002/anie.201201114
25. Hunter, C. A.; Anderson, H. L. *Angew. Chem., Int. Ed.* **2009,** *48,* 7488–7499. doi:10.1002/anie.200902490
26. Ercolani, G.; Schiaffino, L. *Angew. Chem., Int. Ed.* **2011,** *50,* 1762–1768. doi:10.1002/anie.201004201
27. Papp, I.; Sieben, C.; Sisson, A. L.; Kostka, J.; Böttcher, C.; Ludwig, K.; Herrmann, A.; Haag, R. *ChemBioChem* **2011,** *12,* 887–895. doi:10.1002/cbic.201000776
28. Kitov, P. I.; Sadowska, J. M.; Mulvey, G.; Armstrong, G. D.; Ling, H.; Pannu, N. S.; Read, R. J.; Bundle, D. R. *Nature* **2000,** *403,* 669–672. doi:10.1038/35001095
29. Simanek, E. E.; McGarvey, G. J.; Jablonowski, J. A.; Wong, C.-H. *Chem. Rev.* **1998,** *98,* 833–862. doi:10.1021/cr940226i
30. Badjić, J. D.; Balzani, V.; Credi, A.; Lowe, J. N.; Silvi, S.; Stoddart, J. F. *Chem. – Eur. J.* **2004,** *10,* 1926–1935. doi:10.1002/chem.200305687

31. Balzani, V.; Clemente-León, M.; Credi, A.; Lowe, J. N.; Badjić, J. D.; Stoddart, J. F.; Williams, D. J. *Chem. – Eur. J.* **2003,** *9,* 5348–5360. doi:10.1002/chem.200304979
32. O'Sullivan, M. C.; Sprafke, J. K.; Kondratuk, D. V.; Rinfray, C.; Claridge, T. D. W.; Saywell, A.; Blunt, M. O.; O'Shea, J. N.; Beton, P. H.; Malfois, M.; Anderson, H. L. *Nature* **2011,** *469,* 72–75. doi:10.1038/nature09683
33. Kondratuk, D. V.; Perdigao, L. M. A.; O'Sullivan, M. C.; Svatek, S.; Smith, G.; O'Shea, J. N.; Beton, P. H.; Anderson, H. L. *Angew. Chem., Int. Ed.* **2012,** *51,* 6696–6699. doi:10.1002/anie.201202870
34. Timko, J. M.; Moore, S. S.; Walba, D. M.; Hiberty, P. C.; Cram, D. J. *J. Am. Chem. Soc.* **1977,** *99,* 4207–4219. doi:10.1021/ja00455a001
35. Ashton, P. R.; Campbell, P. J.; Glink, P. T.; Philp, D.; Spencer, N.; Stoddart, J. F.; Chrystal, E. J. T.; Menzer, S.; Williams, D. J.; Tasker, P. A. *Angew. Chem., Int. Ed. Engl.* **1995,** *34,* 1865–1869. doi:10.1002/anie.199518651
36. Ashton, P. R.; Chrystal, E. J. T.; Glink, P. T.; Menzer, S.; Schiavo, C.; Spencer, N.; Stoddart, J. F.; Tasker, P. A.; White, A. J. P.; Williams, D. J. *Chem. – Eur. J.* **1996,** *2,* 709–728. doi:10.1002/chem.19960020616
37. Jiang, W.; Schalley, C. A. *Proc. Natl. Acad. Sci. U. S. A.* **2009,** *106,* 10425–10429. doi:10.1073/pnas.0809512106
38. Clifford, T.; Abushamleh, A.; Busch, D. H. *Proc. Natl. Acad. Sci. U. S. A.* **2002,** *99,* 4830–4836. doi:10.1073/pnas.062639799
39. Dong, S.; Zheng, B.; Wang, F.; Huang, F. *Acc. Chem. Res.* **2014,** *47,* 1982–1994. doi:10.1021/ar5000456
40. Amabilino, D. B.; Stoddart, J. F. *Chem. Rev.* **1995,** *95,* 2725–2828. doi:10.1021/cr00040a005
41. Yamaguchi, N.; Gibson, W. H. *Chem. Commun.* **1999,** 789–790. doi:10.1039/a901044k
42. Jiang, W.; Sattler, D.; Rissanen, K.; Schalley, C. A. *Org. Lett.* **2011,** *13,* 4502–4505. doi:10.1021/ol201618f
43. Balzani, V.; Credi, A.; Raymo, F. M.; Stoddart, J. F. *Angew. Chem., Int. Ed.* **2000,** *39,* 3348–3391. doi:10.1002/1521-3773(20001002)39:19<3348::AID-ANIE3348>3.0.CO;2-X
44. Kay, E. R.; Leigh, D. A.; Zerbetto, F. *Angew. Chem., Int. Ed.* **2007,** *46,* 72–191. doi:10.1002/anie.200504313
45. Vukotic, V. N.; Loeb, S. J. *Chem. Soc. Rev.* **2012,** *41,* 5896–5906. doi:10.1039/c2cs35141b
46. Liu, Y.; Flood, A. H.; Bonvallet, P. A.; Vignon, S. A.; Northrop, B. H.; Tseng, H.-R.; Jeppesen, J. O.; Huang, T. J.; Brough, B.; Baller, M.; Magonov, S.; Solares, S. D.; Goddard, W. A.; Ho, C.-M.; Stoddart, J. F. *J. Am. Chem. Soc.* **2005,** *127,* 9745–9759. doi:10.1021/ja051088p
47. Coskun, A.; Banaszak, M.; Astumian, R. D.; Stoddart, J. F.; Grzybowski, B. A. *Chem. Soc. Rev.* **2012,** *41,* 19–30. doi:10.1039/C1CS15262A
48. Bruns, C. J.; Stoddart, J. F. *Acc. Chem. Res.* **2014,** *47,* 2186–2199. doi:10.1021/ar500138u
49. Romuald, C.; Busseron, E.; Coutrot, F. *J. Org. Chem.* **2010,** *75,* 6516–6531. doi:10.1021/jo101234u
50. Clark, P. G.; Day, M. W.; Grubbs, R. H. *J. Am. Chem. Soc.* **2009,** *131,* 13631–13633. doi:10.1021/ja905924u
51. Milgrom, L. R. *The Colours of Life: An Introduction to the Chemistry of Porphyrins and Related Compounds;* Oxford University Press: Oxford, UK, 2001.
52. Ishii, K.; Kobayashi, N. In *The Porphyrin Handbook;* Kadish, K.; Guilard, R.; Smith, K. M., Eds.; Academic Press: Amsterdam, 2003; pp 1–42. doi:10.1016/B978-0-08-092390-1.50007-2
53. Durot, S.; Taesch, J.; Heitz, V. *Chem. Rev.* **2014,** *114,* 8542–8578. doi:10.1021/cr400673y
54. Mandal, S.; Rahaman, M.; Sadhu, S.; Nayak, S. K.; Patra, A. *J. Phys. Chem. C* **2013,** *117,* 3069–3077. doi:10.1021/jp3100188
55. Liu, Y.; Huang, Z.; Liu, K.; Kelgtermans, H.; Dehaen, W.; Wang, Z.; Zhang, X. *Polym. Chem.* **2014,** *5,* 53–56. doi:10.1039/C3PY01036H
56. Fathalla, M.; Strutt, N. L.; Barnes, J. C.; Stern, C. L.; Ke, C.; Stoddart, J. F. *Eur. J. Org. Chem.* **2014,** 2873–2877. doi:10.1002/ejoc.201402018
57. Watanabe, K.; Kitagishi, H.; Kano, K. *Angew. Chem., Int. Ed.* **2013,** *52,* 6894–6897. doi:10.1002/anie.201302470
58. Puglisi, A.; Purrello, R.; Rizzarelli, E.; Sortino, S.; Vecchio, G. *New J. Chem.* **2007,** *31,* 1499–1506. doi:10.1039/b703680a
59. Králová, J.; Kejik, Z.; Bříza, T.; Poučková, P.; Král, A.; Martásek, P.; Král, V. *J. Med. Chem.* **2010,** *53,* 128–138. doi:10.1021/jm9007278
60. Kiba, T.; Suzuki, H.; Hosokawa, K.; Kobayashi, H.; Baba, S.; Kakuchi, T.; Sato, S.-I. *J. Phys. Chem. B* **2009,** *113,* 11560–11563. doi:10.1021/jp905904h
61. Kano, K.; Kitagishi, H.; Dagallier, C.; Kodera, M.; Matsuo, T.; Hayashi, T.; Hisaeda, Y.; Hirota, S. *Inorg. Chem.* **2006,** *45,* 4448–4460. doi:10.1021/ic060137b
62. Kim, Y.-H.; Hong, J.-I. *Chem. Commun.* **2002,** 512–513. doi:10.1039/b109596j
63. D'Souza, F.; Chitta, R.; Gadde, S.; Zandler, M. E.; Sandanayaka, A. S. D.; Araki, Y.; Ito, O. *Chem. Commun.* **2005,** 1279–1281. doi:10.1039/b416736h
64. Even, P.; Boitrel, B. *Coord. Chem. Rev.* **2006,** *250,* 519–541. doi:10.1016/j.ccr.2005.09.003
65. Zhang, H.; Liu, Q.; Li, J.; Qu, D.-H. *Org. Lett.* **2013,** *15,* 338–341. doi:10.1021/ol3032686
66. Jahan, M.; Safari, N.; Khosravi, H.; Moghimi, A.; Notash, B. *Polyhedron* **2005,** *24,* 1682–1688. doi:10.1016/j.poly.2005.04.033
67. Imahori, H.; Fukuzumi, S. *Adv. Funct. Mater.* **2004,** *14,* 525–536. doi:10.1002/adfm.200305172
68. Imahori, H.; Sakata, Y. *Eur. J. Org. Chem.* **1999,** 2445–2457. doi:10.1002/(SICI)1099-0690(199910)1999:10<2445::AID-EJOC2445>3.0.CO;2-G
69. Yong, C.-K.; Parkinson, P.; Kondratuk, D. V.; Chen, W.-H.; Stannard, A.; Summerfield, A.; Sprafke, J. K.; O'Sullivan, M. C.; Beton, P. H.; Anderson, H. L.; Herz, L. M. *Chem. Sci.* **2015,** *6,* 181–189. doi:10.1039/C4SC02424A
70. Parkinson, P.; Knappke, C. E. I.; Kamonsutthipaijit, N.; Sirithip, K.; Matichak, J. D.; Anderson, H. L.; Herz, L. M. *J. Am. Chem. Soc.* **2014,** *136,* 8217–8220. doi:10.1021/ja504730j
71. Liu, J.-Y.; Huang, Y.; Menting, R.; Röder, B.; Ermilov, E. A.; Ng, D. K. P. *Chem. Commun.* **2013,** *49,* 2998–3000. doi:10.1039/c3cc00262d
72. Menting, R.; Lau, J. T. F.; Xu, H.; Ng, D. K. P.; Röder, B.; Ermilov, E. A. *Chem. Commun.* **2012,** *48,* 4597–4599. doi:10.1039/c2cc30286a
73. Burrell, A. K.; Officer, D. L.; Plieger, P. G.; Reid, D. C. W. *Chem. Rev.* **2001,** *101,* 2751–2796. doi:10.1021/cr0000426
74. Yamada, Y.; Okamoto, M.; Furukawa, K.; Kato, T.; Tanaka, K. *Angew. Chem., Int. Ed.* **2012,** *51,* 709–713. doi:10.1002/anie.201107104
75. van Nostrum, C. F.; Picken, S. J.; Schouten, A.-J.; Nolte, R. J. M. *J. Am. Chem. Soc.* **1995,** *117,* 9957–9965. doi:10.1021/ja00145a004

76. Lindsey, J. S.; Schreiman, I. C.; Hsu, H. C.; Kearney, P. C.; Marguerettaz, A. M. *J. Org. Chem.* **1987,** *52,* 827–836. doi:10.1021/jo00381a022
77. Geier, G. R., III; Lindsey, J. S. *Tetrahedron* **2004,** *60,* 11435–11444. doi:10.1016/j.tet.2004.09.081
78. Jiang, W.; Schäfer, A.; Mohr, P. C.; Schalley, C. A. *J. Am. Chem. Soc.* **2010,** *132,* 2309–2320. doi:10.1021/ja9101369
79. Jiang, W.; Schalley, C. A. *J. Mass Spectrom.* **2010,** *45,* 788–798. doi:10.1002/jms.1769

License and Terms

Supporting Information

for

Discrete multiporphyrin pseudorotaxane assemblies from di- and tetravalent porphyrin building blocks

Mirko Lohse[1], Larissa K. S. von Krbek[2], Sebastian Radunz[1], Suresh Moorthy,[2] Christoph A. Schalley*,[2] and Stefan Hecht*,[1]

Address: [1]Department of Chemistry, Humboldt-Universität zu Berlin, Brook-Taylor-Str. 2, 12489 Berlin, Germany. Fax: +49 (0)30 2093-6940; Tel: +49 (0)30 2093-7308 and [2] Institut für Chemie und Biochemie, Freie Universität Berlin, Takustraße 3, 14195 Berlin, Germany. Fax: +49(0)308385-5366; Tel: +49(0)308385-2639

Email: Stefan Hecht - sh@chemie.hu-berlin.de; Christoph A. Schalley - christoph@schalley-lab.de

Detailed synthetic procedures

General methods

Solvents and commercial starting materials were used as supplied. The solvents were dried before use, if necessary, employing an Innovative Technologies solvent purification system (multi-unit micro series). Silica gel for chromatography from Merck (0.035–0.070 mm, 60 Å) was used for column chromatography. The petroleum ether (PE) used had a boiling range of 40–60 °C. NMR spectra were recorded on a 500 MHz (125 MHz for ^{13}C) Bruker AVANCE II 500 spectrometer or on a 300 MHz (75.6 MHz for ^{13}C) Bruker DPX 300 spectrometer at 25 °C using the solvent residual proton signals as internal standard (^{1}H: $\delta(CHCl_3)$ = 7.26 ppm, $\delta(CH_2Cl_2)$ = 5.32 ppm, $\delta(CH_3CN)$ = 1.94 ppm, ^{13}C: $\delta(CHCl_3)$ = 77.16 ppm, ^{13}C: $\delta(CH_2Cl_2)$ = 53.5 ppm, ^{13}C: $\delta(CH_3CN)$ = 118.3 and 1.32 ppm). Ultrahigh-performance liquid chromatography connected to mass spectrometry (UPLC/MS) was performed on a Waters Acquity UPLC equivuipped with a Waters LCT Premier XE Mass detector for high resolution MS (HRMS, ESI^+ ionization) and with Waters Alliance systems (consisting of a Waters Separations Module 2695, a Waters Diode Array Detector 996 and a Waters Mass Detector ZQ 2000). TLC was performed on Merck Silica Gel 60 F254 TLC plates with a fluorescent indicator employing a 254 nm UV lamp for visualization. All procedures linked to photochemistry were performed using spectrophotometric grade solvents.

UV–vis spectroscopy was performed on either a Varian Cary 50 or Varian Cary 60 UV–vis spectrophotometer equivuipped with a Peltier thermostated cell holder at 25 ± 0.05 °C.

Electrospray ionization reflectron-time-of-flight high resolution mass spectrometric (ESI-ReTOF-HRMS) experiments were conducted on an Agilent 6210 ESI-TOF,

Agilent Technologies, Santa Clara, CA, USA. The flow rate was set to 4 µL/min and the spray voltage to 4 kV. The desolvation gas was set to 1 psi (1 bar). All other parameters were optimized for maximum abundance of the respective $[M + H]^+$.

Electrospray ionization quadrupole-time-of-flight high resolution mass spectrometric (ESI-Q-TOF-HRMS) experiments were performed with a Synapt G2-S HDMS, Waters Co., Milford, MA, USA. The flow rate was set to 10 µL/min and the spray voltage to 3 kV (1.5 kV for **A1**$_4$@**C4**). The desolvation gas was set to 1 psi (1 bar). All other parameters were optimized for maximum abundance of the respective $[M]^+$.

Compounds NaBArF [1], **C1** [2], **6** [3], **18** [4] were synthesized according to literature.

Synthetic procedures and compound characterization data

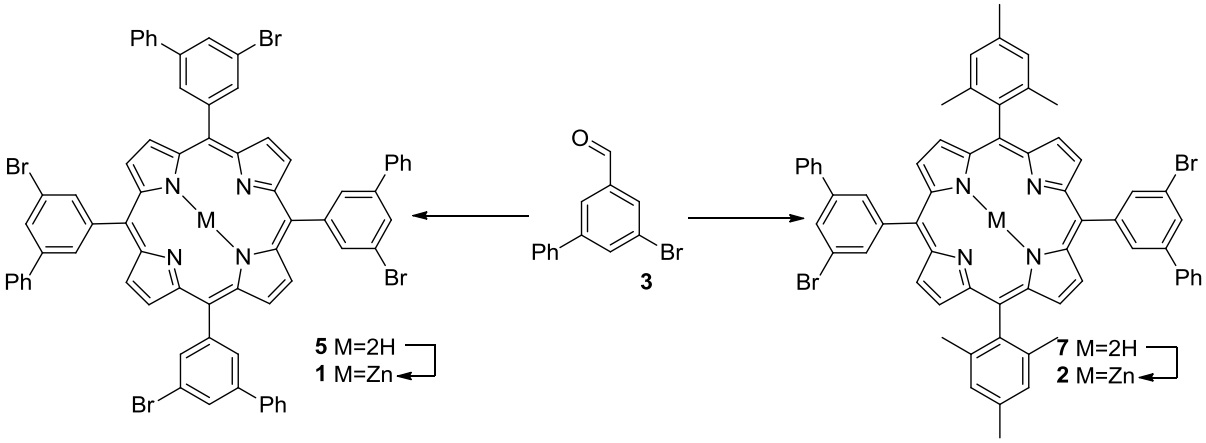

3-Bromo-5-phenyl-benzaldehyde (3)

The reactant 3,5-dibromobenzaldehyde (6.44 g, 24.40 mmol, 1 equiv) was added to a mixture of phenylboronic acid (2.41 g, 21.96 mmol, 0.9 equiv), $Pd(PPh_3)_4$ (70 mg, 1.22 mmol, 0.05 equiv), 2 M aqueous Na_2CO_3 solution (20 mL), ethanol (40 mL) and toluene (120 mL). The reaction mixture was stirred at 90–95 °C under a nitrogen atmosphere overnight. After cooling to room temperature the organic layer was separated and the aqueous layer was extracted with Et_2O (3 x 50 mL). The combined

organic phases were dried over $MgSO_4$ and evaporated to give a crude solid. Purification by column chromatography afforded **5** as a colorless oil (4.787 g, 18.30 mmol, yield 75%). 3,5-Diphenylbenzaldehyde (400 mg) was isolated as the major side-product.

^{1}H NMR (500 MHz, $CDCl_3$): δ = 10.01 (s, CHO), 8.01 (m, $1H_{aryl}$), 7.96 (m, $2H_{aryl}$), 7.59 (m, $2H_{aryl}$), 7.49 (m, $2H_{aryl}$), 7.43 (m, $1H_{aryl}$) ppm **^{13}C NMR** (125 MHz, $CDCl_3$): δ = 190.6, 144.0, 138.2, 138.2, 135.6, 130.9, 129.1, 128.6, 127.0, 126.8, 123.7 ppm. **ESI-MS:** could not be ionized by the ESI-source.

5,10,15,20-Tetrakis{(3-bromo-5-phenyl)-phenyl}porphyrin (5)

Pyrrole (**4**, 0.207 mL, 3.00 mmol, 1 equiv), compound **3** (783 mg, 3.00 mmol, 1 equiv) were dissolved in $CHCl_3$ (400 mL) and 0.6 g molecular sieves (6 Å) were added. The mixture was degassed by bubbling argon through the stirred solution for 15 min after which $BF_3{\cdot}Et_2O$ (0.040 mL, 0.3 mmol, 0.1 equiv) was added dropwise and stirring was continued for 4 h. Afterwards DDQ (680 mg, 3.0 mmol, 1 equiv) was added and stirring was continued for a further hour, followed by the addition of TEA (2 mL). The major impurities were removed by filtration of the crude reaction mixture through a silca plug with CH_2Cl_2 as the eluting solvent. Pure product **5** was obtained by subsequent column chromatography (SiO_2, petroleum ether/CH_2Cl_2 7:3) as shimmering violet crystals (270 mg, 0.88 mmol, 29%).

^{1}H NMR (500 MHz, $CDCl_3$): δ = 9.01 (s, $8H_{aryl}$), 8.42 (m, $8H_{aryl}$), 8.23 (t, J = 1.70 Hz, $4H_{aryl}$), 7.84 (m, $8H_{aryl}$), 7.52 (m, 8H, H_{aryl}), 7.43 (m, $4H_{aryl}$), -2.78 (s, 2H, NH) **^{13}C NMR** (125.75 MHz, CD_2Cl_2): δ = 144.1, 141.4,139.4, 139.3, 135.9, 132.2, 132.2, 129.7, 129.1, 128.2, 127.5, 121.6, 118.9 ppm.

Zinc[5,10,15,20-tetrakis{(3-bromo-5-phenyl)phenyl}porphyrin] (1)

$Zn(OAc)_2$ (461 mg, 2.10 mmol, 10 equiv) was added to a stirring solution of **5** (259 mg, 0.21 mmol, 1 equiv) in 30 mL of a chloroform/methanol solvent and the reaction mixture was stirred at room temperature overnight. After removal of the solvents under reduced pressure, the crude product was redissolved in CH_2Cl_2 and washed with brine. The separated organic layer was dried over $MgSO_4$ and concentrated. Purification by column chromatography (SiO_2, petroleum ether/CH_2Cl_2 7:3) afforded **1** as violet crystals (270 mg, 2.09 mmol, 99%).

^{1}H NMR (500 MHz, $CDCl_3$): δ = 9.01 (s, 8H_{aryl}), 8.45 (s, 8H, H_{aryl}), 8.22 (s, 4H_{aryl}), 7.84 (m, 8H_{aryl}), 7.47 (m, 8H_{aryl}), 7.39 (m, 4H_{aryl}) **^{13}C NMR** (125.75 MHz, $CDCl_3$): δ = 150.1, 144.8, 141.2, 139.4, 135.9, 132.3, 132.1, 129.4, 129.0, 128.1, 127.4, 121.1, 119.8 ppm. **ESI-MS:** 1298.0 (calc. 1298.0 $C_{68}H_{40}N_4Br_4Zn$).

5,15-Bis{(3-bromo-5-phenyl)phenyl}-10,20-(bismesityl)porphyrin (7)

Molecular sieves (6 Å, 0.06 g) were added to a stirring solution of 5-bromo-[1,1'biphenyl]-3-carbaldehyde (**3**, 0.227 g, 0.87 mmol, 1 equiv) and 2,2'-(mesitylmethylene)bis(1*H*-pyrrole) (**6**, 0.230 g, 0.87 mmol, 1 equiv) in 300 mL of chloroform. The mixture was degassed by bubbling argon through the solution for 20 min before $BF_3{\cdot}Et_2O$ (0.03 mL, 0.190 mmol, 0.2 equiv) were added. The reaction mixture was stirred in the dark for 2 h, after which DDQ (0.197 g, 0.87 mmol, 1.0 equiv) was added and the stirring was continued overnight. Afterwards TEA (1 mL) was added and the major impurities were removed by filtration of the crude reaction mixture through a silica plug with CH_2Cl_2 as the eluting solvent. Pure product **7** was obtained by column chromatography (SiO_2, CH_2Cl_2/petroleum ether 1:3) as a purple solid (0.120 g, 0.24 mmol, 28%).

^{1}H NMR (500 MHz, $CDCl_3$): δ = 8.87 (d, J = 4.8 Hz, $4H_{aryl}$), 8.74 (d, J = 4.8 Hz, $4H_{aryl}$), 8.45 - 8.32 (m, $4H_{aryl}$), 8.18 (s, $4H_{aryl}$), 7.87 - 7.75 (m, $4H_{aryl}$), 7.45 (m, $8H_{aryl}$), 7.28 (m, $4H_{aryl}$), 2.62 (s, 6H), 1.85 (s, 12H), -2.64 (s, 2H, NH) **^{13}C NMR** (125.75 MHz, $CDCl_3$): δ =144.4, 141.3, 139.5, 139.4, 139.3, 138.2, 137.9, 135.8, 132.0, 129.6, 129.1, 128.2, 127.9, 127.5, 121.5, 118.9, 117.6, 21.7, 21.5 ppm.

Zinc[5,15-bis{(3-bromo-5-phenyl)phenyl}-10,20-(bismesityl)porphyrin] (2)

Zinc(II) acetate (0.131 g, 0.60 mmol, 5 equiv) was added to a stirring solution of **7** (0.120 g, 0.12 mmol, 1 equiv) in 20 mL of chloroform/methanol 1:1 and stirred overnight at room temperature. Afterwards the solvent was removed under reduced pressure and the crude product was purified by column chromatography (SiO_2, PE/CH_2Cl_2 3:1) to obtain **2** as a purple/red solid (0.110 g, 0.10 mmol, 86%).

^{1}H NMR (500 MHz, $CDCl_3$): δ = 8.98 (d, J = 4.6 Hz, $4H_{aryl}$), 8.80 (d, J = 4.6 Hz, $4H_{aryl}$), 8.52 - 8.32 (m, $4H_{aryl}$), 8.20 (t, J = 1.7 Hz, $2H_{aryl}$), 7.83 (d, J = 7.5 Hz, $2H_{aryl}$), 7.49 (t, J = 7.8 Hz, $2H_{aryl}$), 7.41 (m, $4H_{aryl}$), 7.30 (s, $4H_{aryl}$), 2.62 (s, 6H), 1.82 (s, 12H). **^{13}C NMR** (125.76 MHz, $CDCl_3$): δ =150.2, 149.8, 145.2, 139.7, 139.3, 138.7, 137.6, 135.8, 132.2, 131.2, 129.1, 128.2, 127.8, 127.5, 120.0, 118.5, 21.7, 21.5 ppm. **ESI-MS:** 1072.3 (calc. 1072.3 $C_{62}H_{46}Br_2N_4Zn$)

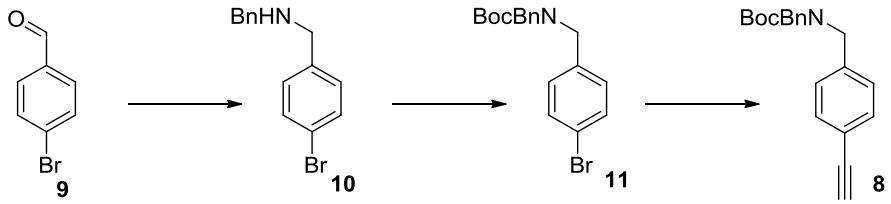

Benzyl-(4-bromobenzyl)amine (10)

Benzylamine (1.158 g, 10.81 mmol, 1 equiv) was added to a solution of 4-bromo-benzaldehyde (**9**, 2.000 g, 10.81 mmol, 1 equiv) in 15 mL of trimethyl orthoformate and stirred overnight. The solvent was removed under reduced pressure to obtain the

desired product in decent purity which was used without further purification (2.91 g, 10.80 mmol, 98%). $NaBH_4$ (0.817 g, 21.59 mmol, 2 equiv) were added to an ice-cooled solution of the imine (2.960 g, 10.80 mmol, 1 equiv) in a 1:1 mixture of THF/MeOH (30 mL each). The mixture was allowed to warm to room temperature and stirred for 2 h. The volatiles were removed under reduced pressure and the crude product was dissolved in ethyl acetate. The slurry mixture was filtered through a celite plug using ethyl acetate as the solvent. Pure product **10** was obtained after removal of the solvent under reduced pressure (2.910 g, 10.79 mmol, 98%).

^{1}H NMR (500 MHz, $CDCl_3$): δ = 7.38(m, $2H_{aryl}$), 7.26(m, $2H_{aryl}$), 7.15(m, $5H_{aryl}$), 3.72(s, 2H), 3.69 (s, 2H) **^{13}C NMR** (125.75 MHz, CDCl3): δ = 155.9, 131.7, 128.5, 27.4, 80.3, 28.5 ppm. **ESI-HRMS** 276.019 (calc. 276.021 $C_{14}H_{15}BrN^+$)

(*tert*-Butyloxycarbonyl)(benzyl)4-bromobenzylamine (11)

Triethylamine (2 mL) was added to a stirred solution of **10** (2,688 g, 9.77 mmol, 1 equiv) and $(Boc)_2O$ (3.271 g, 15.00 mmol, 1.5 equiv) dissolved in 100 mL CH_2Cl_2. After all of the starting material was consumed (TLC, ca 16 h) the solvent was removed under reduced pressure and excess $(Boc)_2O$ was removed by bulb-to-bulb distillation. The crude product was purified by column chromatography (SiO_2, petroleum ether/EtOAc 99:1 → 4:1) affording pure **11** as a colorless oil (2.200 g, 5.87 mmol, 60%).

^{1}H NMR (500 MHz, $CDCl_3$): δ = 7.45 (m $2H_{aryl}$), 7.23 (m,$7H_{aryl}$), 4.34 (br, 4H), 1.49 (s, 9H) **^{13}C NMR** (125.75 MHz, $CDCl_3$): δ = 140.1, 139.3, 131.5, 129.9, 128.5, 128.2, 127.1, 120.7, 53.1, 52.4 ppm. **ESI-HRMS**: 320.056 (calc. 320.040 $C_{15}H_{15}BrNO_2^+$)

(*tert*-Butyloxycarbonyl)(benzyl){4-(trimethylsilyl)ethynylbenzyl}amine (12)

CuI (5 mg, 0.03 mmol, 0.1 equiv), triphenylphosphine (35 mg, 0.14 mmol, 0.5 equiv), and **11** (100 mg, 0.27 mmol, 1 equiv) were dissolved in 4 mL of a 1:1 mixture of dry toluene/triethylamine which was degassed by rapid vacuum–argon cycles (5 times). Afterwards, $Pd(PPh_3)_4$ (31 mg, 0.03 mmol, 0.1 equiv) was added and the solution was degassed again (3 times). After the addition of ethynyltrimethylsilane (0.08 mL, 0.53 mmol, 2 equiv) the solution was stirred at 80 °C for 16 h. When all starting material was consumed (TLC) the mixture was filtered through a plug of celite with ethyl acetate as the eluting solvent. The resulting solution was concentrated under reduced pressure and purified by column chromatography (SiO_2, petroleum ether/EtOAc 15:1 → 9:1) to yield **12** as a colourless solid (0.100 g, 0.26 mmol, 96%).

^{1}H NMR (500 MHz, $CDCl_3$): δ = 7.45 (m, $2H_{aryl}$), 7.34 (m, $7H_{aryl}$), 4.38 (br, 4H), 1.50 (s, 9H), 0.28 (s, 9H) **^{13}C NMR** (125.75 MHz, $CDCl_3$): δ = 155.9, 132.1, 128.5, 128.0, 127.8, 127.4, 127.3, 127.1, 104.9, 94.1, 80.2, 49.3, 28.4, 0.4 ppm. **ESI-HRMS**: 338.158 (calc. 338.157 $C_{20}H_{24}NO_2Si^+$)

(*tert*-Butyloxycarbonyl)(benzyl)4-ethynylbenzylamine (8)

Potassium hydroxide (36 mg, 0.64 mmol, 2.5 equiv) was added to a solution of **12** (100 mg, 0.25 mmol, 1 equiv) in toluene and stirred overnight at room temperature. Afterwards the solvent was removed under reduced pressure and the residue was dissolved in CH_2Cl_2, washed sequentially with 1 M HCl and brine, dried over $MgSO_4$ and concentrated under reduced pressure. The crude product was purified by column chromatography (SiO_2, petroleum ether:EtOAc 9:1) to give an yellowish oil that solidifies upon standing (65 mg, 0.23 mmol, 90%).

^{1}H NMR (500 MHz, $CDCl_3$): δ = 7.51 (m, $2H_{aryl}$), 7.33 (m,$7H_{aryl}$), 4.42 (br, 4H), 3.17 (s, 1H), 1.51 (s, 9H) **^{13}C NMR** (125.75 MHz, $CDCl_3$): δ = 156.1, 132.4, 128.7, 128.2,

128.0, 127.5, 121.1, 80.4, 77.3, 28.6 ppm. **ESI-HRMS**: 338.128 (calc. 338.157 $C_{17}H_{16}NO_2^+$)

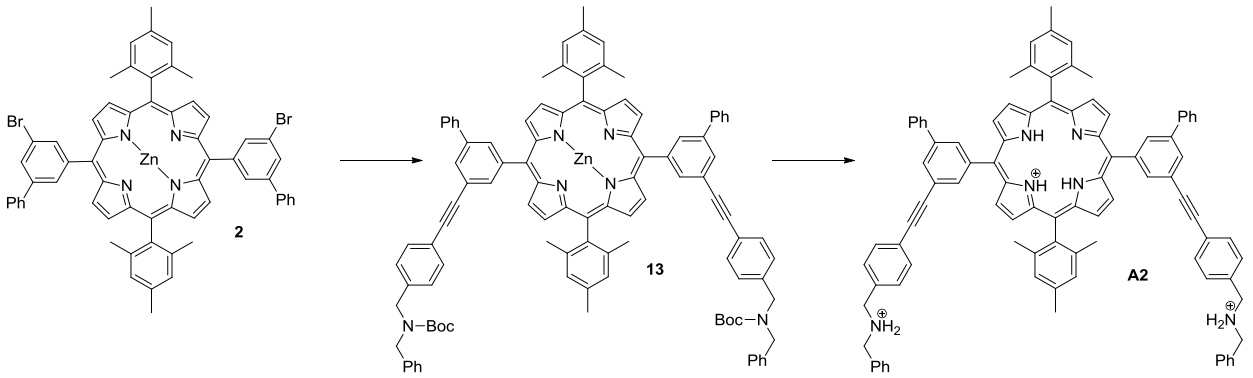

Boc-protected bisammonium precursor porphyrin (13)

CuI (1.7 mg, 0.01 mmol, 0.2 equiv), triphenylphosphine (2.4 mg, 0.01 mmol, 0.2 equiv), and **2** (50 mg, 0.05 mmol, 1 equiv) were dissolved in 2 mL of dry toluene/triethylamine 1:1 and degassed by rapid vacuum–argon cycles (5 times). Afterwards, $Pd(PPh_3)_4$ (11 mg, 0.09 mmol, 0.2 equiv) was added and the solution was degassed again (3 times). After the addition of **8** (75 mg, 0.23 mmol, 5 equiv), the solution was stirred at 80 °C for 3 d under a nitrogen atmosphere. When all starting material was consumed (TLC), the mixture was filtered through a plug of celite with CH_2Cl_2 as the solvent. The resulting solution was concentrated under reduced pressure and purified by column chromatography (SiO_2, CH_2Cl_2). The product was precipitated from CH_2Cl_2/MeOH by slowly removing CH_2Cl_2 under vacuum (72 mg, 0.03 mmol, 69%).

^{1}H NMR (600 MHz, $CDCl_3$): δ = 9.02 (m, $4H_{aryl}$), 3.93 (m, $4H_{aryl}$), 8.45 (br, $4H_{aryl}$), 8.25 (s, $2H_{aryl}$), 7.56 (m, $8H_{aryl}$), 7.35 (m, $20H_{aryl}$), 4.20 (br, 8H), 2.66 (s, 6H), 1.89 (s, 12H), 1.32 (br, 18H) **^{13}C NMR** (125.76 MHz, $CDCl_3$): δ = 155.7, 145.0, 149.8, 143.9, 140.2, 139.4, 139.3, 139.2, 137.7, 137.3, 135.9, 133.1, 132.1, 131.8, 130.8, 129.2, 128.9,

128.9, 128.0, 127.8, 127.6, 127.5, 127.3, 121.8, 119.2, 118.7, 80.1, 65.7, 28.3, 24.1, 21.7 ppm.

Target bisammonium porphyrin salt (A2)

Trifluoroacetic acid (3 mL) was added to a stirring solution of **13** (150 mg, 0.10 mmol, 1 equiv) in CH_2Cl_2 and the resulting solution was stirred for 3 d. When no starting material was left (TLC), the solvent was removed under reduced pressure until dryness, the residue was dissolved in CH_2Cl_2 and washed with 1 M NaOH solution. The combined organic phases were dried over $MgSO_4$ and concentrated under reduced pressure to obtain **14** as a purple solid (120 mg, 0.10 mmol, 97%) which was used without further purification.

^{1}H NMR (300 MHz, MeOD): δ = 9.03 (d, J = 4.9 Hz, $4H_{aryl}$), 8.83 (d, J = 4.9 Hz, $4H_{aryl}$), 8.72 (m ,$2H_{aryl}$), 8.61 (m, $2H_{aryl}$), 8.41 (m, $2H_{aryl}$), 7.96 (d, J = 7.8 Hz, $4H_{aryl}$), 7.76 (d, J = 8.2 Hz, $4H_{aryl}$), 7.50 (m, $28H_{aryl}$), 4.29 (s, 4H), 4.28 (s, 4H), 2.65 (s, 6H), 1.95 (s, 12H) ppm.

To a solution of **14** (120 mg, 0.10 mmol, 1 equiv) in 20 mL chloroform/methanol 1:1 was added 3 mL of 1 M HCl solution. After stirring for 5 min the solution was concentrated to dryness under reduced pressure to obtain a green solid. This process was repeated three times to fully protonate the compound. The hydrochloride of **14** (100 mg, 0.07 mmol, 1 equiv) was then dissolved in methanol and NaBArF (196 mg, 0.22 mmol, 3.1 equiv) was added. The desired product was precipitated by adding water to the solution and subsequent centrifugation. The obtained sticky solid was dissolved in MeOH, again precipitated with water and centrifuged. This process was repeated three times. **A2** was obtained as a purple solid after lyophilisation from benzene (0.160 mg, 0.02 mmol, 58%).

^{1}H NMR (600 MHz, CD_2Cl_2): δ = 9.20 (s, 4H_{aryl}), 9.01 (s, 4H_{aryl}), 8.56 (m, 2H_{aryl}), 8.45 (m, 2H_{aryl}), 8.34 (s, 2H_{aryl}), 7.88 (m, 4H_{aryl}), 7.70 (m, 4H_{aryl}), 7.66 (m, 24H_{aryl}), 7.54 (m, 16H_{aryl}), 7.49 (s, 8H_{aryl}), 7.33 (m, 12H_{aryl}), 4.23 (br, 8H), 2.63 (s, 6H), 1.81 (s, 12H) **^{13}C NMR** (125.76 MHz, MeOD): δ =163.7, 163.3, 162.4, 135.8, 133.5, 131.3, 131.0, 130.9, 130.6, 130.4, 130.4-130.3 , 129.1 - 128.9, 128.5, 126.9, 124.7, 118.5, 52.3, 51.8, 49.9 **^{19}F NMR** (470 MHz, MeOD) -63.85 ppm. **ESI-HRMS**: 645.317 (calc. 645.313)

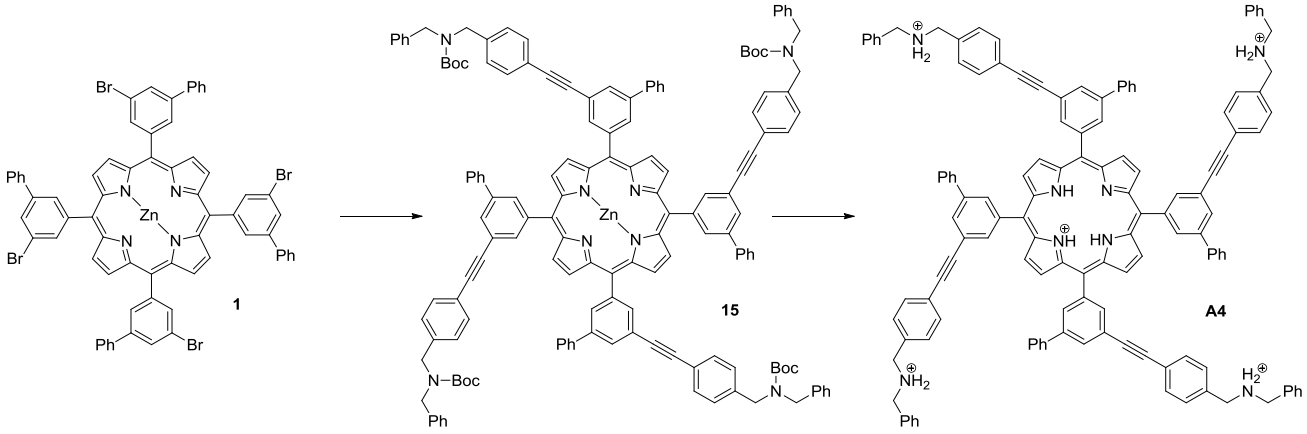

Boc-protected tetraammonium precursor porphyrin (15)

Porphyrin **1** (260 mg, 0.20 mmol, 1.0 equiv), PPh_3 (21 mg, 0.08 mmol, 0.4 equiv) and CuI (15 mg, 0.08 mmol, 0.4 equiv) were dissolved in 40 mL toluene/TEA 1:1 and degassed by rapid vacuum–argon cycles (5 times). Afterwards, $Pd(PPh_3)_4$ (92 mg, 0.08 mmol, 0.4 equiv) was added and the flask was degassed again (3 times). After **8** (643 mg, 2.00 mmol, 10.0 equiv) was added the solution was stirred at 80 °C for 3 d under a nitrogen atmosphere. Purification was conducted on a short silica plug with CH_2Cl_2 as the eluent, followed by column chromatography (silica gel, CH_2Cl_2/MeOH 100:1) and finally precipitated from (MeOH/CH_2Cl_2) by slowly removing the CH_2Cl_2 under vacuum to obtain pure **15** (421 mg, 0.19 mmol, 93%) as a purple solid.

^{1}H NMR (500 MHz, $CDCl_3$): δ = 9.12 (s, $8H_{aryl}$), 8.47 (s, $4H_{aryl}$), 8.40 (s, $4H_{aryl}$), 8.24 (s, $4H_{aryl}$), 7.89 (m, $8H_{aryl}$), 7.55 (m, $8H_{aryl}$), 7.52 (m, $8H_{aryl}$), 7.42 (m, $4H_{aryl}$), 7.31 (m, $8H_{aryl}$), 7.26 (m, $4H_{aryl}$), 7.13 (m, $16H_{aryl}$), 4.28 (m, 16H), 1.40(s, 36H) **^{13}C NMR** (125.76 MHz, $CDCl_3$): δ = 156.7, 150.3, 143.6, 140.1, 139.6, 137.7, 136.1, 133.4, 132.3, 131.9, 129.4, 129.0, 128.6, 128.0, 127.9, 127.5, 127.3, 122.1, 120.2, 89.7, 80.2, 49.2, 28.3 ppm.

Target tetraammonium porphyrin salt (A4)

Precursor **15** (396 mg, 0.18 mmol, 1.0 equiv) was dissolved in 20 mL of CH_2Cl_2 and 6 mL of TFA was added. After stirring overnight at room temperature the reaction mixture was concentrated under reduced pressure. The crude solid was redissolved in CH_2Cl_2 and washed with 2 M aqueous $NaHCO_3$ solution. The combined organic phases were dried over $MgSO_4$ and the solvent was removed under reduced pressure to obtain the desired compound **16** (310 mg, 0.18 mmol, 98%) as a purple solid that was used without further purification.

Compound **16** (314 mg, 0.18 mmol, 1.0 equiv) was dissolved in 40 mL of a 1:1 $CHCl_3$/MeOH mixture and 3 mL 1 M aqueous HCl were added. After 5 min of stirring the volatiles were removed under reduced pressure and this procedure was subsequently repeated another 3 times. The so obtained solid was dried under vacuum overnight. The above hydrochloride of **16** (0.335 g, 0.17 mmol, 1 equiv) was dissolved in 20 mL MeOH and NaBArF (825 mg, 0.93 mmol, 5.5 equiv) was added. After 10 min of stirring, H_2O was added slowly until the precipitation of the desired compound occurs. The precipate was collected by centrifugation and was then redissolved in MeOH to repeat the precipitation. This procedure was repeated two more times to obtain **A4** (703 mg, 0.12 mmol, 68%).

^{1}H NMR (500 MHz, CD_2Cl_2): δ = 9.30 (s, 8H_{aryl}), 8.60 (s, 8H_{aryl}), 8.39 (s, 4H_{aryl}), 8.03 (m, 8H_{aryl}), 7.88 (m, 8H_{aryl}), 7.61 (s, 40H_{aryl}), 7.43 (s, 20H_{aryl}), 7.54-7.34 (m, 40H_{aryl}), 4.28 (m, 16H) **^{13}C NMR** (126 MHz, MeOD) δ 163.5, 163.1, 162.7, 162.3, 135.8, 133.5, 132.2, 131.3, 131.0, 130.9, 130.6, 130.4, 130.3, 130.1, 129.4, 129.0, 128.5, 126.9, 125.7, 124.7, 122.5, 118.5, 91.4, 90.3, 52.2, 51.7 **^{19}F NMR** (470 MHz, MeOD) -64.40 ppm

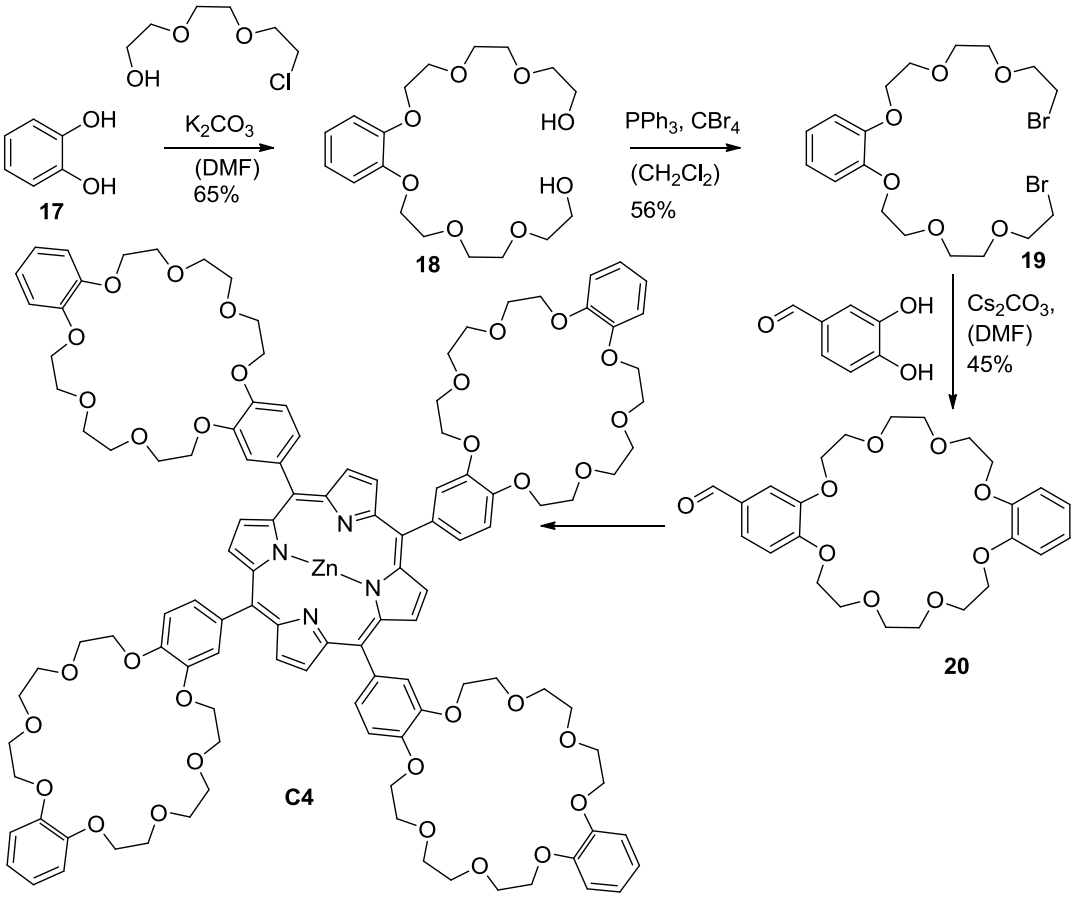

1,2-Bis(2-(2-(2-bromoethoxy)ethoxy)ethoxy)benzene (19)

PPh_3 (56.71 g, 261.40 mmol, 6 equiv) followed by CBr_4 (71.710 g, 261.40 mmol, 6 equiv) were added to a stirring solution of **18** (13.494 g, 36.04 mmol, 1 equiv) in CH_2Cl_2. The mixture was stirred overnight at room temperature, concentrated under reduced pressure and purified by column chromoatography (SiO_2, CH_2Cl_2/PE 9:1) to obtain **19** as a yellow oil (10.34 g, 20.54 mmol, 57%).

^{1}H NMR (300 MHz, $CDCl_3$): δ = 6.92 (s, $4H_{aryl}$), 4.17 (m, 4H), 3.87 (m, 4H), 3.81 (m, 4H), 3.72 (m, 8H), 3.47 (m, 4H) **^{13}C NMR** (126 MHz, $CDCl_3$) δ = 148.6, 121.3, 114.6, 70.8, 70.4, 70.2, 69.5, 68.6, 30.2 ppm. **ESI-HRMS**: 499.030 (calc. 499.025 $C_{18}H_{28}O_6Br_2^+$)

3-Formyl-dibenzo[24]crown-8 (20)

3,4-Dihydroxybenzaldehyde (1.381 g, 10.00 mmol, 1 equiv) was dissolved in 100 mL of dry DMF in two necked round-bottomed flask and Cs_2CO_3 powder (11.40 g, 35.00 mmol, 3.5 equiv) was added. The mixture was allowed to stir for 15 min, after which **19** (5.50 g, 12.66 mmol, 1.1 equiv) dissolved in 100 mL of dry DMF was added dropwise over 2 h at 60 °C. Then the temperature was raised to 85 °C and the reaction mixture was stirred for 5 d at this temperature. Afterwards the solvent was removed under reduced pressure, 100 mL of water were added to the residue and the mixture was extracted with CH_2Cl_2 three times. The combined organic extracts were dried over anhydrous sodium sulfate and the solvent was removed under reduced pressure to give the crude product. Subsequent purification by column chromatography (SiO_2, CH_2Cl_2/MeOH 98:2) yielded **20** (2.1 g, 4.00 mmol, 40%) as a white powder.

^{1}H NMR (300 MHz, $CDCl_3$): δ = 9.79 (s, 1H), 7.40 (dd, J = 8.2, 1.9 Hz, $1H_{aryl}$), 7.35 (d, J = 1.9 Hz, $1H_{aryl}$), 6.92 (dd, J = 8.5, 3.5 Hz, $1H_{aryl}$), 6.88 - 6.81 (m, $4H_{aryl}$), 4.19 (m, 4H), 4.15 - 4.09 (m, 4H), 3.96 - 3.85 (m, 8H), 3.82 (d, J = 3.8 Hz, 8H) **^{13}C NMR** (126 MHz, $CDCl_3$) δ = 190.8, 162.4, 154.2, 151.6, 149.0, 148.7, 130.0, 126.7, 121.6, 113.8, 111.8, 110.9, 72.5, 71.4, 71.3, 71.1, 70.3, 69.8, 69.3. ppm. **ESI-HRMS**: 499.030 (calc. 494.238 $C_{25}H_{32}O_9NH_4^+$)

5,10,15,20-Tetrakis (dibenzo[24]-crown-8)porphyrin (21)

Pyrrole (0.1 mL, 1.50 mmol, 1 equiv) was added to a hot solution (100 °C) of **20** (720 mg, 1.50 mmol, 1 equiv) in 115 mL of propionic acid and the solution was refluxed for 3 h. After removal of the solvent by distillation, the black crude product was purified by column chromatography (neutral alumina, CH_2Cl_2) and preparative GPC to obtain **21** as a purple solid (100 mg, 0.19 mmol, 13%).

^{1}H NMR (300 MHz, $CDCl_3$): δ =9.02 (s, $8H_{aryl}$), 7.74 (m, $8H_{aryl}$), 7.24 - 7.16 (m, $8H_{aryl}$), 6.98 - 6.81 (m, $16H_{aryl}$), 4.29 (m, 16H), 4.20 - 3.99 (m, 32H), 3.96 - 3.81 (m, 16H), 3.81 - 3.69 (m, 32H) **^{13}C NMR** (125.75 MHz, $CDCl_3$): δ = 172.1, 171.5, 170.1, 149.0, 148.8, 147.0, 153.3, 128.0, 121.5, 120.6, 119.8, 114.16, 111.88, 104.9, 96.9, 82.0, 80.2, 77.3, 71.6, 71.5, 71.4, 70.19, 70.13, 70.08, 70.06, 69.7, 69.6, 69.5, 69.4, 29.8, 14.6, 1.1 ppm

Zinc [5,10,15,20-tetrakis(dibenzo[24]-crown-8)porphyrin] (C4)

Zinc acetate (21 mg, 0.10 mmol, 2 equiv) was added to a stirring solution of **21** (100 mg, 0,05 mmol, 1 equiv) in 20 mL of chloroform/methanol 1:1 and stirred at room temperature overnight. The purple solution was concentrated to dryness and purified by column chromatography (neutral alumina, CH_2Cl_2) to obtain **C4** as a purple solid (93 mg, 0.04 mmol, 90%).

^{1}H NMR (300 MHz, CD_2Cl_2): δ =9.02 (s, $8H_{aryl}$), 7.74 (m, $8H_{aryl}$), 7.24 - 7.17 (m, $4H_{aryl}$), 6.89 (m, $16H_{aryl}$), 4.25 (m, 16H), 4.10 - 3.99 (m, 24H), 3.96 - 3.85 (m, 16H), 3.81 - 3.72 (32, 4H) **^{13}C NMR** (125.75 MHz, CD_2Cl_2): δ =150.7, 149.4, 148.9, 147.7, 136.8, 132.3, 128.3, 121.7, 121.1, 114.6, 112.4, 71.3, 70.1, 70.1, 70.0 ppm**. ESI-HRMS**: 2179.81 (calc. 2179.80 $C_{116}H_{132}O_{32}N_4ZnNa^+$)

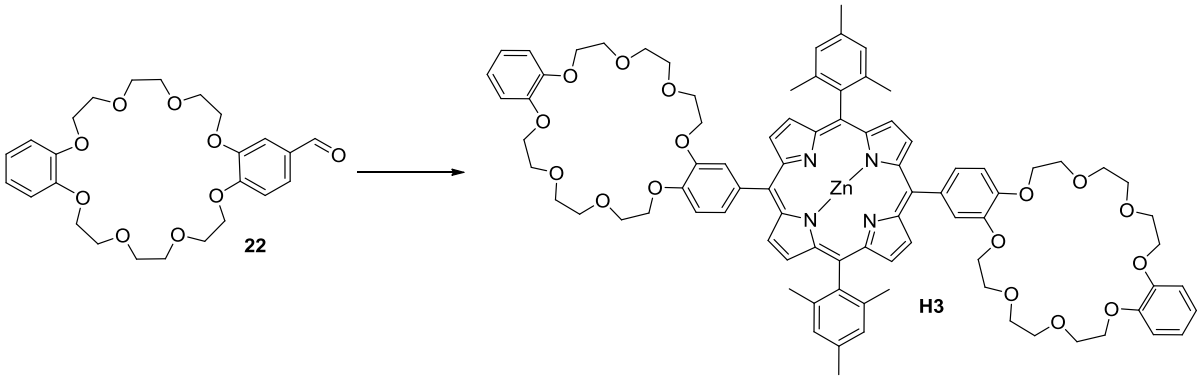

5,15-Bis(dibenzo[24]-crown-8)-10,20-bis(mesityl)porphyrin (22)

Molecular sieves (6 Å, 0.06 g) were added to a stirring solution of **20** (0.903 g, 1.90 mmol, 1 equiv), 2,2'-(mesitylmethylene)bis(1H-pyrrole), and **6** (0.501 g, 1.90 mmol, 1 equiv) in 300 mL chloroform. The mixture was degassed by bubbling argon through the solution for 20 min before $BF_3 \cdot Et_2O$ (0.03 mL, 0.19 mmol, 0.2 equiv) was added and the mixture was stirred in the dark for 3 h at room temperature. Afterwards, DDQ (0.430 g, 1.90 mmol, 1.0 equiv) was added and stirring was continued overnight. Then TEA (1 mL) was added and the major impurities were removed by filtration through a silica plug using CH_2Cl_2 as eluent. The pure product was obtained by column chromatography (neutral alumina, CH_2Cl_2/petrolether 1:3) and preparative GPC as a purple solid (0.80 g, 1.12 mmol, 59%).

^{1}H NMR (300 MHz, CD_2Cl_2): δ = 8.90 (d, J = 4.8 Hz, $4H_{aryl}$), 8.69 (d, J = 4.8 Hz, $4H_{aryl}$), 7.83 (d, J = 2.0 Hz, $4H_{aryl}$), 7.77 (dd, J = 8.1, 2.0 Hz, $2H_{aryl}$), 7.34 (s, $4H_{aryl}$), 7.29 (d, J = 8.2 Hz, $2H_{aryl}$), 7.05 - 6.88 (m, $8H_{aryl}$), 4.51 - 4.41 (m, 4H), 4.31 (m, 4H), 4.26 - 4.15 (m, 8H), 4.13 - 4.05 (m, 4H), 3.95 (m, 24H), 3.85 (m, 8H), 2.66 (s, 6H), 1.89 - 1.83 (m, 12H) **^{13}C NMR** (125.75 MHz, $CDCl_3$): δ = 149.0, 148.7, 147.5, 139.4, 127.8, 121.5, 114.1, 71.4, 70.0, 69.4, 21.7, 21.4 ppm.

Zinc [5,15-bis(dibenzo[24]-crown-8)-10,20-bis(mesityl)porphyrin] (C2)

Zinc acetate (229 mg, 1.04 mmol, 5 equiv) was added to a stirred solution of **22** (300 mg, 0,21 mmol, 1 equiv) in 20 mL of chloroform/methanol 1:1 and stirred overnight at room temperature. The purple solution was concentrated to dryness under reduced pressure and purified by column chromatography (neutral alumina, CH_2Cl_2) to obtain **C2** as a purple solid (298 mg, 0.20 mmol, 95%).

^{1}H NMR (500 MHz, $CDCl_3$): δ =8.81 (dd, J = 4.6, 1.8 Hz, $4H_{aryl}$), 8.68 (dd, J = 4.6, 2.5 Hz, $4H_{aryl}$), 7.69 - 7.60 (m, $4H_{aryl}$), 7.20 (s, $4H_{aryl}$), 7.06 (dd, J = 7.9, 6.5 Hz, $2H_{aryl}$), 6.85 - 6.74 (m, $8H_{aryl}$), 4.23 (m, 4H), 4.09 - 4.06 (m, 4H), 4.03 (s, 2H), 4.02 - 3.99 (m, 2H), 3.98 - 3.94 (m, 2H), 3.91 (m, 2H), 3.88 (s, 4H), 3.85 - 3.82 (m, 4H), 3.77 - 3.71 (m, 8H), 3.68 - 3.62 (m, 4H), 3.57 (s, 4H), 3.49 (s, 2H), 3.43 (s, 4H), 2.55 (s, 6H), 1.75 (s, 12H) **^{13}C NMR** (126 MHz, $CDCl_3$) δ = 150.1, 149.8, 148.8, 148.2, 148.1, 146.5, 146.4, 139.2, 137.3, 135.9, 132.3, 130.7, 127.6, 121.3, 119.7, 119.0, 113.9, 71.0, 70.9, 70.7, 70.6, 70.4, 70.3, 69.7, 69.5, 69.4, 69.3, 69.3, 69.2, 69.1, 68.9, 68.8 ppm. **ESI-HRMS**: 1523.573 (calc. 1523.570 $C_{86}H_{92}N_4O_{16}ZnNa^+$)

^{1}H NMR titrations of the pseudorotaxanes

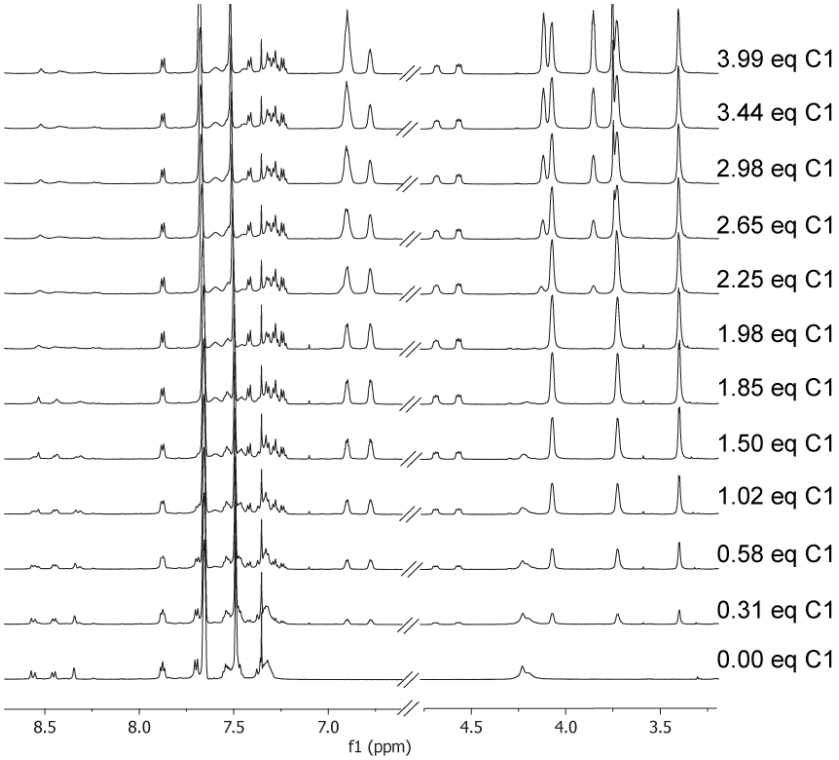

Figure S1: NMR titration (500 MHz, 298 K, CD_2Cl_2) of **C1** to a 3 mM solution of **A2** showing a slow exchange and signal shifts up to the expected 2:1 ratio.

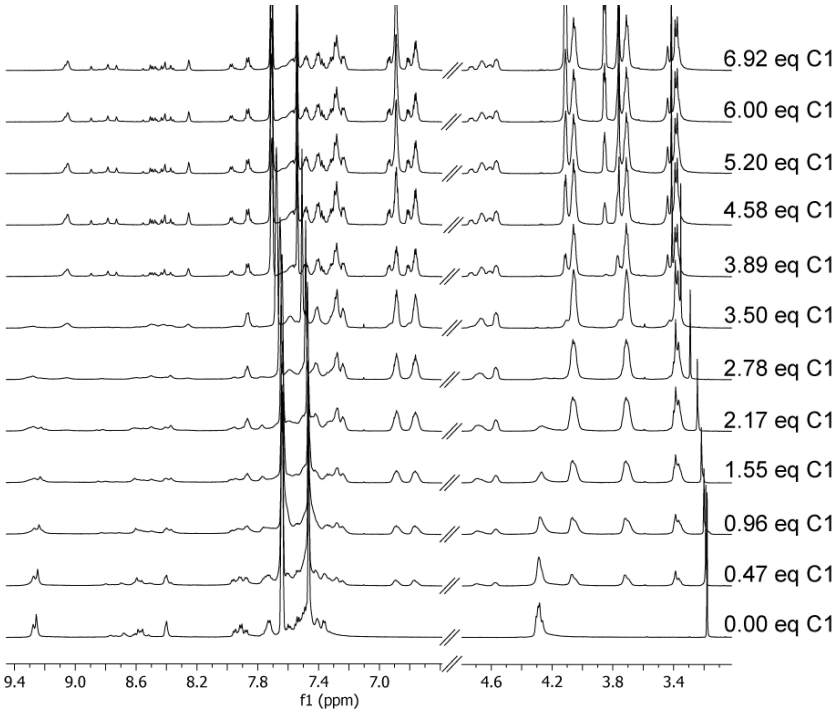

Figure S2: NMR titration (500 MHz, 298 K, CD_2Cl_2) of **C1** to a 3 mM solution of **A4** showing a slow exchange and signal shifts up to the expected 4:1 ratio.

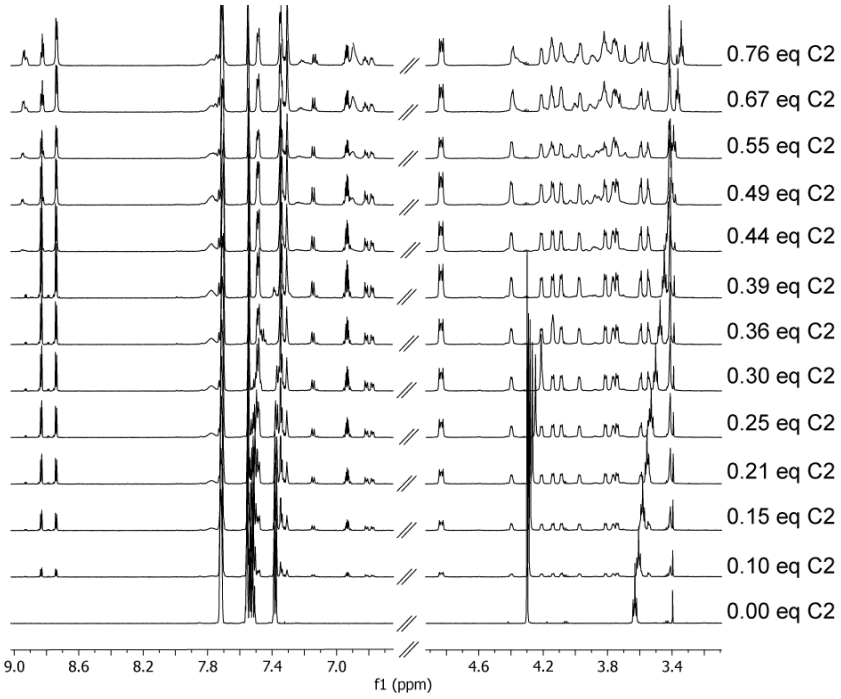

Figure S3: NMR titration (500 MHz, 298 K, CD_2Cl_2) of **C4** to a 3 mM solution of **A1** showing a slow exchange and signal shifts up to the expected 1:4 ratio.

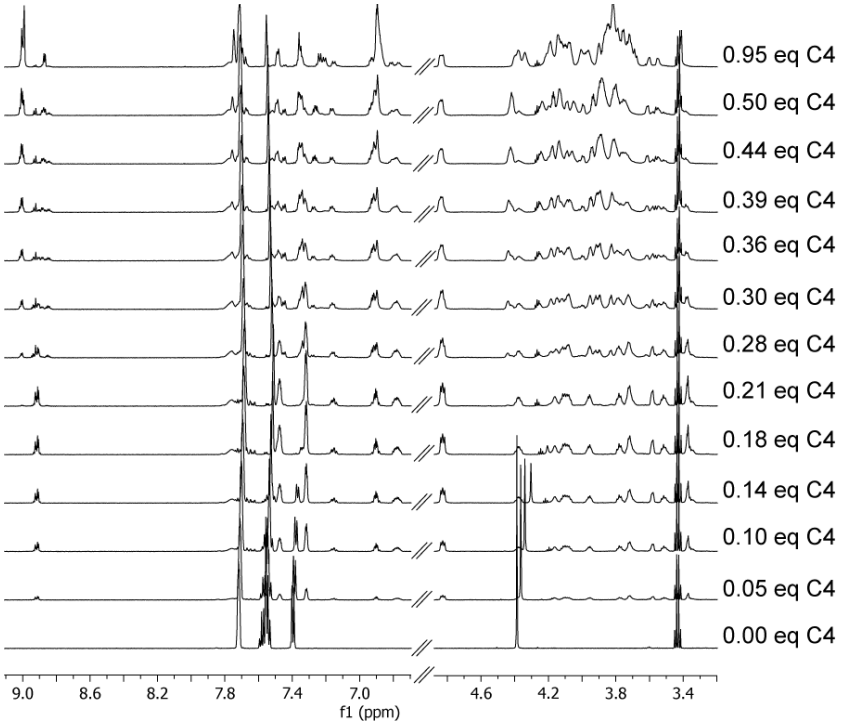

Figure S4: NMR titration (500 MHz, 298 K, CD_2Cl_2) of **C2** to a 3 mM solution of **A1** showing a slow exchange and signal shifts up to the expected 1:2 ratio.

Mass spectrometric analysis

[3]- and [5]Pseudorotaxanes with monovalent building blocks A1 or C1

The samples for mass spectrometric analysis of the [3]- and [5]pseudorotaxanes were prepared as follows. Separate solutions of hosts and guests were prepared (CH_2Cl_2, **A1**/**C1**: 4 mM, **A2**/**C2**: 2 mM, **A4**/**C4**: 1 mM), combined in the respective 1:2, 1:4, 2:1 and 4:1 molar ratios and allowed to equilibrate for 24 hours at room temperature. The solutions of the pseudorotaxanes were diluted to 0.2 µM prior to analysis.

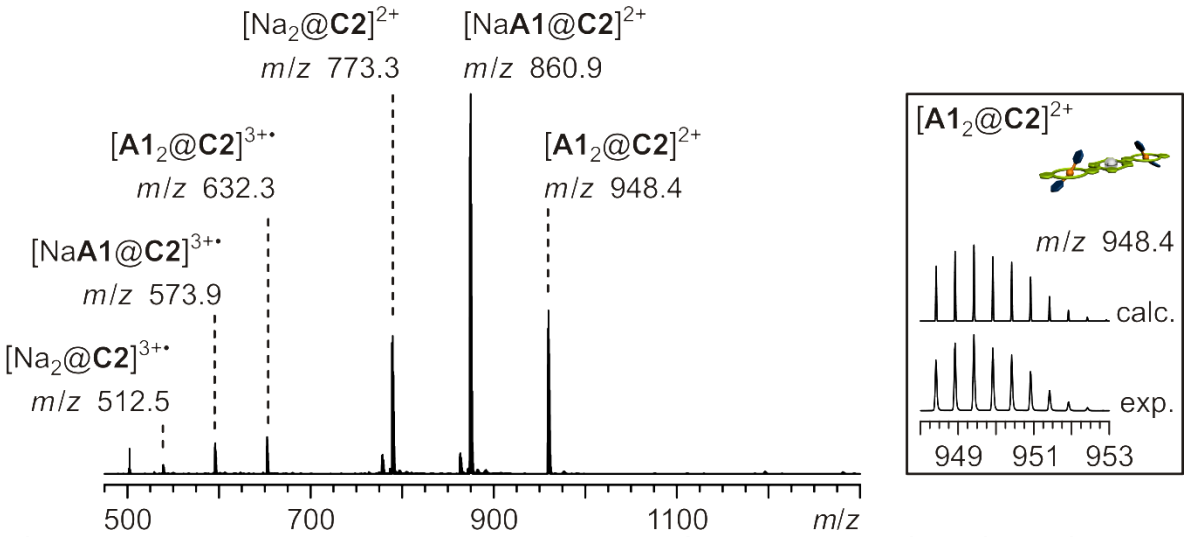

Figure S**5:** ESI-Q-TOF-MS spectrum of a 2:1 mixture of **A1** and **C2** (CH_2Cl_2, 0.2 µM; left hand side) and respective experimental and calculated isotopic patterns of the desired [3]-pseudorotaxane [**A1**$_2$@**C2**]$^{2+}$ (*m*/*z* 948.4; right hand side).

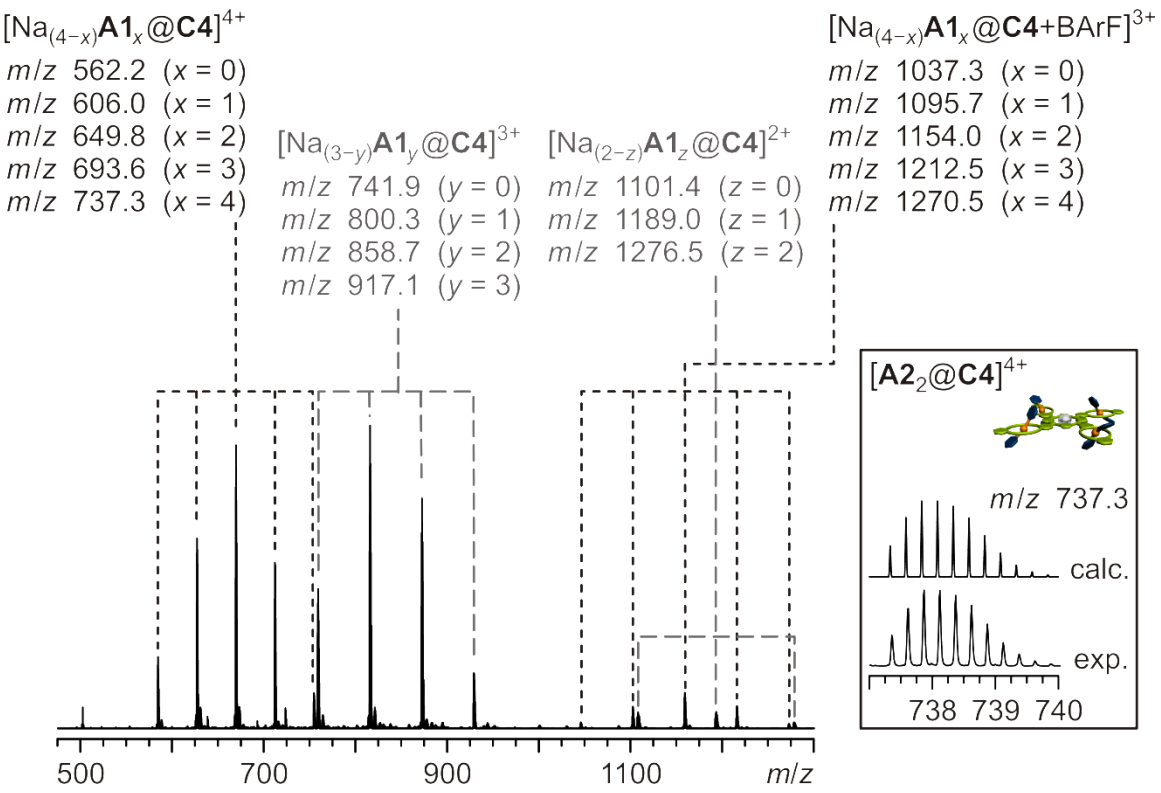

Figure S6: ESI-Q-TOF-MS spectrum of a 4:1 mixture of **A1** and **C4** (CH_2Cl_2, 0.2 µM; left hand side) and respective experimental and calculated isotopic patterns of the desired [5]-pseudorotaxane [**A1**$_4$@**C4**]$^{2+}$ (*m*/*z* 1093.5; right hand side).

[2]- and [3]Pseudorotaxanes with di- and tetravalent building blocks A2, A4, C2 and C4

The samples for mass spectrometric analysis of the multivalent [2]- and [3]pseudorotaxanes were prepared as follows. Separate solutions of hosts and guests were prepared (CH_2Cl_2, **A2**/**C2**: 0.6 mM, **A4**/**C4**: 0.3 mM). They were mixed in the respective 1:1, 1:2 and 2:1 molar ratios and allowed to equilibrate for 14 hours at 6 °C. The pseudorotaxane solutions were diluted to 0.2 µM prior to analysis.

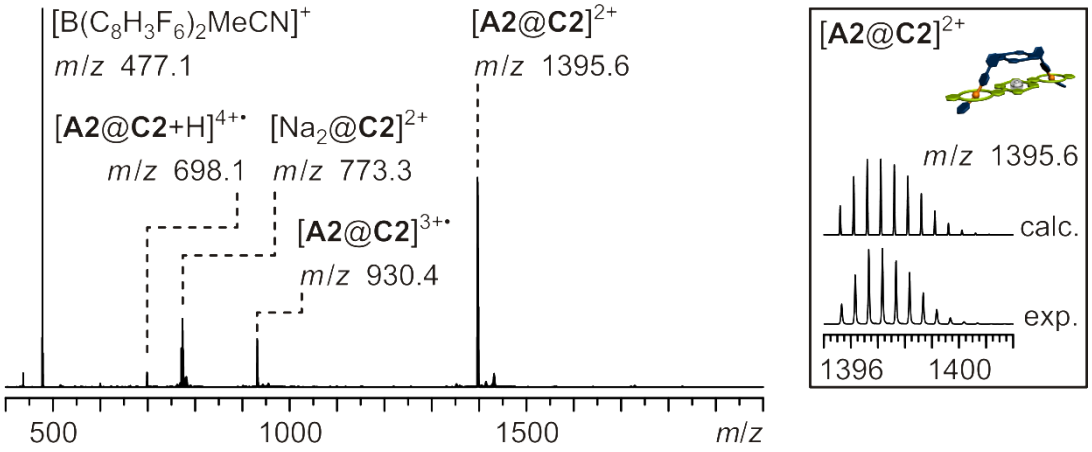

Figure S7: ESI-Q-TOF-MS spectrum of a 1:1 mixture of **A2** and **C2** (CH_2Cl_2, 0.2 µM; left hand side) and respective experimental and calculated isotopic patterns of the desired [2]pseudorotaxane [**A2**@**C2**]$^{2+}$ (*m/z* 1395.6033 (exp.), 1395.6039 (calc.); right hand side).

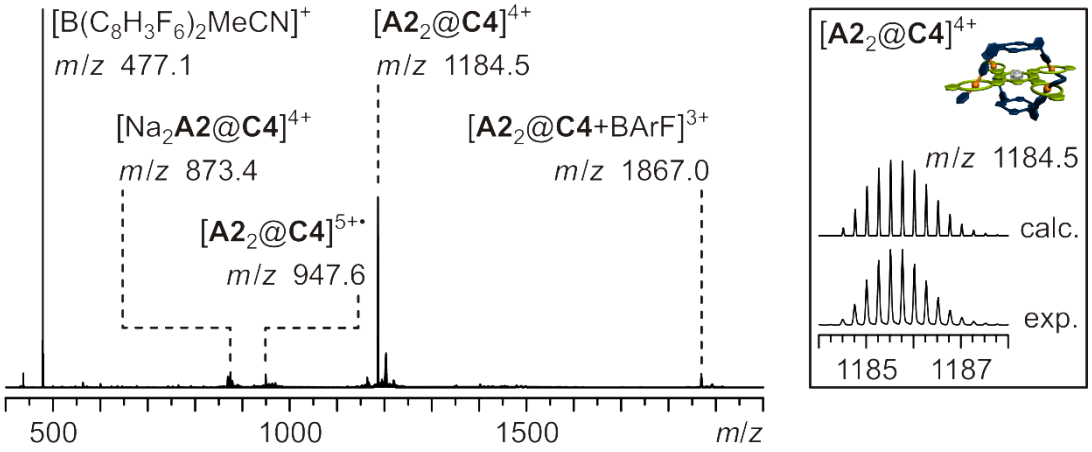

Figure S8: ESI-Q-TOF-MS spectrum of a 2:1 mixture of **A2** and **C4** (CH_2Cl_2, 0.2 µM; left hand side) and respective experimental and calculated isotopic patterns of the desired [3]-pseudorotaxane [**A2**$_2$@**C4**]$^{4+}$ (*m/z* 1184.5020 (exp.), 1184.5168 (calc.); right hand side).

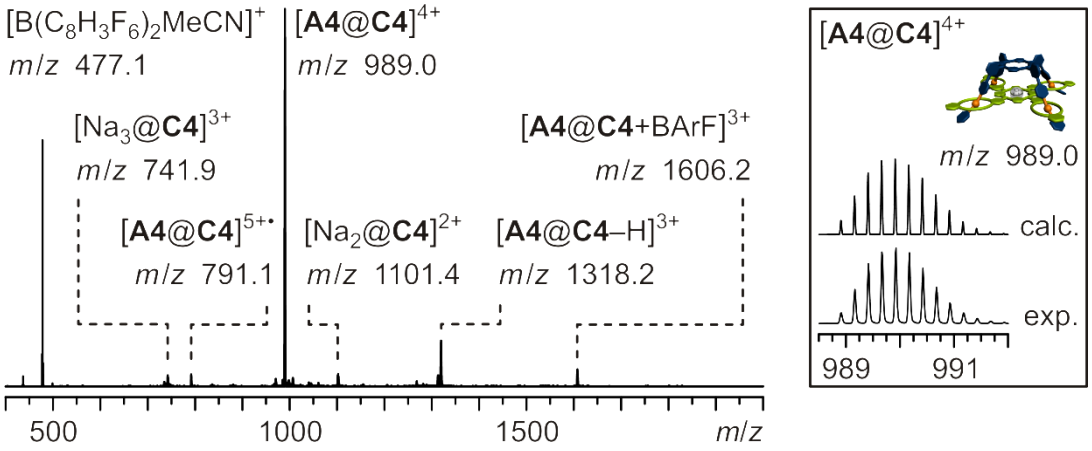

Figure S9: ESI-Q-TOF-MS spectrum of a 1:1 mixture of **A4** and **C4** (CH_2Cl_2, 0.2 µM; left hand side) and respective experimental and calculated isotopic patterns of the desired [2]-pseudorotaxane [**A4**@**C4**]$^{4+}$ (*m/z* 988.9071 (exp.), 988.9080 (calc.); right hand side).

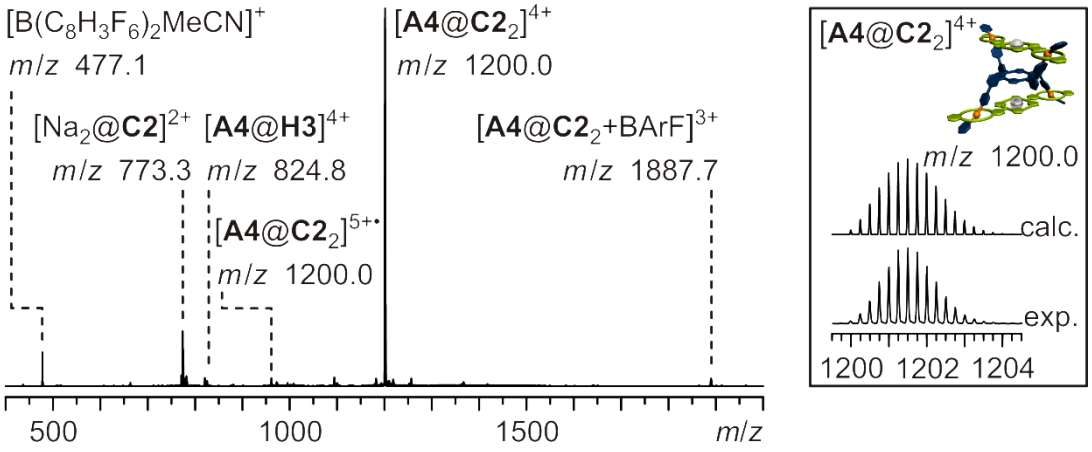

Figure S10: ESI-Q-TOF-MS spectrum of a 1:2 mixture of **A4** and **C2** (CH_2Cl_2, 0.2 µM; left hand side) and respective experimental and calculated isotopic patterns of the desired [3]-pseudorotaxane [**A4**@**C2**$_2$]$^{2+}$ (*m/z* 1199.9935 (exp.), 1199.9951 (calc.); right hand side).

References

1. D. L. Reger, T. D. Wright, C. A. Little, J. J. S. Lamba and M. D. Smith, *Inorg. Chem.*, **2001**, *40*, 3810-3814.

2. C. R. South, M. N. Higley, K. C. F. Leung, D. Lanari, A. Nelson, R. H. Grubbs, J. F. Stoddart and M. Weck, *Chem. Eur. J.*, **2006**, *12*, 3789-3797.

3. J. Frey, G. Kodis, S. D. Straight, T. A. Moore, A. L. Moore and D. Gust, *J. Phys. Chem. A*, **2012**, *117*, 607-615.

4. T. Bogaschenko, S. Basok, C. Kulygina, A. Lyapunov and N. Lukyanenko, *Synthesis*, **2002**, *2002*, 2266-2270.